Fall 2020

Steady-State and Transient Study of Flow Boiling in Microchannels With Microgrooves/Micronozzles

Congcong Ren

STEADY-STATE AND TRANSIENT STUDY OF FLOW BOILING IN MICROCHANNELS WITH MICROGROOVES/MICRONOZZLES

by

Congcong Ren

Bachelor of Engineering
University of Birmingham, 2013

Bachelor of Science
Huazhong University of Science & Technology, 2013

Master of Science
University of Bath, 2014

Submitted in Partial Fulfillment of the Requirements

For the Degree of Doctor of Philosophy in

Mechanical Engineering

College of Engineering and Computing

University of South Carolina

2020

Accepted by:

Chen Li, Major Professor

Jamil Khan, Committee Member

Guiren Wang, Committee Member

Guoan Wang, Committee Member

Cheryl L. Addy, Vice Provost and Dean of the Graduate School

DEDICATION

To my parents and my younger brother, for their endless love, support and encouragements without which I would not be who I am, where I am.

ACKNOWLEDGEMENTS

With immense pleasure and great respect, I express my deep regards and sincere thanks to my advisors Dr. Chen Li for his invaluable guidance, insightful suggestion, and countless support throughout my Ph. D study at the University of South Carolina. He is the one who introduced me to the world of academic research. His encouragements and help have been the constant source of inspiration. It is my great honor to work with him and his team. The experiences and knowledge I gained these years will be invaluable treasure in my life.

I would like to thank my committee members, Dr. Jamil Khan, Dr. Guiren Wang, and Dr. Guoan Wang for their invaluable advice and help throughout my research.

I would like to express my sincere regards and thanks to all my lab mates, especially Dr. Wenming Li and Dr. Wei Chang for their suggestions, constant encouragements, and generous help through all stages of my research.

Last but not least, I would show my sincere thanks to my parents for their endless love, support and encouragement, without which I would not come this far.

This work was supported by the Office of Naval Research under the Grant N00014-16-1-2956 and N000141612307, and National Science Foundation under the award 1357920 and 1336443.

ABSTRACT

Microchannel flow boiling is one of the most desired cooling solutions for high power electronics. Owing to the high latent heat of vaporization, high heat fluxes can be achieved through phase-change heat transfer. However, the enhancements of (critical heat flux) CHF and heat transfer coefficient (HTC) are usually inhibited by the transitional flow patterns, which highly influence the liquid rewetting. In the past two decades, many techniques have been explored to enhance the liquid rewetting in microscale.

In this dissertation, four parallel micro-grooves fabricated on the bottom of five microchannels (W=200 μm, H=250 μm, L=10 mm) were designed to promote the liquid rewetting ability through the enhanced capillary pressure. Experiments were conducted with deionized water flowing through the micro-grooved microchannels at a wide mass flux range. The experimental studies demonstrate that the configuration of micro-grooves is effective in mitigating the local dry-out and then significantly increases CHF without escalating the pressure drop. On the other hand, enhanced thin film evaporation was also observed to increase the heat transfer rate.

Another topic of this dissertation is the transient heat transfer performance of flow boiling in microchannels under dynamic heat loads. New understandings about microchannels with the microgrooves or the multiple micronozzles were developed to study the performance of the devices to dissipate heat that generated instantly. The heat

was applied to the system in the form of heat pulse and the transient behaviors of the wall temperature, the wall temperature increase rate and the HTC were investigated in this study. The video was captured synchronously, and different flow patterns were matched with the transient thermal characteristics. The effects of heat pulse amplitude and mass velocity were investigated. The results were compared to that of plain-wall microchannel and significant enhancement was noticed along all the boiling stages. The highest enhancement of the HTC in the stable stage was 225% with mass flux of 380 kg/m^{2}s and heat flux of 160 W/cm^2. Different from the flow boiling phenomena with DI-water, the boiling of HFE-7100 expanded to the entire channel instantly. A temperature spike was noticed at the ONB resulted from the growing vapor layer beside the wall after the boiling was initiated, which enabled the identifying of ONB from temperature profile. Apart from the visualization study, the effect of heat pulse amplitude on the ONB time and ONB temperature was determined.

TABLE OF CONTENTS

LIST OF FIGURES

LIST OF SYMBOLS

A	Area, m^2
C_p	Heat capacity at constant pressure, J/kg·K
f	Rewetting Frequency, Hz
$\bar{h}$	Total heat transfer coefficient, $W/m^2 \cdot K$
h_{fg}	Latent heat of vaporization, kJ/kg
H	Microchannel height, m
I	Electrical current, A
k	Thermal conductivity, W/m·K
L	Microchannel Length, m
m	Parameter for fin efficiency
$\dot{m}$	Mass flow rate, kg/s
Na	Nucleation site density, sites/cm^2
Δp	Pressure drop, kPa
p	Pressure
P	Power, W
q''	Heat flux, W/cm^2
R	Electrical resistance, Ω
R_h	Hydraulic radius, m

k	Slope of linear function, Ω/K
k_s	Thermal conductivity, W/mK
t	Thickness between heater and microchannel base, m
t	Time, s
T	Temperature, °C
$\overline{T}$	Overall temperature, °C
V	Electrical voltage, V
W	Microchannel width, m
W_f	Fin width, m
ρ	Density, kg/m^3
χ	Vapor quality
σ	Surface tension, N/m
θ	Contact angle, ^{o}
η	Ratio
η_f	Fin efficiency
τ	Duration, s

LIST OF ABBREVIATIONS

0 ..... Initial

2ϕ ..... Two-phase

b ..... Base

c ..... Cross-sectional

cap ..... Capillary

CHF ..... Critical heat flux

e ..... Exit

eff ..... Effective

exp ..... Experimental

f ..... Frictional

f ..... Fin

fg .....Latent

h.....Hydraulic

HTC..... Heat Transfer Coefficient

in ..... Inlet

l ..... Liquid

m ..... Mixture

NP ..... Nanoparticles

out.....Outlet

ONB ..... Onsite of boiling

PR ..... Photo resist

RIE ..... Reactive ion etching

DRIE..... Deep reactive ion etching

R .....Constant resistant

s ..... Solid

sat ..... Saturated

Si ..... Silicon

tf .....Thin film

v..... Vapor

wet.....wetted

CHAPTER 1 BACKGROUND

The continuous growth of electronic devices, transportation industry, diode lasers and nuclear industry brings exponential increasing heat generated, which consequently increases the risk of device damaging caused by high temperature [1] [2]. Even though great efforts have been made on high heat flux dissipation for over 30 years, it is still challenging when designing systems to address the largest expected heat fluxes, which may be in excess of 1 kW/cm^2 in the background, with local hotspots exceeding 5 kW/cm^2 [3]. Due to such high heat fluxes, a large coolant flow rate and associated pressure drop are required to maintain the temperature of devices at reasonable constraints. In fact, traditional cooling technics are not able to dissipate these assumed heat fluxes. Thus, a new generation of thermal management technics are developed. For example, porous media, microchannel heat sink and spray cooling are very promising cooling technics with multiple applications on compact devices. Compare to the traditional air forced cooling or single-phase liquid cooling methods, two-phase cooling can effectively reduce the coolant flow rate and pressure drop due to the high heat transfer coefficient with the advantage of latent heat. As a result, two-phase cooling has been studied extensively in the past decades and enormous improvements were achieved. Compare to the convectional scale cooling system, the heat and mass transfer in microsystem is more efficient with high surface to volume ratio. In response, less coolant and pressure drop are required to dissipate high heat fluxes with good temperature uniformity. Moreover, the light weight and compact size of the two-phase

mini/micro scale channel heat sink make it one of the most popular cooling technics[4-7]. Two-phase microsystem cooling has been widely used in many applications [8], including water cooled turbine blades [9], computer and IT industry (CPUs, GPUs, memory cards, data storage devices) [10-13], miniature refrigeration systems [14-17], cooling of Insulated gate bipolar transistors (IGBTs) [18, 19], and Cooling of PEM fuel cells [20, 21]. As one of the most promising cooling technics, extensive studies were focused on two-phase transport in microchannels. To design an ideal microchannel system, efforts were made to improve the efficiency to transport heat and mass, minimize instability, and decrease the weight, size and cost. Generally, the main challenges for heat and mass transporting are to decrease instability, enlarge working condition range, and enhance heat transfer coefficient (HTC) and critical heat flux (CHF) without the cost of extra pressure drop.

The enhancement of HTC was achieved with various techniques such as inlet restrictors microcavities [22-24], micronozzles [25, 26], bridged channel [27], micro-pin fins [28, 29], nanowire coating [30], and change of working liquid[23, 31, 32]. Particularly, microcavities, bridged channels, and nanowire coating can effectively enhance nucleate boiling by increasing nucleation sites density while thin film evaporation can be significantly improved with nanowire coating by promoting wettability.

Bubbly flow, slug flow, and annular flow are three main flow patterns during flow boiling along the microchannel.

Figure 1.1 shows the schematics of the heat transfer coefficient corresponding to two distinct heat transfer regimes: nucleate and convective boiling dominant heat transfer regimes. Bubbly and slug flow occupy most of the length of the microchannel in the

nucleate boiling dominant heat transfer regime while the annular flow is the major pattern in convective boiling dominant heat transfer regime. For the nucleate boiling dominant regime, HTC is highest at the onsite of nucleate boiling (ONB) decreases with gradual suppression of nucleate boiling. For the convective boiling dominate regime, HTC increases with gradual thinning of liquid film. Besides, the HTC decreases from the incipience of the dry-out condition in both regimes. It suggests that HTC can be enhanced by promoting nucleate boiling or annular liquid film evaporation. Particularly, the annular flow regime was proved to be dominant in the heat transfer configurations. Moreover, it becomes more prevalence with decreasing channel diameter [33] [34].

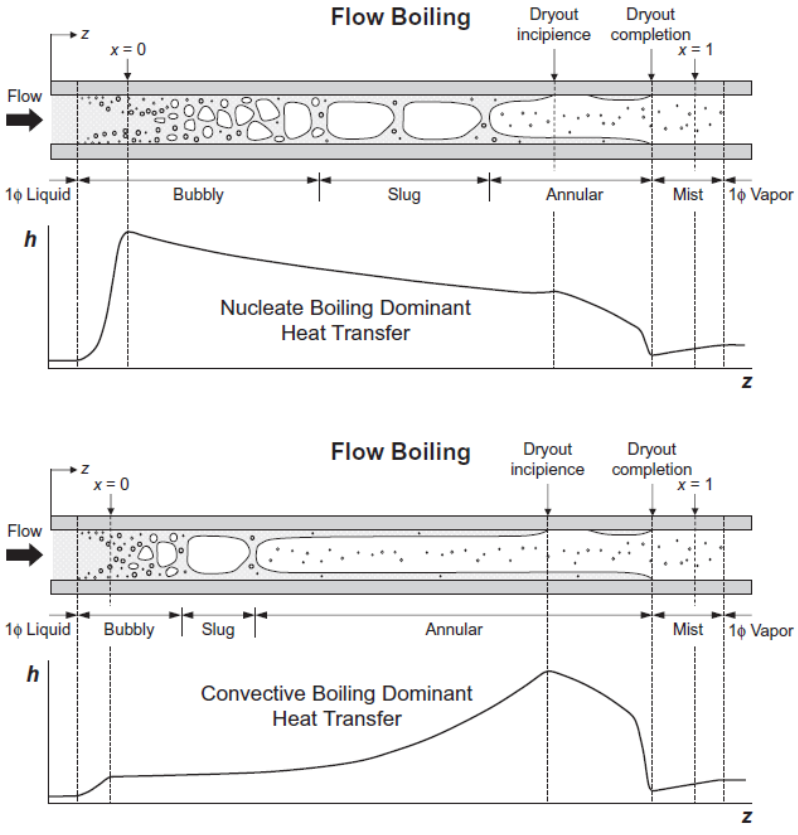

.

Figure 1.1 Schematics of flow regimes, and variation of heat transfer coefficient in mini/microchannels with uniform circumferential heat flux [7]

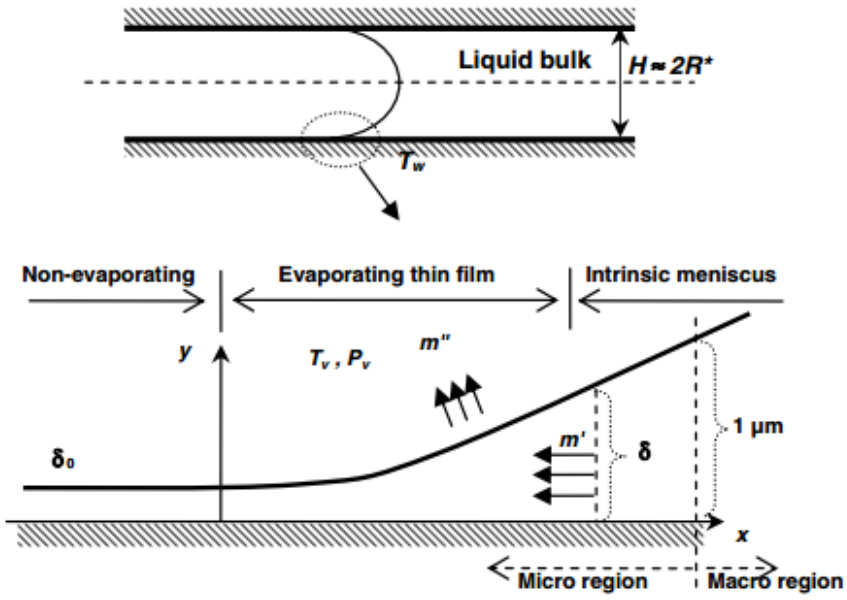

Figure 1.2 Schematic diagram and coordinate system for an evaporating thin film in a channel [35]

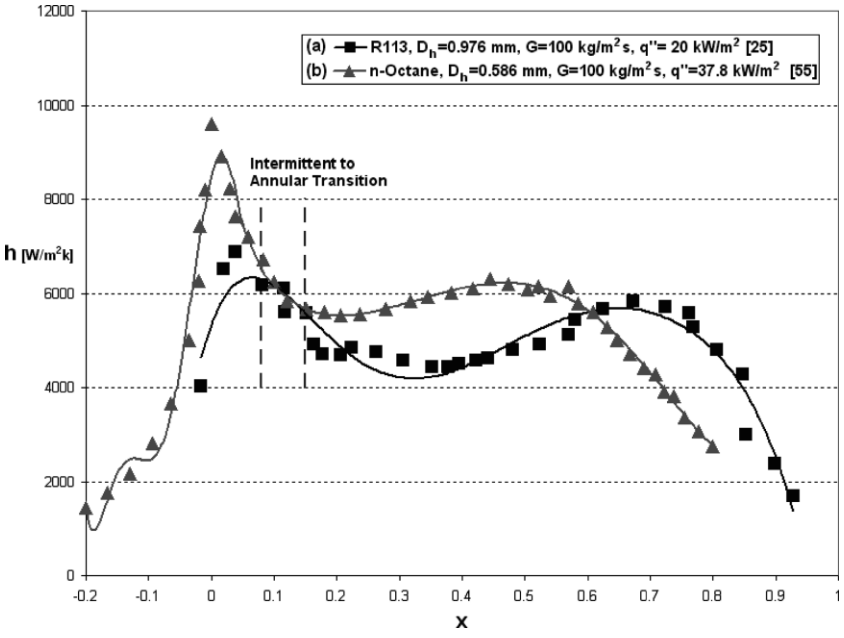

Figure 1.3 Characteristic heat transfer coefficient curve in microchannels [36]

Figure 1.2 illustrates three typical regions of the extended meniscus when liquid wets a solid. The thin film region is characterized by high heat transfer rates due to the low thermal resistant across the thin film. Enormous researches proved that the macro region is the main contributor to the overall heat transfer rate and most of the phase change happens here [37]. Also, capillary pressure plays an important role in determining the film profile throughout the extended meniscus. Plenty of researches presented the positive effect of capillary force on film thinning and thermal performance [38] [39].

In response to the different flow patterns and the nature of different phase-change mechanisms, a possible characteristic, M shaped, of the HTC behaviors in terms of vapor quality for the flow boiling in microchannels is illustrated in Figure 1.3. The HTC rises steeply from a subcooled condition to the saturated condition, where the vapor quality is approximately zero. The peak value appeared at the onsite of the nucleate boiling, which results in acceleration of the bulk liquid velocity in bubble flow region. This obviously raises the HTC substantially above the single-phase region, where forced convection is the only heat transfer mechanism. With the increased vapor quality after that, the bubble agglomeration limits the increasing in heat transfer rate, especially when it is transferred to intermittent flow dominated by vapor slug. The HTC reached a bottom level at the end of the intermittent flow, which followed by annular flow. Due to the dominance of film evaporation, the HTC starts another positive slop with the reducing in the film thickness. For even higher vapor quality, a decreasing trend is observed again when the thin film is developed to non-evaporating film, or even local dry-out happens.

As the nature of two-phase flow phenomenon and heat transfer mechanisms associated with the flow boiling in microchannels, the promotion in nucleate boiling and thin film evaporation are the main methods to enhance the heat transfer rate. Various techniques were developed to enhance the flow boiling performance through these two ways [22, 25, 40-43]. For example, the nucleate boiling can be promoted by increasing nucleation sites density and extend bubbly flow region through integration of micro/nano-structures [42, 44, 45] or microcavities [46] and the thin film evaporation can be promoted by the micro-structure created on the bottom of channel [31, 47, 48].

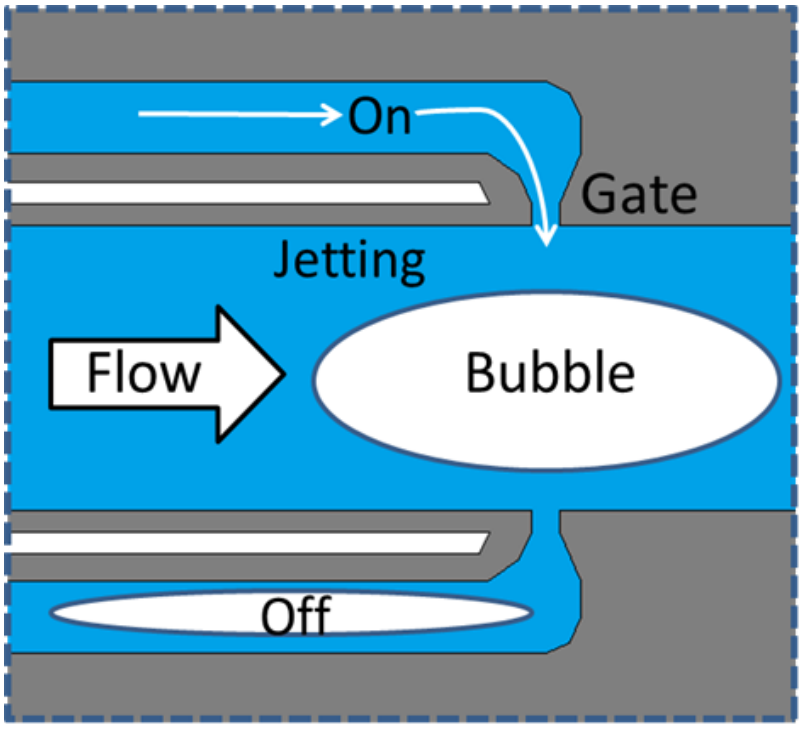

Figure 1.4 Concept of microbubble switched oscillator to modulate bubble growth/collapse in this main channel [49].

Except for the promotion of nucleate boiling and thin film evaporation, the heat transfer rate also can be enhanced by promoting the collapse of the bubble and bubble slug. Recently, a microfluidic transistor with auxiliary channels and micronozzles was developed

to efficiently collapse the bubble slugs. The highly desirable two-phase mixing was achieved by the fast jetting flow generated by the self-sustained two-phase oscillators in our previous [25, 43]. Developed from the two-nozzle microchannel device, a four-nozzle configuration was reported earlier to extend the enhanced mixing to the entire channel [26].

Besides the enhancement on heat transfer rate, the enhancement on CHF is also an important aspect to ensure the safety of electronic devices. Many efforts have also been conducted to increase CHF to enlarge the working margin of high-power density electronics. CHF condition can be triggered by the stable vapor film on the heating surface and may result a sudden increase of temperature and decrease of thermal heat transfer rate [50]. Exceeding CHF may cause permanent damage to both the testing system and device. Explosive boiling, two phase instability and local dry-out are three main factors that can trigger the CHF crisis. In the condition of explosive boiling, the lifetime of the elongated bubble decreases and the bubble grows rapidly, which prevents the rewetting of the heating surface and leads to the premature of CHF [51]. Except for that, two-phase flow instabilities can also result in severe reverse flows, which may result in liquid supply crisis. Compared to conventional cooling systems, it is more challenging to regulate two-phase flows to enhance flow boiling in the microscale cooling devices due to the bubble confinement effect [52]. Various mechanisms such as suppressing flow instability, regulating bubble slugs and enhancing liquid rewetting were developed in the past decades to enhance CHF [43]. Many researchers modify the wettability of the surface of the channel with nano or micro structure to improve flow boiling performance [42, 53]. Nano/microscale coating such as nanowire was proved an important way to enhance nucleation boiling [31, 42, 54, 55] with the unique properties of high nucleate site density,

super hydrophilicity and enhanced capillary effect. Auxiliary channels and micro nozzles were applied to generate intense mixing through jetting flow [25, 26] and enhanced CHF with stable vapor columns in the auxiliary channel [43]. Reentrant cavity [23, 32, 56] and bridged channels [27] were effective methods to enhance both CHF and HTC through promoting liquid rewetting.

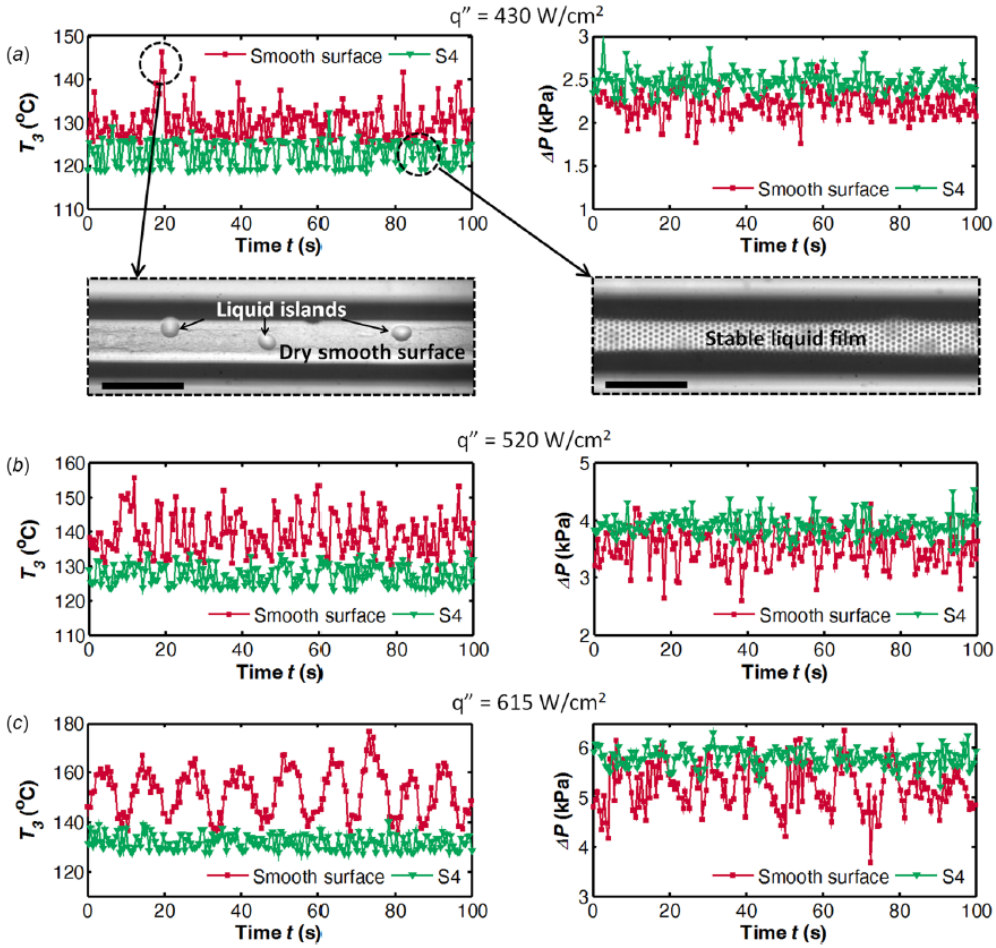

Figure 1.5 Temperature and pressure fluctuation during flow boiling in microchannels with smooth surface and pin fin [47].

Most research on the flow boiling in the microchannel are focused on steady-state study under constant heat flux. In the experimental study of flow boiling under steady-state

conditions, the heat applied to the tested system is increased gradually from zero to CHF and the data was acquired when steady-state condition is reached. The temperature is closely related to the flow pattern and subject to change over time even under steady heat loads. Many researchers studied the temperature fluctuation and the amplitude was reported as high as 40 ^{o}C for the plain-wall microchannel even under steady-state condition [47, 57]. Technics such as micro pin fins and micronozzles were developed to reduce the instability and maintain the temperature at a relative moderate level. However, thermal engineers are faced with further challenges related to the unsteady heat generated by the high-power systems under dynamic working conditions, for example, the startup period. Devices usually work under dynamic working conditions and heat is more likely to be generated instantly. The high temperature changing rate may cause server damage to the cooling system, especially during the startup period. As a result, the transient flow boiling heat transfer must be well understood and comprehensive knowledge is required on this topic. Effective heat dissipation techniques should be developed to efficiently cool the high-power devices under both steady state conditions and dynamic conditions. Nonetheless, there is lack of studies investigating the transient nature of the flow boiling behaviors under dynamic heat loads.

Some researches can be found in the literature on the thermal response of flow boiling under transient heat loads were conducted on a microheater or a single microchannel [58-63]. Their transient processes were initiated by the cold startup, step change heating or pulse heating. For a step change, the heat flux is changed from one value to another and maintained at the later level. A pulse heating implies alternating the heat flux with a constant frequency. Different waveforms such as square and sinusoidal were

applied to study on the thermal response of flow boiling. Temperature response, flow patterns, and boiling incipience time are the main highlights of the transient researches and the effects of mass flux, pulse width and heating frequency were studied [61, 63-65]. The transient temperature field of an integrated thermal microsystem was studied under step-current inputs [62, 66]. It was found that the periodic temperature field can stabilize the tested system and avoid the appearance of the local dry-out. Furthermore, the heating-up time was found decreased with input heat flux, but the cooling-down time did not vary a lot. Another study plotted the various flow regimes: single phase, nucleate boiling, film boiling and dry out, with increasing heat flux under fixed mass flux under high-frequency pulsed heating [61, 67]. Even though the transient temperature profile has been widely investigated, there is still lack of research was conducted to investigate the transient heat transfer rate of the microdevices. Only a few literatures reported in the aspect of heat transfer rate [59, 60, 68], the dynamic behavior of the heat transfer rate and temperature changing rate have not been fundamentally studied.

CHAPTER 2 LITERATURE REVIEW

With the continuous increasing on the demand of the high capability to dissipate large amount of heat, significant improvement is required on the cooling performance of the heat dissipation unit. Extended studies have been conducted to enhance the thermal performances of microchannel devices in terms of HTC, CHF, and flow stabilities regarding temperature fluctuation and pressure drop fluctuations. On the other hand, experimental studies were also conducted to investigate the transient nature of the flow boiling in microchannels under dynamic heat loads. In this dissertation, the literatures review will strongly focus on the enhanced techniques to promote the thermal performance of the flow boiling in microchannels under steady state conditions and the transient thermal behaviors of microchannel devices under transient heat loads, such as heat pulse and step change in heat flux.

2.1 Enhancement of flow boiling in microchannels under constant heat loads

Extensive efforts were made to improve flow boiling performances in terms of heat transfer coefficient [69, 70], critical heat flux [71-74], and stabilization of two-phase flows [56, 75, 76]. Numerous researches proved that flow boiling performances can be significantly enhanced by decorating microstructures or surface modifications in microchannels [22, 23, 25, 26, 77, 78], such as inlet/outlet restrictor, auxiliary channel, and microcavity. On the other hand, to suppress the instability of reversal two-phase flows,

microchannels with inlet restrictors (IRs) were developed. With the improvement of two-phase flow stability, HTC and CHF were enhanced noticeably [77-81].

Theoretical study showed that the HTC can be maintained in a higher range during the bubbly flow and annular flow regimes. Reduced nucleate boiling leads to the poor heat transfer rate during the slug flow stage. In the slug flow regime in micro-scale domains, heat transfer coefficient is affected by the evaporation of the thin liquid film that surrounds the elongated vapor bubbles rather than the nucleate boiling [82]. In the microscale domain, laminar flow is dominant. It is challenging to remove confined bubbles and improve mixing. Recently, microchannels combined auxiliary channels and micronozzles were investigated to address the bubble confinement in microchannels by Yang et al. and Li et al. [25, 26]. The enhanced mixing was achieved owing to the rapid bubble collapse with the effect of jetting flows from micronozzles. Thus, the heat transfer rate was substantially increased.

Besides enhanced mixing, enhanced nucleate boiling is an important factor for the increase of heat transfer rate [69, 83]. The experimental study of Steinke and Kandlikar [84] showed a decreasing trend in two-phase HTC with increasing vapor quality and suggested the dominant role of nucleate boiling in the heat transfer mechanism of flow boiling in the microchannel. Many techniques have been explored to increase the nucleation sites density such as microcavities [22-24], bridged channel [27] and nanowire coating [30]. The third enhancer of HTC is enhanced thin film evaporation, which can be promoted by forming a stable thin liquid film. To achieve this aim, micro pin fin array [28] [29] decorated the bottom surface was studied to enhance thin film evaporation, thus, high HTC is achieved. It was proved that silicon nanowires can significantly improve capillary flow to enhance liquid spreading, thus thin liquid film can be formed [31].

As an important aspect of flow boiling performances, many efforts have also been conducted to increase CHF to enlarge the working margin of high-power density electronics. A sudden huge increase in temperature indicates the occurrence of CHF conditions, resulting in the failure of the cooling device. Explosive boiling, two-phase instabilities including pressure drop, temperature oscillation, and local dry-out are seen as three main factors that can trigger the CHF crisis.

The occurrence of explosive boiling is induced because of the low heat transfer rate at the liquid-solid interface in microchannel [51]. Additionally, various approaches were developed to enhance CHF such as surface modifications [42, 53] to enhance rewetting, IRs [78] to suppress flow instabilities, multiple micronozzles [42, 53] to enhance liquid supply. To prevent local dry-out, reentrant cavity [23, 32, 56] and bridged channels were developed as effective methods to promote rewetting owing to the enhanced capillary effect.

The micro pin fin array that was decorated on the bottom surface of the microchannel is effective to promote the thin film evaporation and HTC and CHF are drastically enhanced [47]. However, the type of fabrication process is complicated. In this study, parallel microgrooves were fabricated on the bottom of microchannels with aims to promote the liquid spreading because of the enhanced capillary flow. Porous and grooved surfaces are effective ways to produce thin films [35]. Microgrooves can effectively promote the formation of the thin film. Also, the larger capillary pressure can sustain the liquid film and enhance the liquid spreading. HTC and CHF are assumed to be enhanced because of enhanced thin film evaporation and enhance liquid rewetting.

2.2 Transient study of flow boiling in microchannels under dynamic heat loads

Different from the research on the steady-state condition of flow boiling in microchannels, quite a few experimental studies on such transient thermal behavior of microchannel evaporators during flow boiling are available in the literature. Most of the related researches can be found are focused on the temperature response and flow patterns.

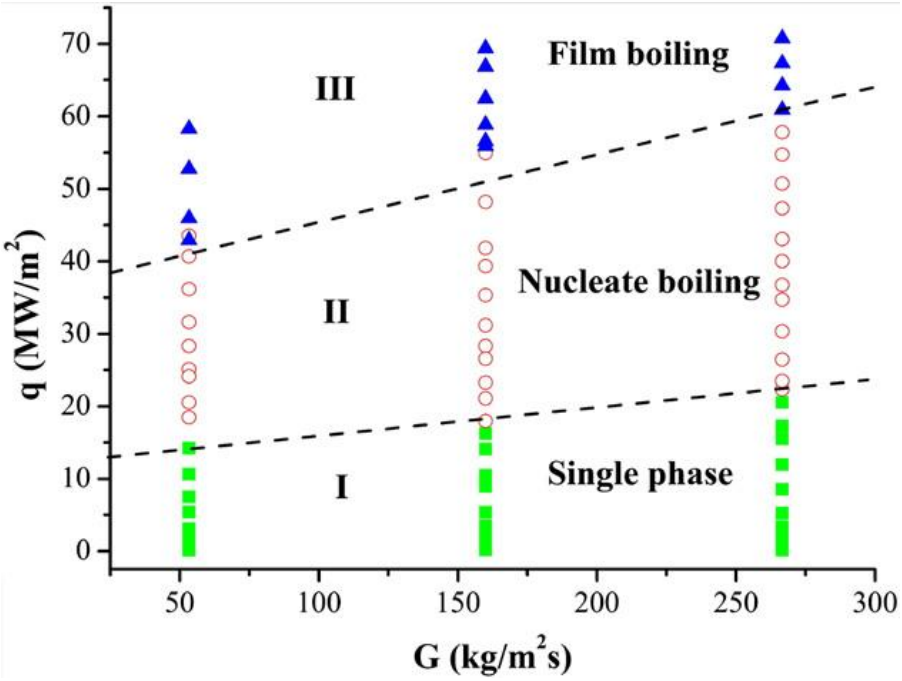

Figure 2.1 Flow boiling map on the microheater under pulse heating [61]

The study of transient flow boiling was mainly focused on the boiling phenomenon under high-frequency heat pulse. Most of the research were limited to bubble dynamic analysis with heating applied to micro-heaters. Chen [61] investigated the flow boiling phenomenon and thermal response on the surface of micro-heater under high-frequency rectangular heat pulse. A map, showing the effects of heat and mass fluxes on nucleate and film boiling on a microheater under pulse heating, was obtained (Figure 2.1). Different

types of nucleate boiling were observed at different mass flux. Film boiling phenomenon was observed at high heat flux at all mass fluxes. It was concluded that boiling inception would start earlier with increasing of heat flux. The effects of pulse width and mass flux were also investigated with pulse width ranging from 50 μs to 2 ms and mass flux ranging from 45 kg/m^{2}s to 225 kg/m^{2}s [67].

Another experimental transient study on pin fin microchannel was developed with R134a as coolant [59]. The heat flux was increased linearly respect to time to keep the wall temperature increasing linearly in the interval of 10 s. The heat transfer coefficient was studied with both steady-state and transient experiments and the transient HTC is higher. It was proved that that pin-fin microchannel heat sink enables to keep an electronic device near uniform temperature under conditions of steady-state and time-varying high heat fluxes. The study of flow boiling on a single was conducted by Basu [58] with HFE 7000 as coolant. The transient heat load was applied in the form of a step change in heat flux and a rectangular pulse. Similar to Chen's studies, the effect of mass flux and heat flux or pulse amplitude were studied. In addition to that, the onsite boiling condition was discussed. A temperature drop or spike were reported at the onsite of the boiling phenomenon and the wall superheat temperature at this point was very high due to low contact angle and high heating rate. The wall superheat at the onset conditions increased with increasing heat flux. The time taken to initiate boiling was studied. It was found that the heat flux affected the time significantly in low heat flux range and less variation was observed in the high heat flux range. Chen [67] also investigated the boiling incipience time with water as working liquid. Similarly, decreased rapidly initially with increasing heat flux but quickly reached a constant value at higher heat fluxes.

A recent published study of the effect of transient power hotspots on flow boiling inside single microscale channels provides more insights on the transient heat transfer rate. The hotspot region undergoes over-sinusoidal, square, and sawtooth heat pulsation at different frequencies and pulse amplitudes. The typical behaviors of HTCs were shown in Figure 2.2. It was found that the maximum HTC was always higher for pulsed heat flux when compared to steady heating and it closely associated with the wall temperature.

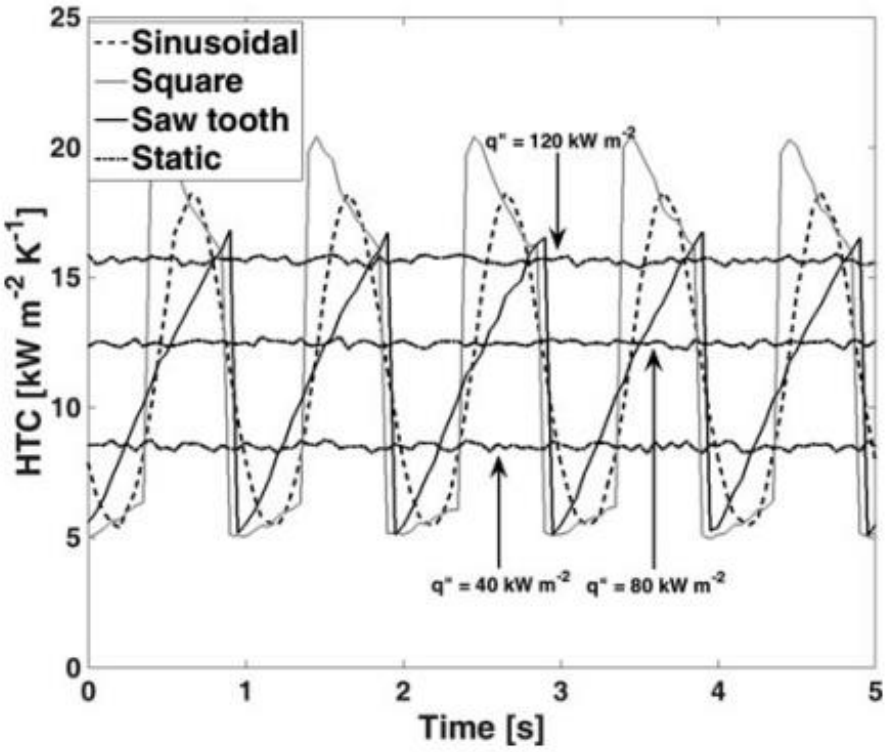

Figure 2.2 Dynamic behaviors of HTC with different waveform types

Except for the study on the single microchannel, an experimental study was also conducted on multi microchannels by Huang [64]. This study includes cold start-up conditions and periodic heating conditions using two different test sections (different inlet orifice) and two coolants (R236fa and R245fa). Experiments were conducted under quite

wide conditions including different mass flux, heat flux or pulse amplitude, inlet subcooling temperature, outlet saturation temperature, and surface roughness. The transient base temperature response was recorded simultaneously with the flow regime to study the flow pattern at different base temperatures. The time required to initiate boiling increases with the inlet orifice width, mass flux, inlet subcooling, outlet saturation temperature, and fluid surface tension, but decreases with the heat pulse amplitude.

Overall, the current literatures provide insights on the temperature responses and flow patterns during flow boiling in a single microchannel. Further investigations on the temperature changing rate and heat transfer rate are required to provide a deep understanding of flow boiling under transient loads.

CHAPTER 3 ENHANCED FLOW BOILING IN THE MICROCHANNEL BY PROMOTING CAPILLARY PRESSURE USING MICROGROOVES

Due to their unfavorable liquid rewetting it is challenging to promote the flow boiling performance, particularly critical heat flux (CHF). Inlet restrictors (IRs) have been successfully used to manage two-phase instabilities in flow boiling microchannels. However, IRs would result in extremely high pressure drop. In this study, without using IRs, 4 parallel microgrooves (W=50 μm, H=250 μm, L=10 mm) are fabricated on the bottom of five parallel microchannels (W=200 μm, H=250 μm, L=10 mm) to effectively manage two-phase flow instabilities without sacrificing pressure drop. Our visualization study shows that these micro-grooves can enable rewetting at a very high frequency and enhance thin film evaporation with a high thin film ratio. A highly desirable periodic rewetting mechanism to substantially delay CHF conditions and enhance heat transfer rates. Flow boiling in the present microchannel configuration has been systematically characterized in mass flux ranging from 100 kg/m^{2}s to 600 kg/m^{2}s. Compared to plain-wall microchannels, flow boiling heat transfer coefficient (HTC) is significantly enhanced due to the sustainable thin film evaporation. Moreover, CHF is also substantially enhanced due to the rapid and periodic rewetting enabled by these decorated microgrooves. We also observed that the enhancement of HTC fades when mass flux exceeds 600 kg/m^{2}s due to flooding.

3.1 Experimental study

3.1.1 Design and fabrication of microdevices

Poor liquid rewetting and liquid supply are the main reasons to trigger premature CHF crisis in plain microchannels. Efforts have been conducted to increase the rewetting capability by decorating silicon nanowires or micro-pillar arrays in channels to enhance the capillary effect [47, 85]. The enhanced capillary effect has a significant effect in promoting the liquid rewetting by altering the surface wettability.

In this study, parallel microgroove ducts on the channel bottom surface are created to increase the liquid spreading along the channel length by enhancing capillary effect compared to plain-wall microchannels. The enhanced capillary pressure induced by the microgrooves would facilitate liquid spreading. Also, the increased capillary effect could favor the formation of thin liquid film on the bottom surface to increase the evaporation. Figure 3.1 shows the tested device to experimentally investigate the flow boiling performances of DI-water. The microdevice consists of five parallel microchannels (W=200 μm, H=250 μm, L=10 mm). Four microgrooves were fabricated on the bottom wall of each microchannel. The dimensions of the microgrooves are width=50 μm, depth=15 μm and length=10 mm.

A micro heater, which was made of a thin aluminum film, was deposited onto the back side of silicon microchannels. The heater area (W=2 mm, L=10 mm) was identical to the total base area of microchannel arrays. It served as a thermistor and the temperature of the heater can be calculated form the electrical resistant. An inlet port, an outlet port, and two pressure ports were fabricated on the microchannel device. The diameter of the ports

is 1mm. The inlet to exit pressure drop was calculated as the pressure difference between the two pressure ports. All the microchannels are independent from each other. A micro-pinfin array was fabrication between the inlet port and the entrance to the parallel microchannels. These micro pin fins can work as a flow stabilizer, which aim to form uniform liquid flow. To minimize heat loss, two thermal isolation gaps (air gaps) were created on both sides of microchannel arrays. A Pyrex glass wafer was anodically bonded to the silicon substrate to seal the device. The transparent glass cover enables the visualization of the flow patterns in the microchannels.

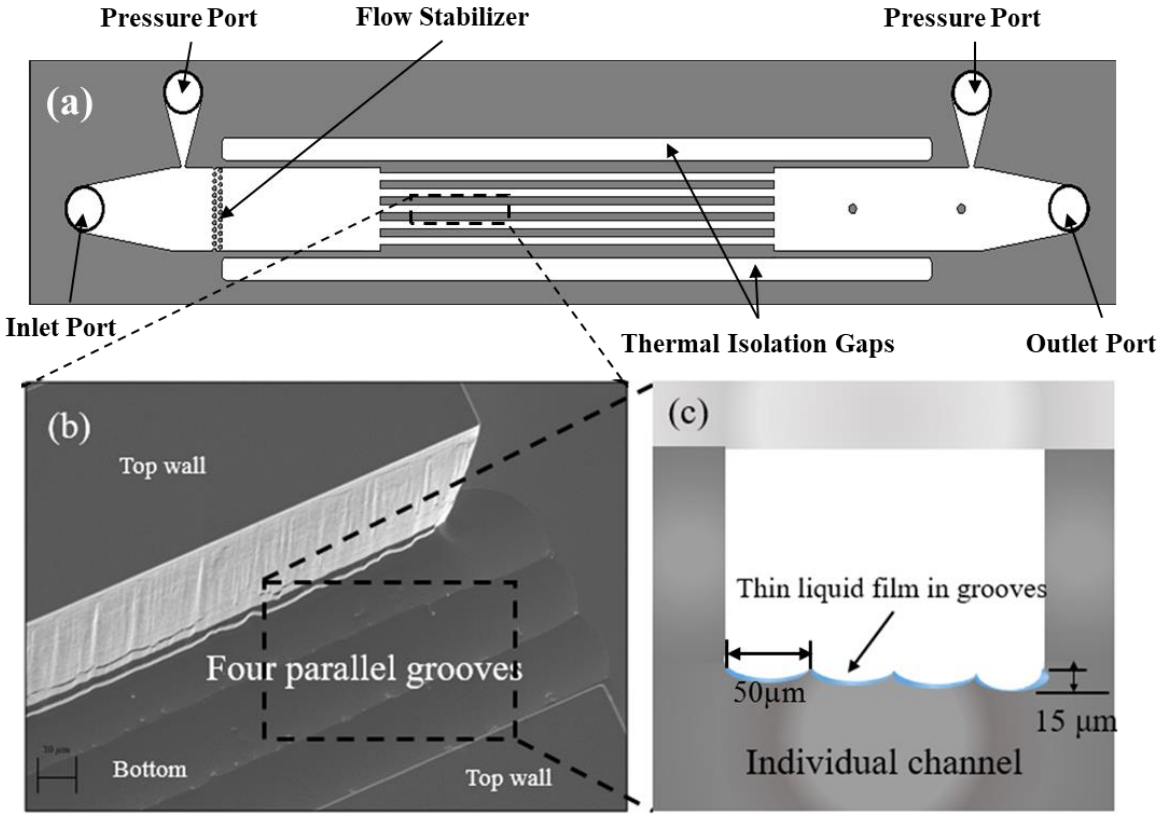

Figure 3.1 The microchannels integrated microgrooves on the bottom surface (a) Geometric configuration of the working zone of the tested device, including five parallel plain-wall microchannels. (b) SEM of the individual microchannel. (c) Schematic of the thin liquid film in the microgrooves.

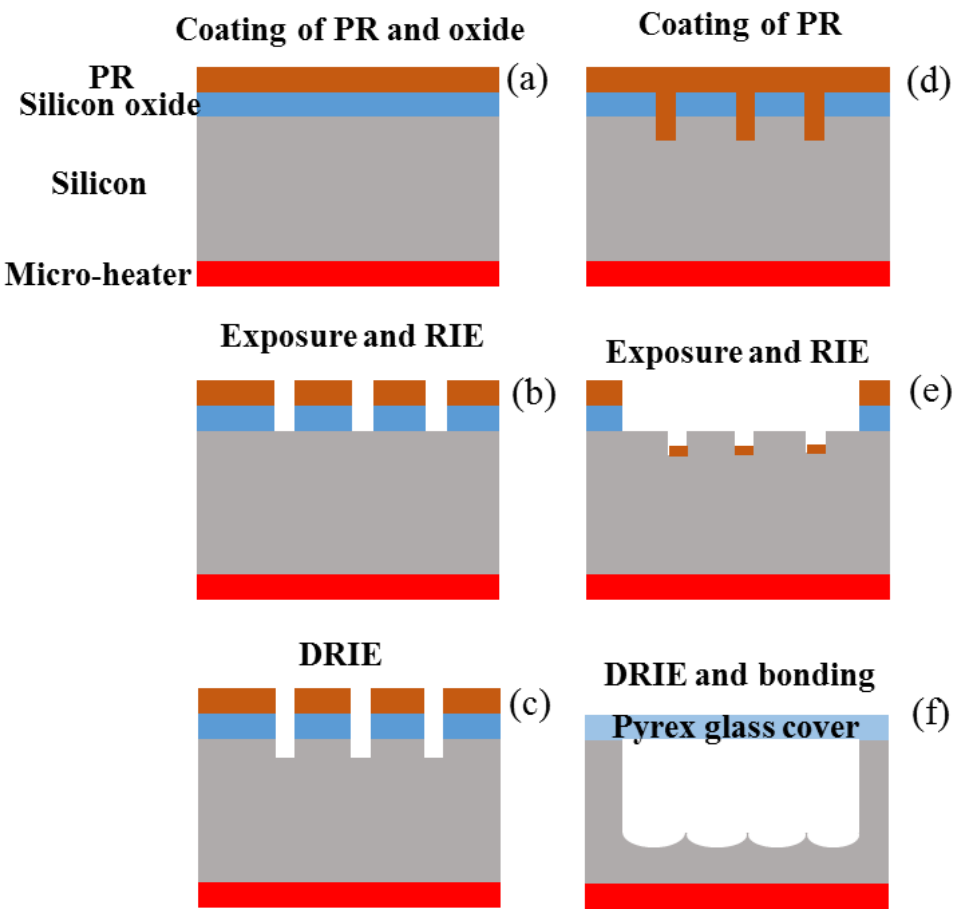

Figure 3.2 Main steps of the microfabrication process of the tested microdevice.

Before etching processes on the topside of the chip, a thin metal film resistor (10 mm × 2 mm) made of 1 μm thick of aluminum was deposited on the backside of the chip to generate uniform constant heat flux. Micro-resistor also serves as a thermistor to measure the average temperature of the heater. The silicon oxide film provides electrical insulation for the micro heater and serves as an etching mask. Silicon oxide was etched off by reactive ion etching (RIE) and the five parallel microchannels ad four microgrooves in each microchannel were etched by deep reactive ion etching (DRIE). After etching processes, anodic bonding was applied to bond a 500 μm thick Pyrex glass wafer to a 500

μm thick silicon wafer substrate. Visualization study can be carried out through the glass window as well. The individual microchannel device (W=10 mm, t=1 mm, L=30mm) was cut from the wafer by a dice–saw. Figure 3.2 has illustrated the main steps of the microfabrication process of the tested microdevice.

3.1.2 Experimental setup and procedure

The present study utilizes exactly the same setup (Figure 3.3) as our previous study [25].

Figure 3.4 shows how the microchannel device was assembled at the test package module, which provided hydraulic ports and connected to power supplies. Mechanical fasten unit consists of two fasten bolts and two holding clamps and is used to locate and fasten the microchannel devices. The tested devices were supported at two ends and the middle part was suspended on two heating probe fins. The probe fins connected to the power supply were pressed on the heater, two bolts were used to adjust the heights of the probe-pins. The connection of the heating probe fins and the heater was carefully adjusted to minimize contact resistance. Also, this packaging was carefully designed to minimize the stresses on the heater and to reduce heat loss. Six micro o-rings were placed between the silicon tested device and the holding clamps to achieve mechanical seals and balance the stress on the tested device. Two pressure transducers were connected to the pressure ports to measure pressure drops.

Prior to the test, the heater, which also works as a thermistor, is calibrated with a proportional-integral-derivative controller in the isothermal oven to estimate the correlation between the temperature and thermal resistance of the heater. Meanwhile, the

heat loss from the system to the surrounding is evaluated as a function of the temperature difference between the heat exchanger temperature and ambient temperature. The heater temperature was plotted as a function of input heat flux without working liquid flow through the test system. The correlation of the input heat flux and temperature difference was linear fitted. Therefore, the heat loss at different heater temperature can be estimated with the correlation. Both the heater temperature and heat loss are evaluated with high accuracy. The pressurized DI water tank was degassed with heat supply to maintain the water temperature to 40 ^{o}C prior to the test. With the pumping power of compressed nitrogen and a flow meter of Krohne Optimass 3300c with a ± 0.1% resolution (density with ± 2 kg/m^3), the DI water flowed through the system at a constant mass flow rate. Inlet/outlet pressure and temperature were measured with pressure transducers and K-type thermocouples respectively. The average temperature of the heater was calculated with the correlation obtained with calibration prior to the test. A high precision digital programmable power supply (BK-PRECISION XLN10014) was used to supply electrical power. The voltage applied to the microheater was measured by an Agilent digital multimeter (34972A). Flow rate, local pressure, inlet, and outlet temperature, and voltage and current were recorded by a customized data acquisition system developed from NI LabVIEW®. A visualization system comprised of a high-speed camera (Phantom V 7.3) and an Olympus microscope (BX-51) with 400× amplifications were used to study the two-phase flow patterns. All measurements were carried out at 1 atm ambient pressure and room temperature of ~18 °C and all data were collected by an Agilent 34972A data acquisition system.

The system was heated from ambient temperature and data was collected with step of 5°C on wall temperature before boiling and 5 W/cm^2 on effective heat flux after boiling was initiated. After the steady-state condition was reached, 90 data points (current, voltage, local pressure and temperature at inlet and outlet) were collected with frequency of 0.67 Hz to obtain the average parameters. The experiments were conducted with mass flux of 100 kg/m^{2}s, 210 kg/m^{2}s, 303 kg/m^{2}s, 346 kg/m^{2}s, 389 kg/m^{2}s, and 600 kg/m^{2}s.

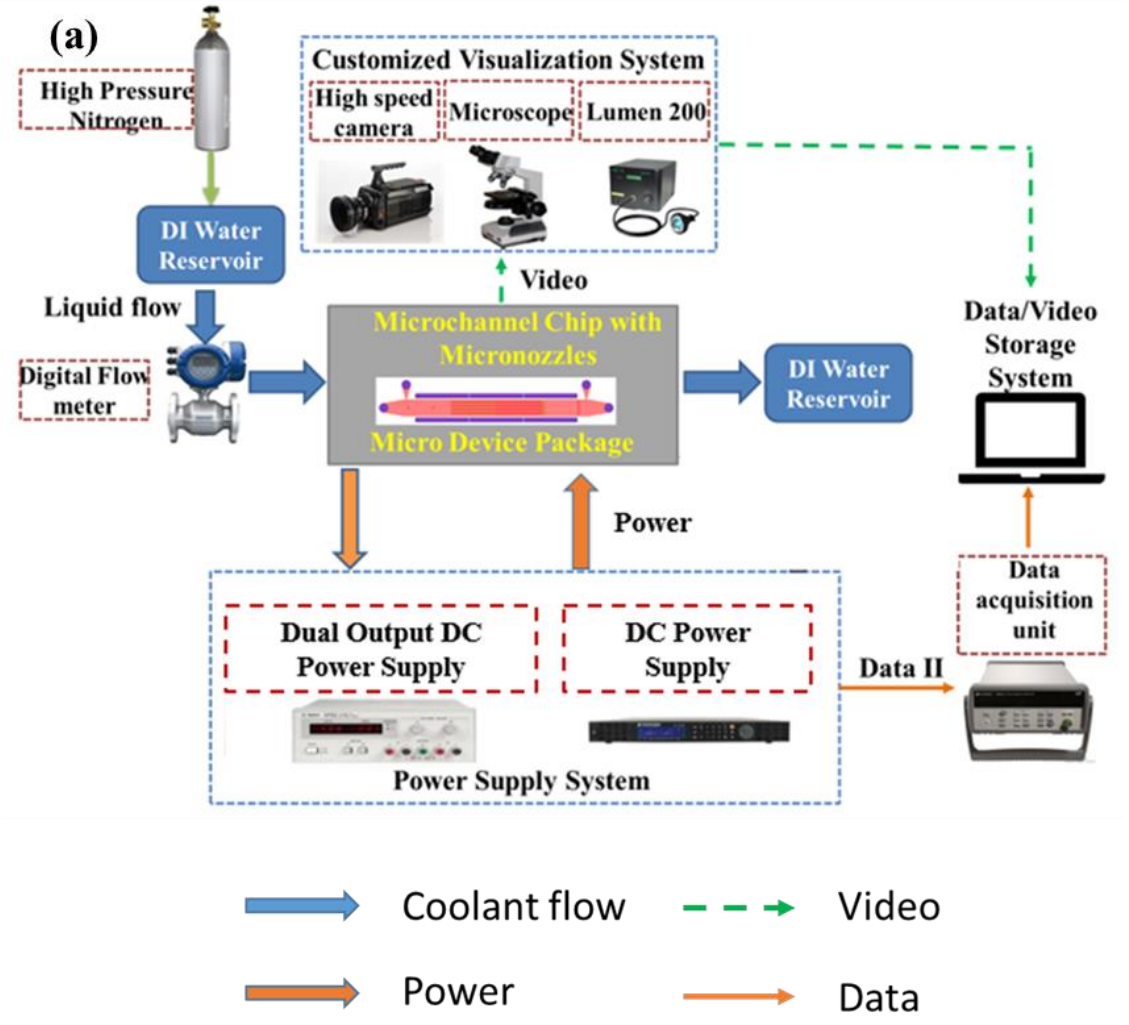

Figure 3.3 Test setup: Experimental procedure

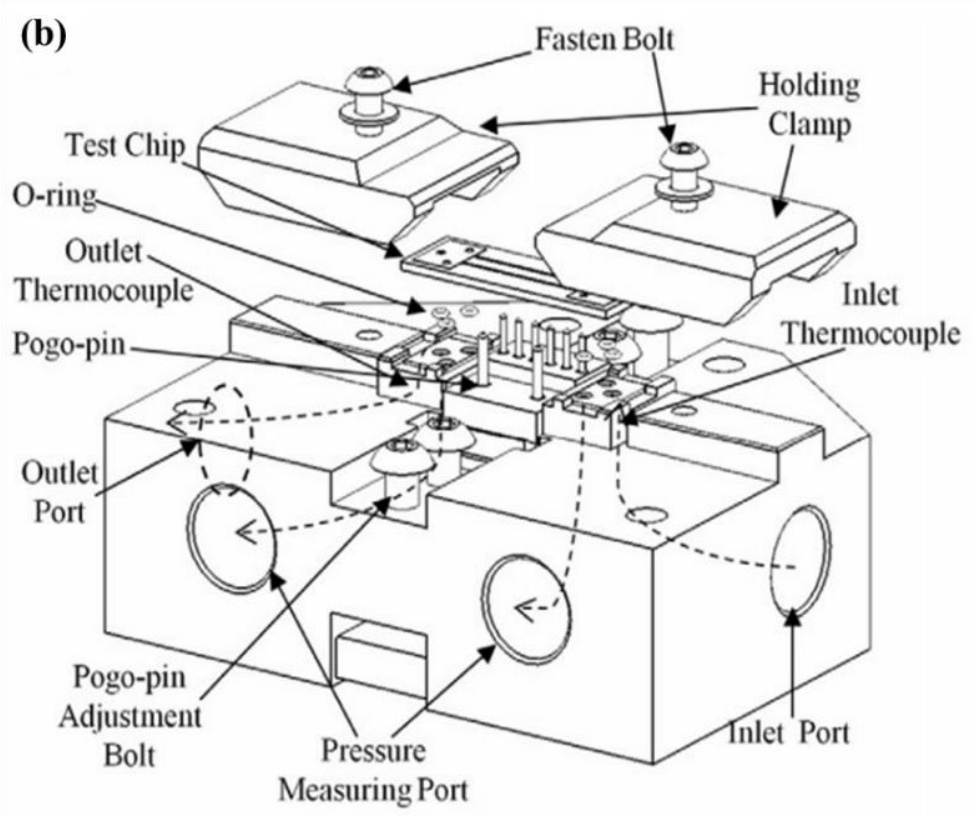

Figure 3.4 Test setup: An exploded 3D model of the test package module

3.1.3 Data reduction

Before the test procedure calibration is conducted to predict the correlation between temperature and resistance of the thermistor. The average temperature of the heater can be calculated as:

$$\bar{T}_{heater} = k(R - R_0) + T_0 \quad (1)$$

Where k is the slope of the heater temperature vs electrical resistance curve, the correlations were fitted from calibration data. R_0 is the electrical resistance at room temperature and T_0 is the room temperature. The resistance of the heater R is calculated from the input voltage (V) and current (I).

$$R = \frac{V}{I} \tag{2}$$

The input power is:

$$P = V \times I \tag{3}$$

The effective heat input is calculated by deducting heating loss to the surrounding from the original heat input:

$$P_{eff} = P - P_{loss} \tag{4}$$

The heat transferring of the heater and the bottom of the microchannel is considered as pure conduction and the average temperature of this surface is computed as:

$$\bar{T}_{wall} = \bar{T}_{heater} - \frac{q''_{eff} t}{k_s} \tag{5}$$

Where q''_{eff} is the effective heat flux and can be calculated as

$$q''_{eff} = \frac{P_{eff}}{A_b} \tag{6}$$

The two-phase effective heat transfer coefficient is calculated as:

$$\bar{h}_{tp} = \frac{P_{latent}}{(\sum(WL + 2HL\eta_f))(T_{wall} - T_{sat})} \tag{7}$$

Where P_{latent} is latent heat which is calculated as:

$$P_{latent} = P_{eff} - \dot{m}C_p(T_{out} - T_{in}) \tag{8}$$

η_f is the fin efficiency:

$$\eta_f = \frac{\tanh(mH)}{mH} \tag{9}$$

$$m = \sqrt{2\bar{h}_{tp}(L + W_f)/k_s W_f L} \tag{10}$$

The thermal conductivity of Pyrex glass is relatively small (approximately 1%) compare to that of silicon, the interface between the microchannel wall and the cover glass is assumed to be thermal insulated in the fin approximation.

The exit vapor quality is computed as:

$$\chi = \frac{P_{latent}}{\dot{m}h_{fg}} \tag{11}$$

In addition to that, the overall heat transfer coefficient is calculated as:

$$\bar{h} = \frac{P_{eff}}{A_b(\overline{T}_{wall} - T_{sat})} \tag{12}$$

Capillary pressure is calculated as

$$P_{cap} = \frac{2\sigma cos\theta}{R_h} \tag{13}$$

Where σ is the surface tension of the working fluid, θ is the contact angle and R_h is the hydraulic radius.

Wetted ratio and thin film ratio are calculated as

$$\eta_{wet} = \frac{\tau_{wet}}{\tau} \tag{14}$$

$$\eta_{tf} = \frac{\tau_{tf}}{\tau} \tag{15}$$

Where τ_{wet} is the duration of wetting, τ_{tf} is the duration of thin liquid film and τ is the total time of one period of dry-out and rewetting process.

3.1.4 Uncertainty analysis

The measurement uncertainties of flow rate, pressure, voltage, current, ambient temperature, wall temperature, and microfabrication resolution are ±1%, ±1.5%, ±0.5%, ±0.5%, ±1 °C, ±1%, and 3 μm, respectively [74]. Uncertainty propagations are calculated using methods developed by S. J. Kline and F. A. McClintock [86]. Uncertainties of the effective heat flux and overall HTC have been estimated to be less than ±3 W/cm^2 and ±2.4 kW/m^{2}k, respectively.

3.2 Results and discussion

3.2.1 Thermal performance of the present design

Figure 3.5 shows the average wall temperature as a function of effective heat flux with mass fluxes in the range of 100 kg/m^{2}s to 600 kg/m^{2}s. The wall temperatures rise sharply in the single-phase region then tends to be flat after the onset of nucleate boiling (ONB). The superheats at ONB are 5-8 °C and slightly increase with mass flux. Figure 3.6 depicts the overall HTCs calculated based on the area of heating as a function of effective heat flux and exit vapor quality for mass fluxes ranging from 100 kg/m^{2}s to 346 kg/m^{2}s. With the increase of effective heat flux, the overall HTCs decrease sharply in the early boiling stage, when nucleate boiling dominated the boiling mechanisms, and then become flat during the fully-developed boiling region, where convective boiling dominated. The

trends of boiling curves agree with previous studies [25, 36, 87]. Figure 3.6 also indicates that HTCs are closely related to mass fluxes, higher mass flux leads to higher HTC in the same working loads. The increased convection owing to a higher flow rate should be the main reason for the higher HTCs. As shown in Figure 3.6 (b), an exit vapor quality of 0.48 is achieved at the low flow rate of 100 kg/m^{2}s. The early dry-out near the outlet section may result in a small exit vapor quality.

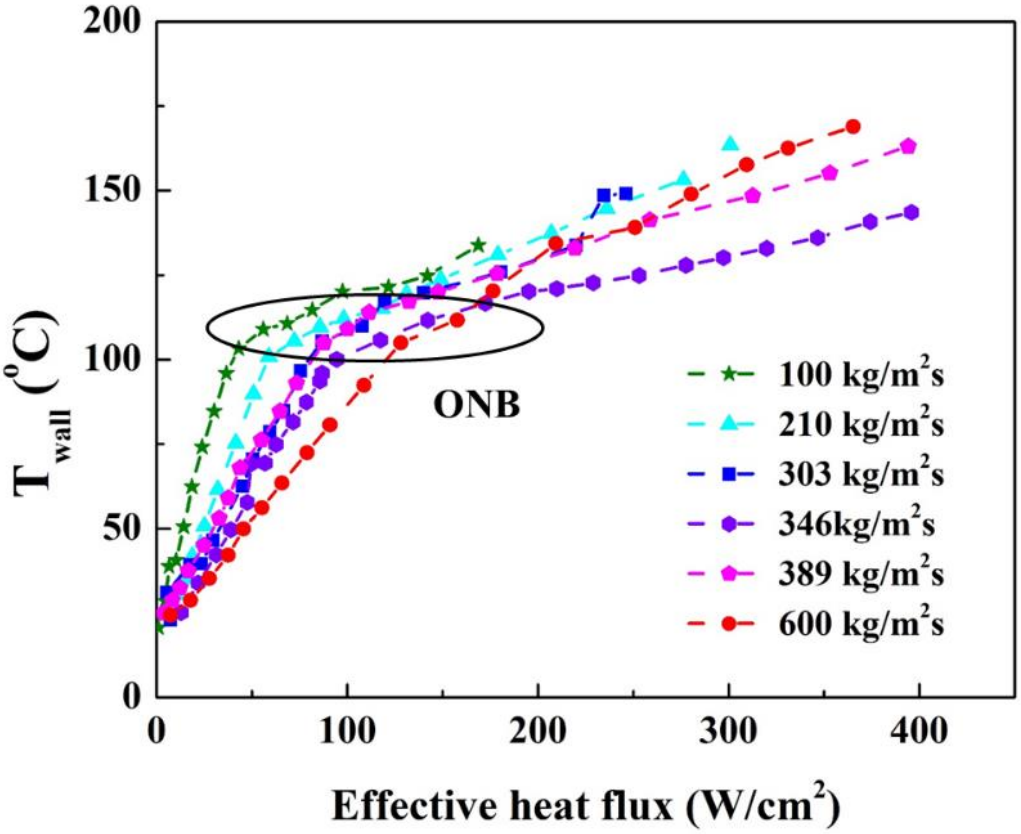

Figure 3.5 Average wall temperature as a function of effective heat flux

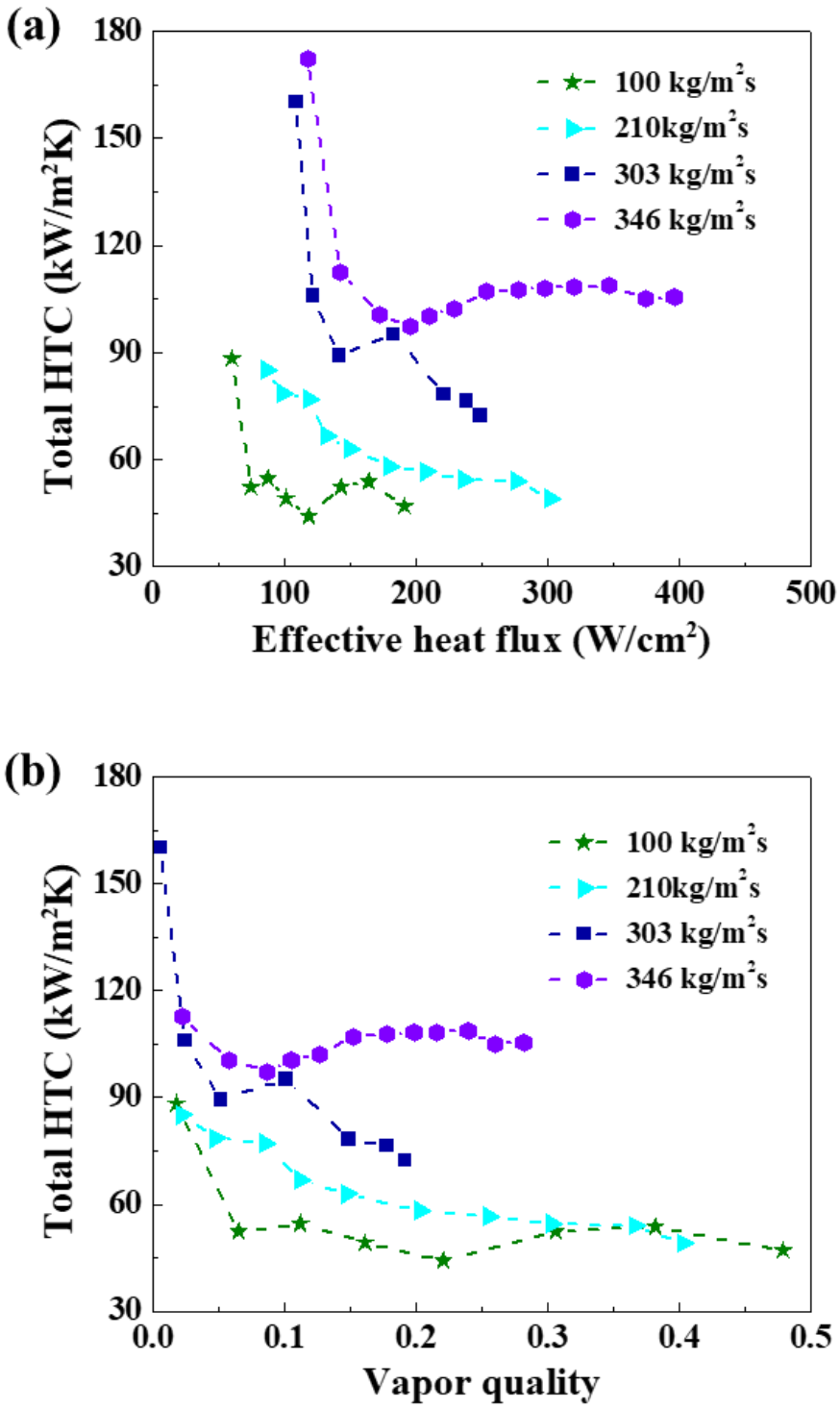

Figure 3.6 Overall HTC as a function of (a) effective heat flux (b) exit vapor quality.

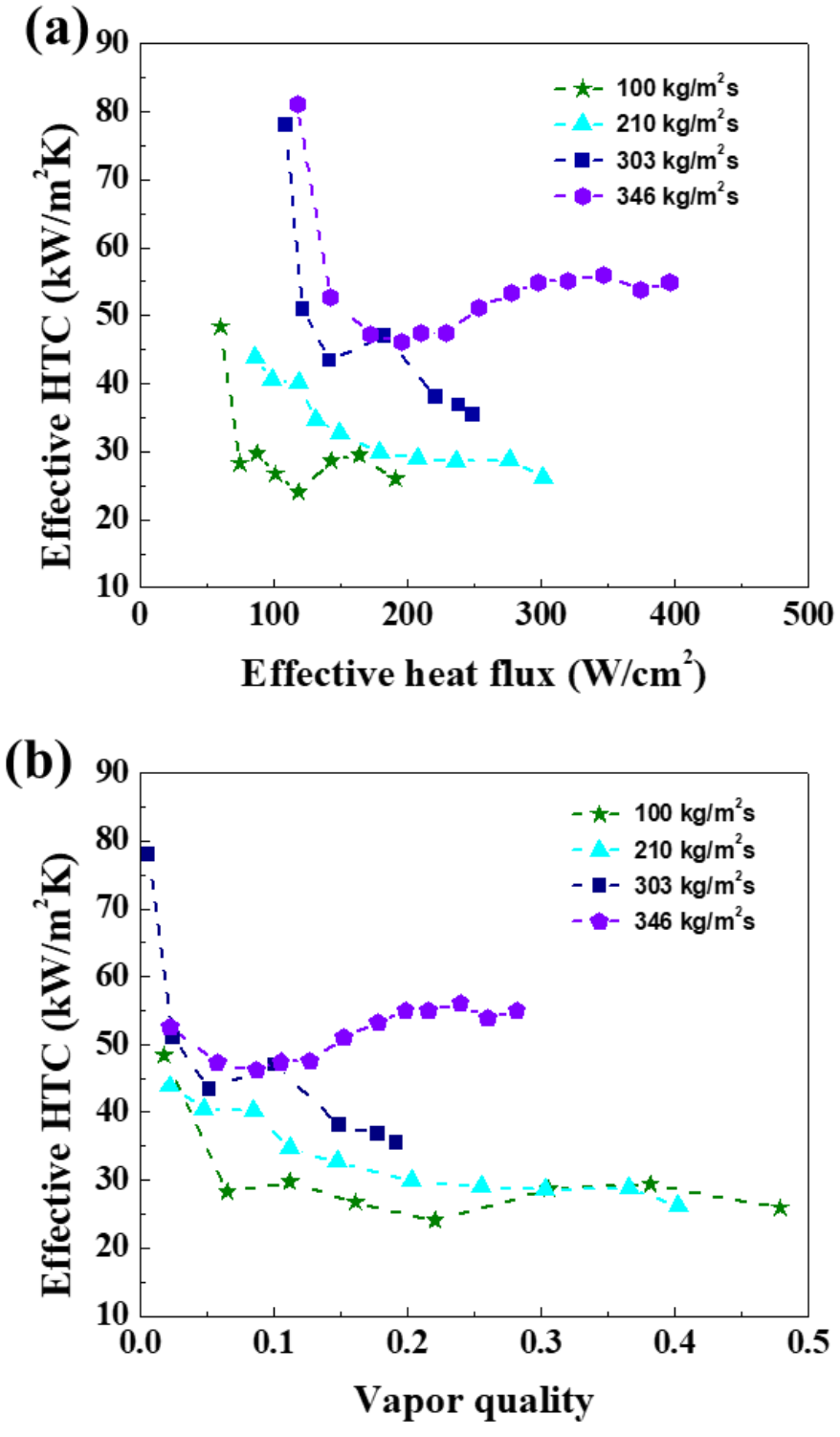

Figure 3.7 Effective HTC as a function of (a) effective heat flux (b) Exit vapor quality.

To better illustrate the heat transfer performance of the present design, Figure 3.7 shows the effective HTCs considering the fin effect in the calculation. Besides, the effective HTC excluded the sensible heat used for the temperature change of the liquid, which means it only considered the heat contributed to phase change. The effective HTCs vary from 20 kW/m^2K to 81 kW/m^2K for the mass flux ranging from 100 kg/m^2s to 346 kg/m^2s in this study. Similarly, the effective HTCs achieve highest value in the bubbly flow regime, where nucleate boiling dominant region and then decrease to a moderate value in the fully developed boiling region, where thin film evaporation is the main flow boiling mechanism. Particularly, during the thin film evaporation dominate period, the HTCs slightly increase with reducing thin film thickness then decrease due to the gradual local dry-out before CHF [7].

3.2.2 Enhanced flow boiling

Figure 3.8 shows the effective HTCs by considering all the heat transfer area are significantly enhanced on the present design compared to a plain-wall configuration. Enhancements of HTC around 72% and 51% have been achieved at a mass flux of 100 kg/m^2s and 210 kg/m^2s, respectively. The enhancement increases with the increase in mass flux during the fully developed boiling region. Also, the HTCs curve of plain-wall microchannels fluctuates at a low mass flux of 100 kg/m^2s, indicating the serious instabilities. Additionally, the exit vapor quality of the present design is about seven-fold higher than that of plain-wall configuration at a mass flux of 210 kg/m^2s owing to increased thin film evaporation. At the same exit vapor quality, the HTCs of the present design are enhanced by about 24 % and 57%, respectively. Enhanced thin film evaporation has been identified by decorating silicon nanowires or micro-pillar arrays in channels [47, 85].

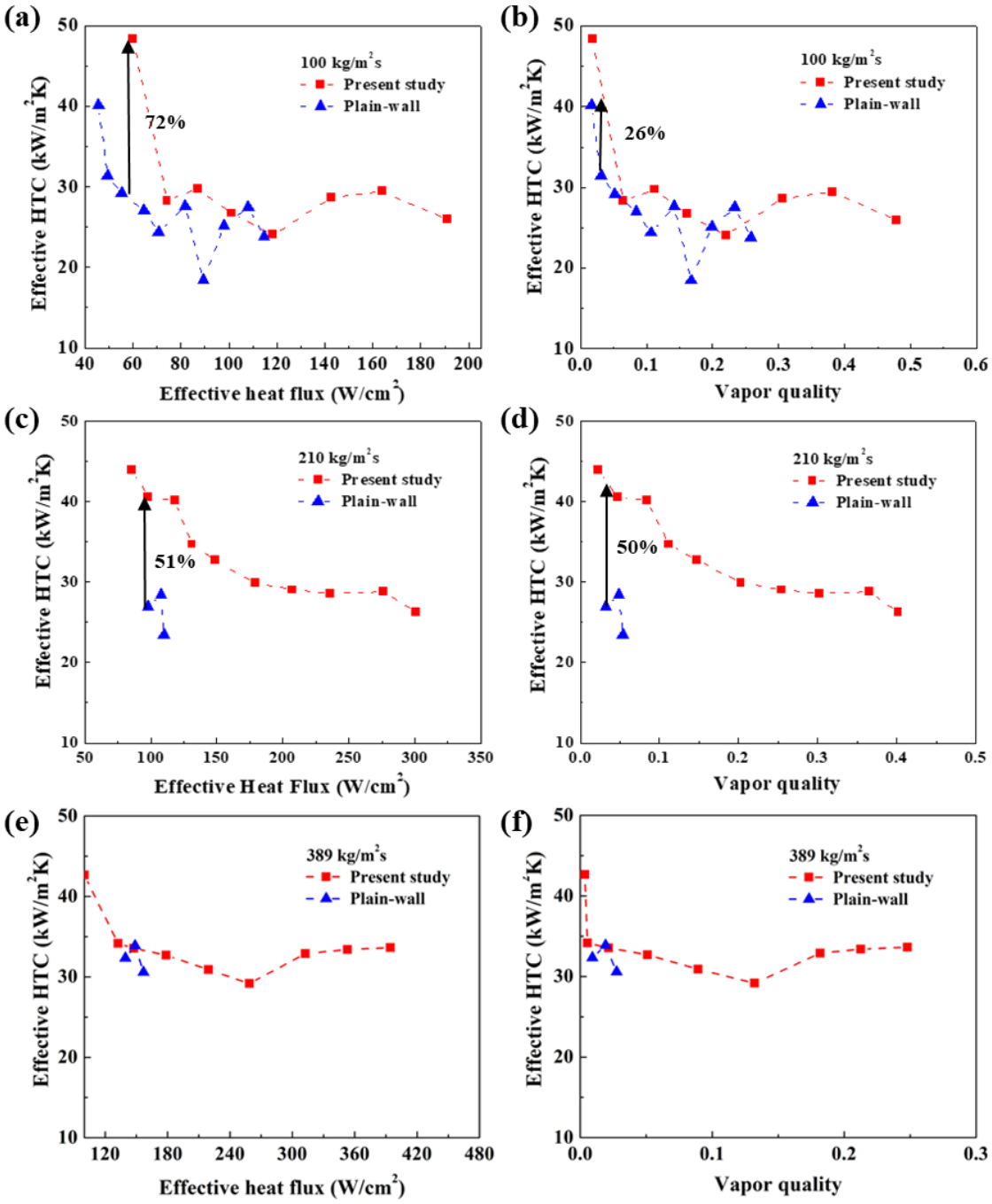

Figure 3.8 Effective HTCs by considering all heat transfer areas vary with the effective heat flux and exit vapor quality at the mass flux of 100 kg/m^{2}s, 210 kg/m^{2}s, and 389 kg/m^{2}s, respectively.

Similarly, microgrooves can increase the thin film evaporation through promoting capillary pressure on the bottom surface, leading to enhanced HTCs. Moreover, the plain-wall microchannel can only work under a small range of heat flux due to severe two-phase instabilities, which exacerbates at high mass flux. However, at high mass flux, more liquid was driven to the hotspot by the additional capillary force and form thick liquid film. In comparison, the liquid film in the plain-wall microchannel was relative thin. This leaded to reduced enhancement, as it was shown in Figure 3.8 (e) and (f).

3.2.2.1 Nucleate boiling phenomenon

Nucleate boiling has been observed in this study. Figure 3.9 (a) shows the nucleate boiling phenomenon after ONB near the inlet section at a mass flux of 600 kg/m^{2}s and a heat flux of 100 W/cm^2. The active nucleation sites density was calculated by dividing the number of the sites that can generate bubbles in a certain area by the area. It is estimated at 9333 sites/cm^2 in the micro-grooved microchannel compared to 4285 sites/cm^2 in the plain-wall microchannel under similar working conditions. The bubbles nucleate from the middle section, grow up, merge as a large bubble then departure from the wall and flow downstream. With the expand of the bubble near the outlet section, the formation of vapor slug is observed because of bubbles coalesce, as shown in Figure 3.9 (b). The vapor slug firstly expands to the flow coming direction and then collapses due to direct condensation on vapor slug interface. The collapse frequency is measured at ~54 Hz.

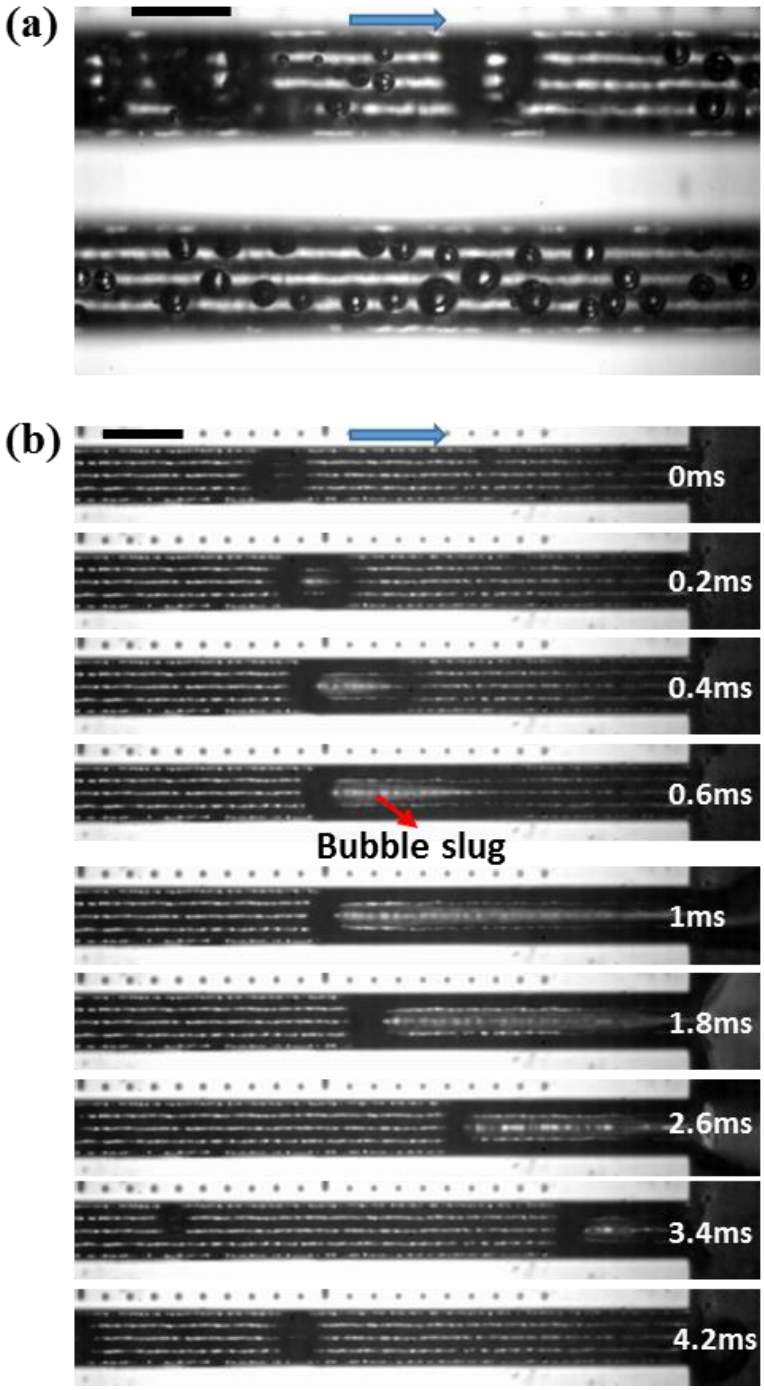

Figure 3.9 Nucleate boing the microchannels with microgrooves. (a) Nucleate boiling in the middle section at a mass flux of 600 kg/m^{2}s and a heat flux of 100 W/cm^2 (Scale bar is 200 μm) (b) Vapor slug near the outlet section (Scale bar is 300 μm)

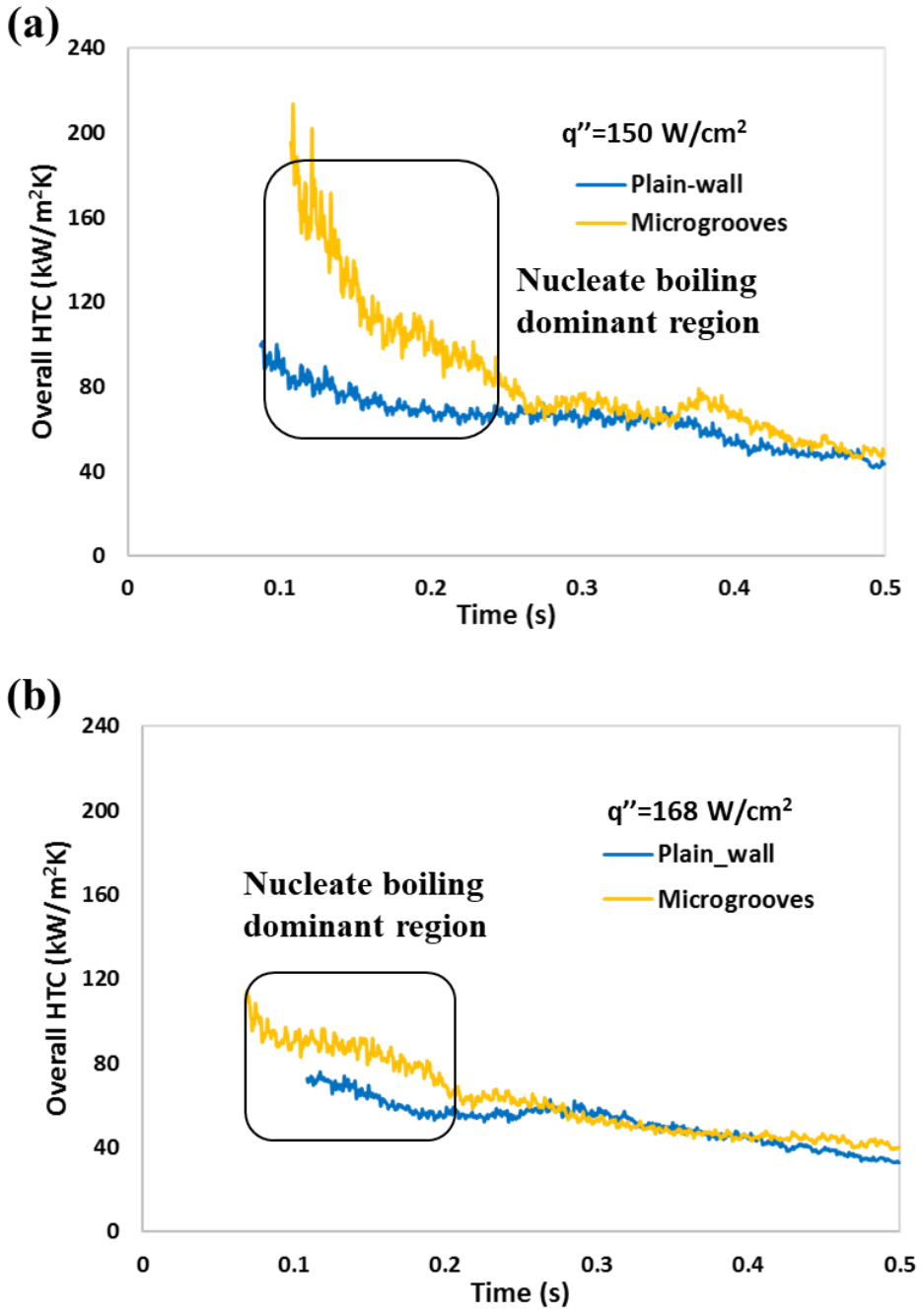

Figure 3.10 Enhancement of nucleate boiling in the transient study under heat pulse. (a) q''=150 W/cm^2, (b) q''=168 W/cm^2 (G=389 kg/m^{2}s)

For the experiments under constant heat flux, the heat was increased manually, and data was captured with certain heat flux intervals, so we cannot guarantee to capture the whole nucleation boiling stage. To further investigate the enhancement of the present

configuration in nucleate boiling, Figure 3.10 shows the comparison of the performance the present design and plain-wall microchannels under a transient condition. Square heat pulse with heating frequency of 1 Hz and heating duty of 50% was applied to both the tested systems. Transient data was collected when the systems reached relative steady state condition, which means the initial temperature did not change with time. The flow was in single phase before heating and the flow boiling was gradually developed under sudden application of heat loads, we can capture the whole boiling process, which make it possible to show the enhancements with different flow regimes. As it is indicated by Figure 3.10, the HTC is significantly higher in the early boiling stage, where nucleate boiling dominates. Clearly, the present design can improve the nucleate boiling dramatically. Also, the thin film evaporation was also slightly enhanced. This is consistent with the data reported in Figure 3.8.

3.2.2.2 Enhanced thin film evaporation

Thin film evaporation plays an important role in the heat transfer mechanism of flow boiling. More than 50% of the overall heat transfer and 90% of the interfacial temperature drop happen in the thin film region [35]. Heat transfer rate increases with gradual thinning of liquid film [7], which means the HTC can be enhanced by reducing the thin film thickness. With the present design, the formation of thin liquid film is supposed to be significantly enhanced owing to the increased capillary effect on the bottom of microchannels decorated with microgrooves.

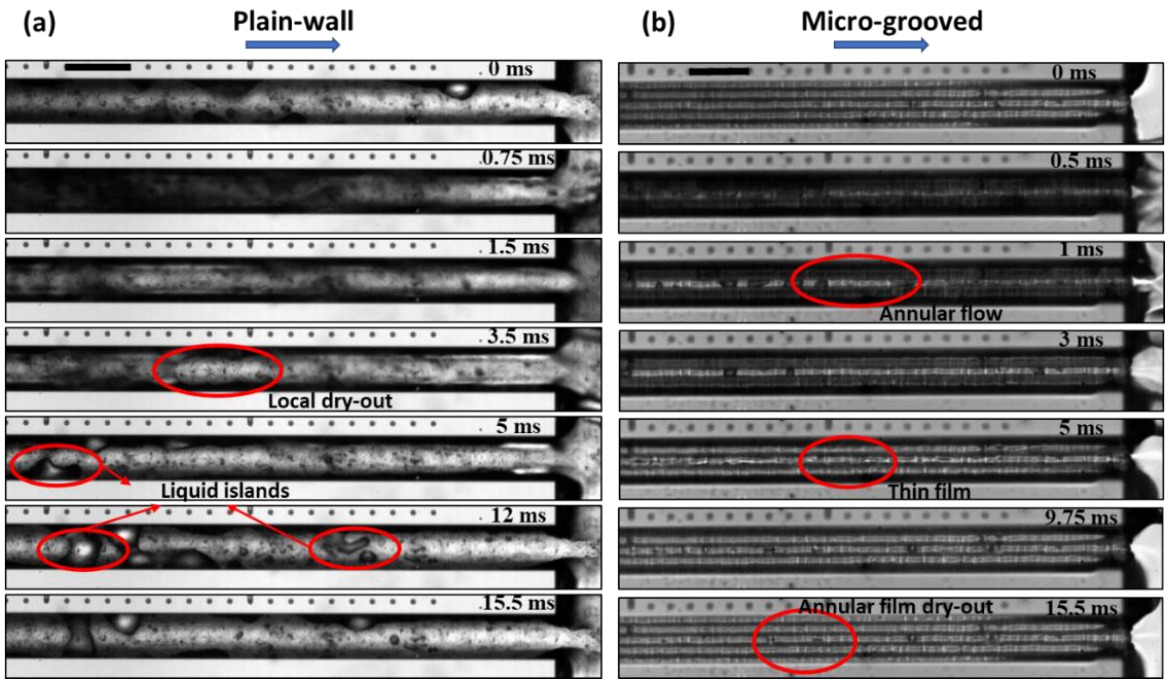

Figure 3.11 Evolution of thin liquid film in (a) plain-wall microchannels and (b) in the present design at a mass flux of 210 kg/m^{2}s and a heat flux of 104 W/cm^2. (Scale bars are 300 μm)

Figure 3.11 illustrates the evolution of thin film in plain-wall and microgroove microchannels. It suggests that the thin liquid film in the present design lasts nearly 5 times longer than that in plain-wall microchannels (i.e., 13.5 ms compared to 2.75ms), the maximum thin film region is also 30% larger. Once the channel is rewetted, thin liquid film is quickly formed. The enhanced capillary effect induced by the parallel microgrooves can increase the liquid spreading along the channel length, which significantly extends the thin film region and enhances thin film evaporation. By contrast, in plain-wall microchannels, local dry-out occurs near the outlet instantly after the channel is rewetted while thick liquid film still exists in upstream. As it is shown in Figure 3.12 (a), large dry surfaces appear from 3.5 ms. What is more, lots of liquid islands were observed in plain-wall microchannels from 5 ms due to the inability to spread liquid along the channel length, which decreases

the heat transfer rate. Also, hot spots may be induced due to lack of timely liquid rewetting. The significant enhancement of thin film evaporation is critical to heat transfer performance [34, 48]. Enhanced heat transfer performance by promoting thin film evaporation was reported by Zhu et al. [47] and Yang et al. [31].

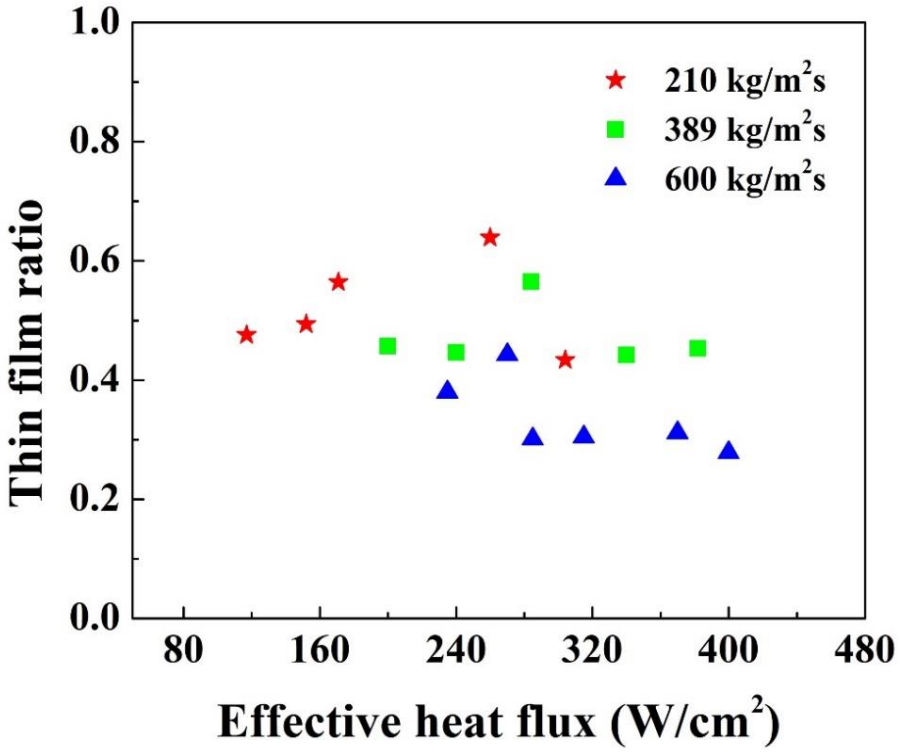

Figure 3.12 Comparison of thin film ratio at different working conditions.

To further evaluate the effect of present design in thin film evaporation, the thin film ratio was calculated based on the ratio that the thin film duration to the rewetting period. It indicates the ability of the structure to maintain the thin liquid film in the microchannel. The liquid film is considered as thin film when the edge of the microgroove is exposed from the liquid. Figure 3.12 (a) shows the plot of thin film ratio versus effective heat flux. The highest thin film ratio reached is 0.65 at a mass flux of 210 kg/m^{2}s. However,

we cannot observe regular thin films in the plain-wall microchannels. Liquid islands are formed instead of thin film as it was presented in Figure 3.11 (a). The relatively high thin film ratio indicates more sustainable thin liquid film. This would lead to enhanced HTC as illustrated in Figure 3.8. Furthermore, the thin film ratio decreases with the increase of mass flux, which suggests reduced heat transfer rate with mass flux increasing in the high mass flux range.

3.2.3 Deteriorated HTCs due to liquid flooding

As discussed in the previous section that at the same heat flux, HTCs increase with mass flux in the range of 100-346 kg/m2s. However, when the mass fluxes exceed the range, an inverse trend is observed.

Figure 3.13 shows the HTCs decrease with the increase of mass flux. The flooding should be the primary cause that interrupts the formation of thin liquid film and hence, leads to deteriorated HTC. Figure 3.14 compares the rewetting process at the mass flux of 303 kg/m2s and 600 kg/m2s. As shown in Figure 3.14(a), the formation of thin liquid film in the microchannel is observed at mass flux of 303 kg/m2s. In contrast, thin liquid film area is much smaller at mass flux of 600 kg/m2s, the duration of thin film is also shorter. Most of the time, the microchannel is occupied by thick liquid film. This is consistent with the trend of thin film ratio plotted in Figure 3.12. The thick liquid film would lead to large thermal resistance, decreasing the heat transfer rate. Furthermore, due to large thick liquid film areas, the present structure does not show obvious enhancement compared to the plain-wall microchannel at high mass flux.

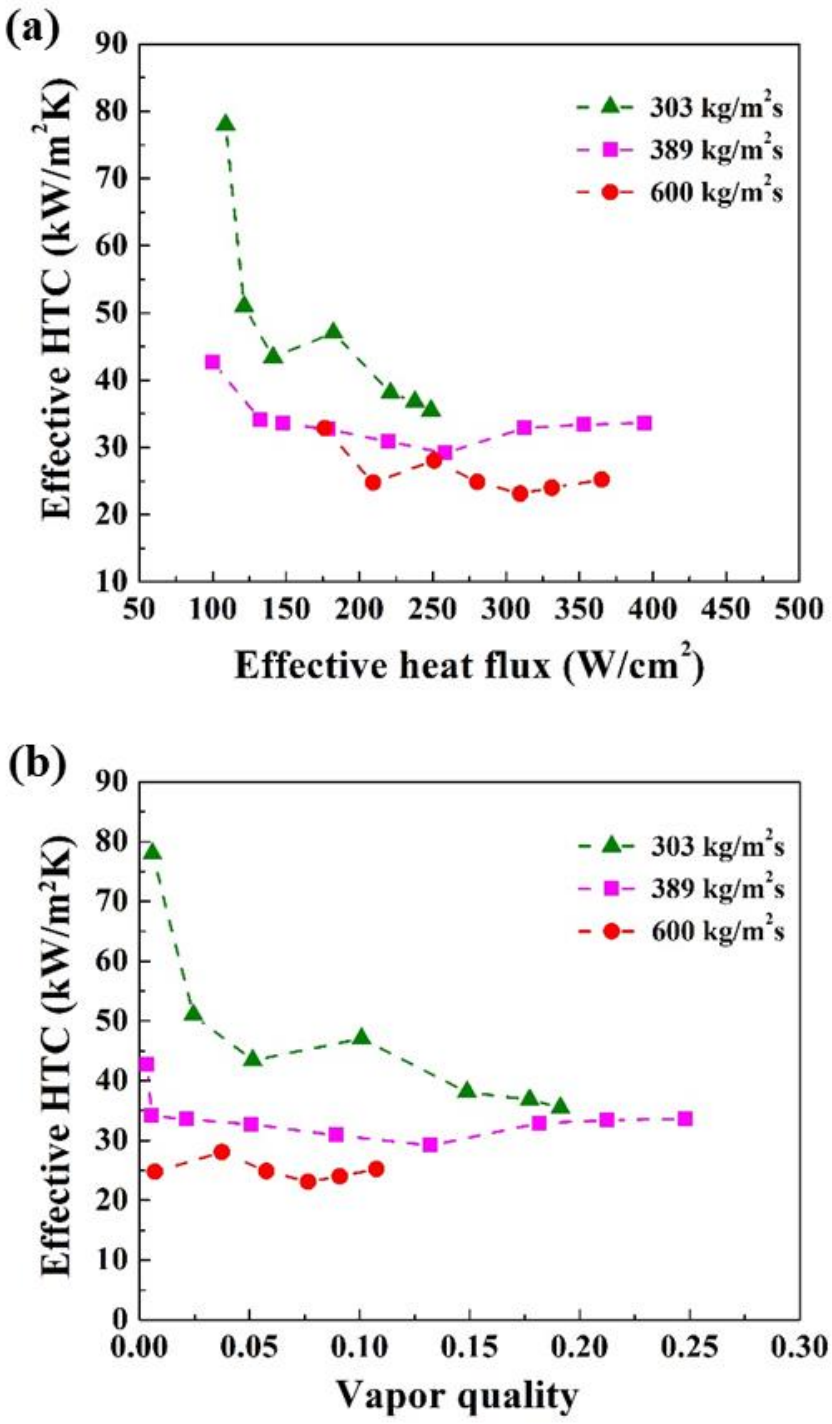

Figure 3.13 Effective HTC as a function of (a) effective heat flux (b) exit vapor quality at higher mass flux

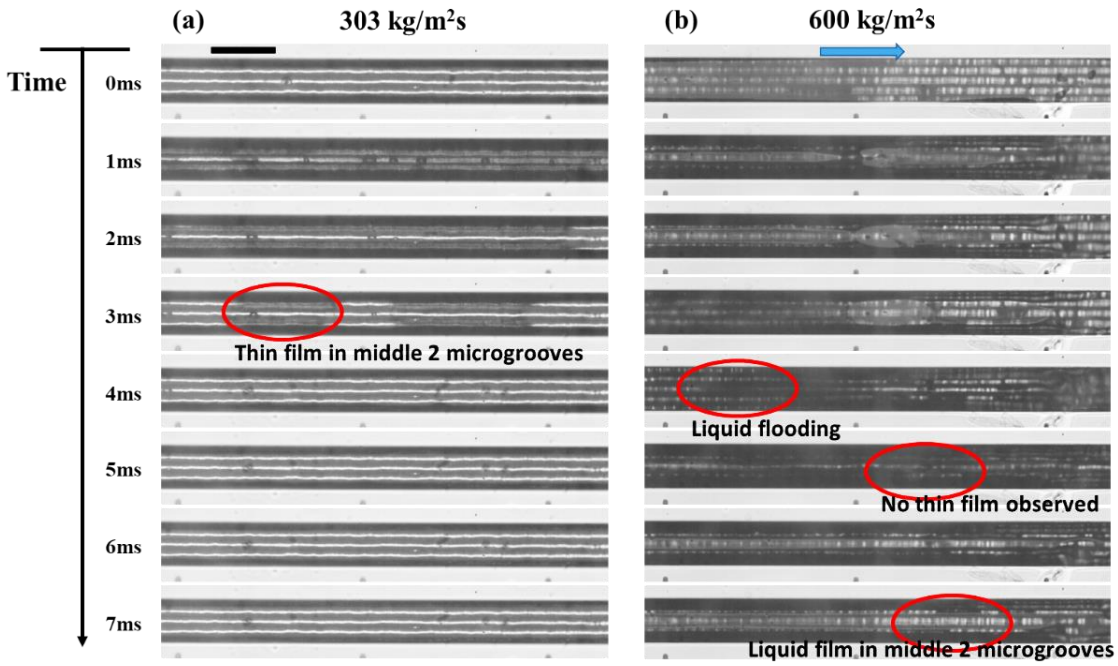

Figure 3.14 Thin liquid film distributions in low and high mass fluxes: (a) Liquid distribution at mass flux of 303 kg/m^{2}s and heat flux of 104 W/cm^2 (b) Liquid distribution at mass flux of 600 kg/m^{2}s and heat flux of 104 W/cm^2 (Scale bars are 300 μm).

3.2.4 Enhanced CHF

Figure 3.15(a) shows significantly enhanced CHF on the present design compared to plain-wall microchannels at the different mass fluxes. An enhancement of ~155% is achieved at the mass flux of 389 kg/m^{2}s. As aforementioned, flooding would result in severe flow instabilities, decreasing the rewetting and heat transfer rate. Figure 3.16 shows the premature of CHF because of wetting crisis near the outlet section. The wetting crisis point can be observed clearly in each microchannel. When the wetting crisis occurs, the liquid cannot effectively wet the heating surface. A vapor film would be formed on the heating surface, leading to CHF conditions.

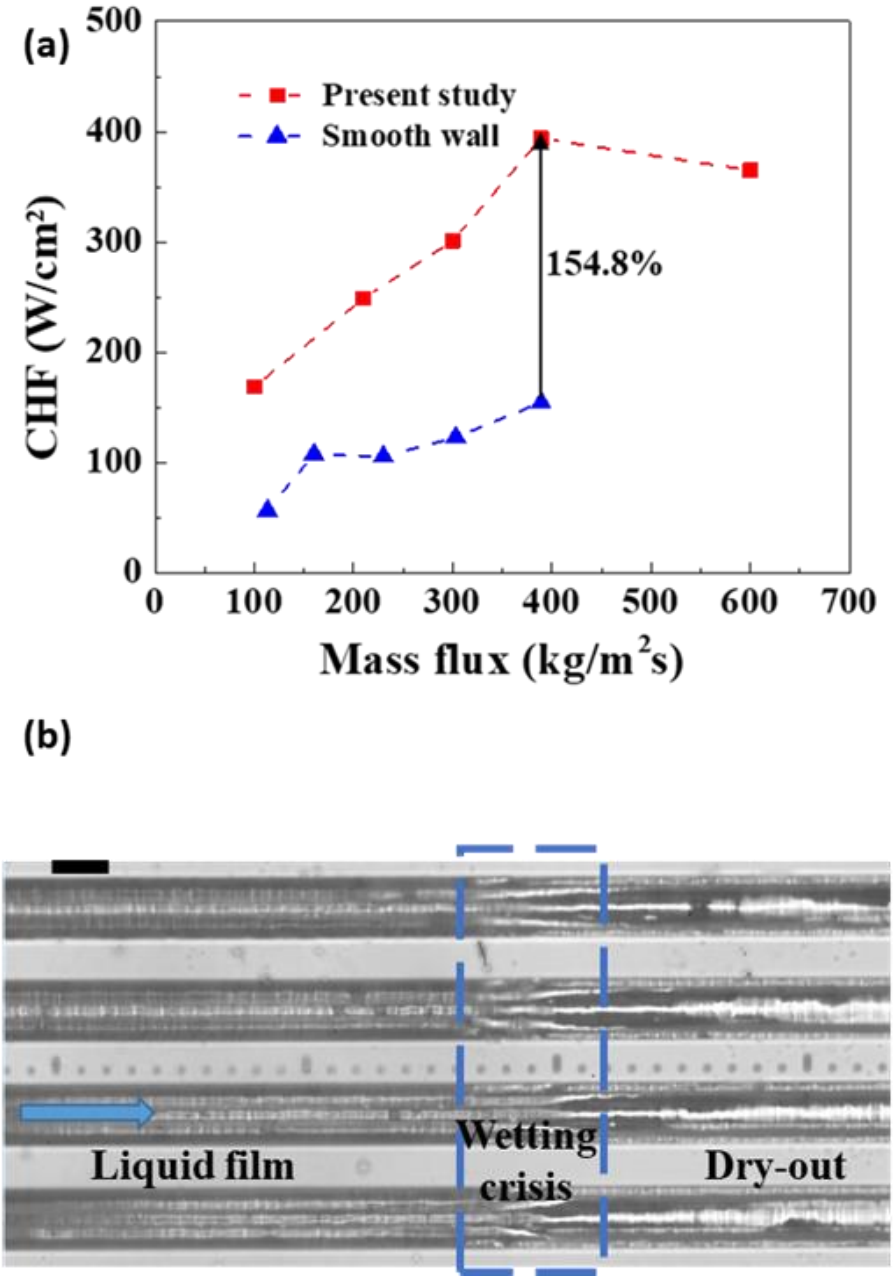

Figure 3.15 Enhanced CHF on the present design compared to plain-wall microchannels. (Scale bar is 200μm)

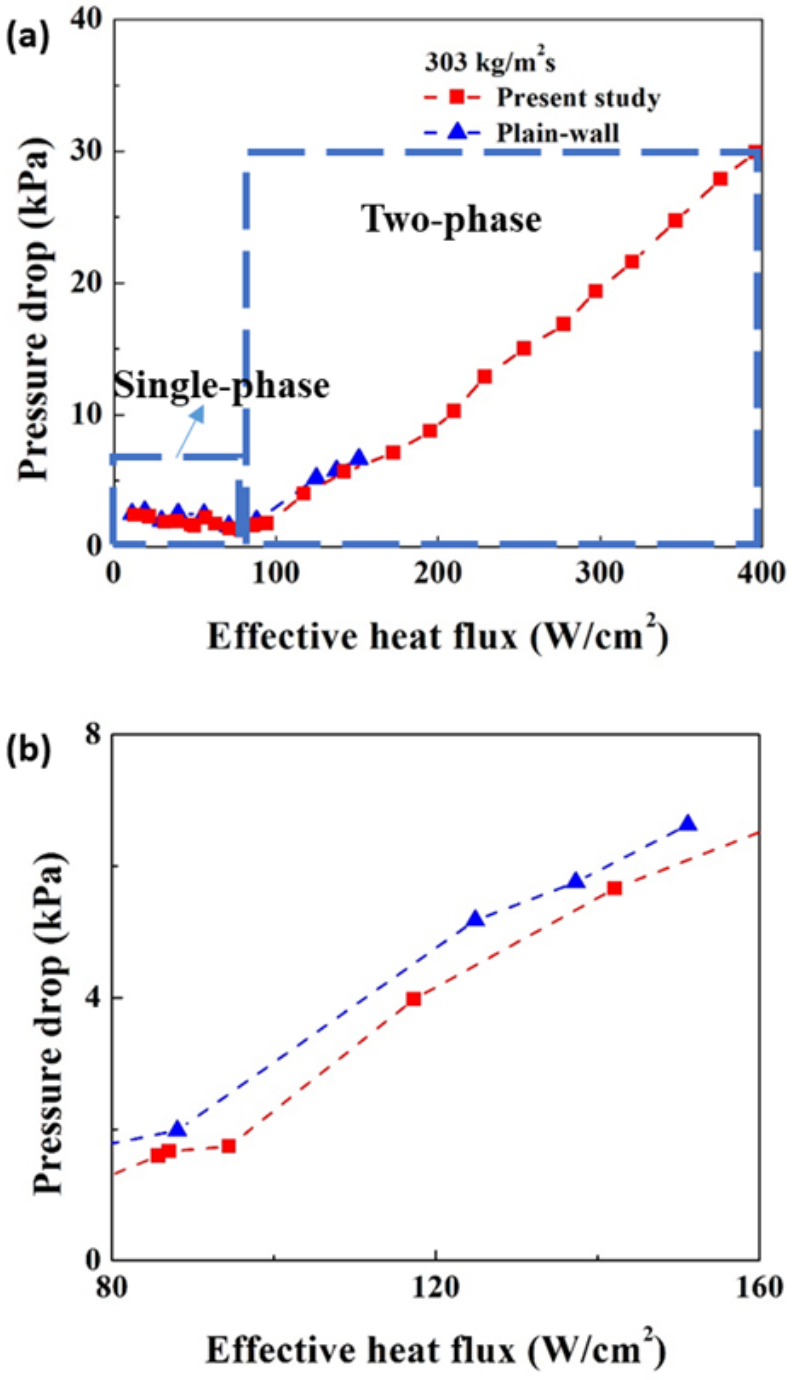

Figure 3.16 Compare of the pressure drop of the present design to the plain-wall microchannel without IRs: (a) all stages (b) early two-phase region

Moreover, Figure 3.16 a shows the pressure drop in the present design and plain-wall microchannels is nearly overlapped in the single-phase region. A slightly reduced pressured drop has been observed in the early two-phase region (Figure 3.16 b).

The enhanced rewetting is one of the main enhanced mechanisms of CHF. The hydraulic diameter of the microgroove is 86 μm compared to 222 μm of the plain-wall microchannel, which increase the capillary pressure by nearly 1.6 times (Calculated from $P_{cap} = \frac{2\sigma cos\theta}{R}$, the capillary pressure is increased to 2364 Pa from 916 Pa). The enhanced capillary effect significantly promotes the rewetting process. Enhanced CHF by promoting capillary flow using nanowire coating was also reported [85, 88]. Figure 3.17 shows the present microchannels can be rewetted in a short time of 0.75 ms.

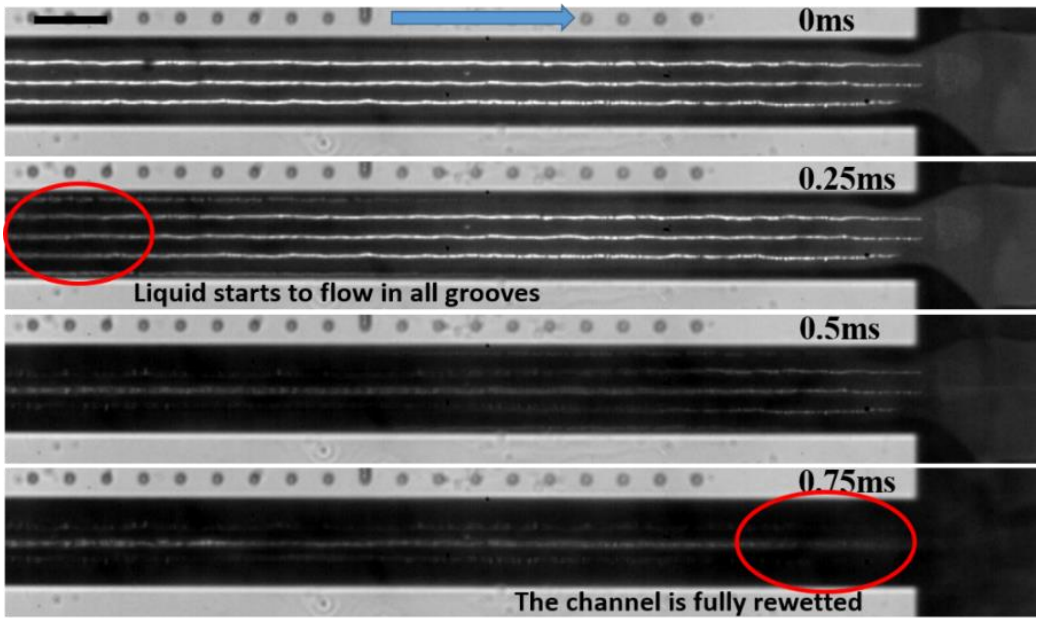

Figure 3.17 Rewetting process at mass flux of 303 kg/m^{2}s and heat flux of 160 W/cm^2. (Scale bar is 200 μm).

The whole rewetting process of the plain-wall microchannel and micro-grooved microchannel are compared in Figure 3.18. As it is illustrated in Figure 3.18 (a), apparent dry surface appears at the central part of plain-wall microchannels from 2 ms. For comparisons, the present microchannel configuration can be kept rewetted in the first 10 ms with a better uniformity of thin liquid film distributions. Thus, the local dry-out phenomenon is drastically mitigated by the promoted capillary flows. Additionally, the microgrooves can delay the dry-out compared to plain-wall microchannels, for example, longer wetted duration of 27 ms versus 17.5 ms.

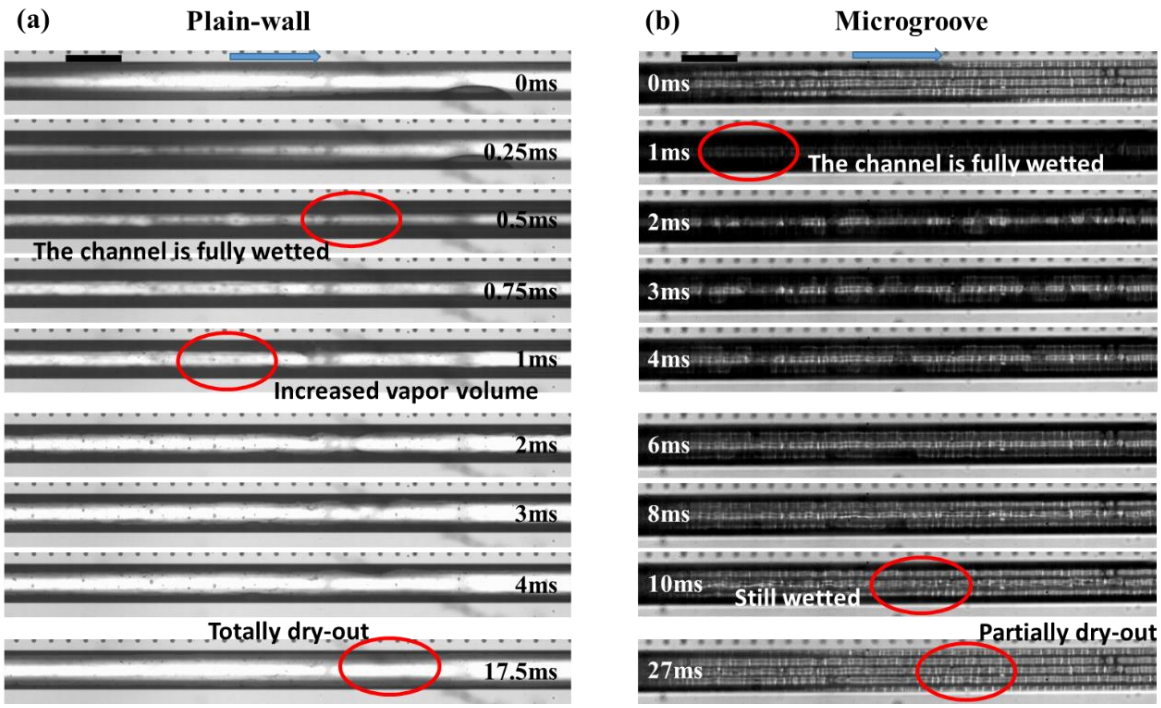

Figure 3.18 Comparisons of the rewetting cycle of microchannels with plain-wall and microgrooves at mass flux of 210 kg/m^{2}s and heat flux of 110W/cm^2. (Scale bars are 300 μm).

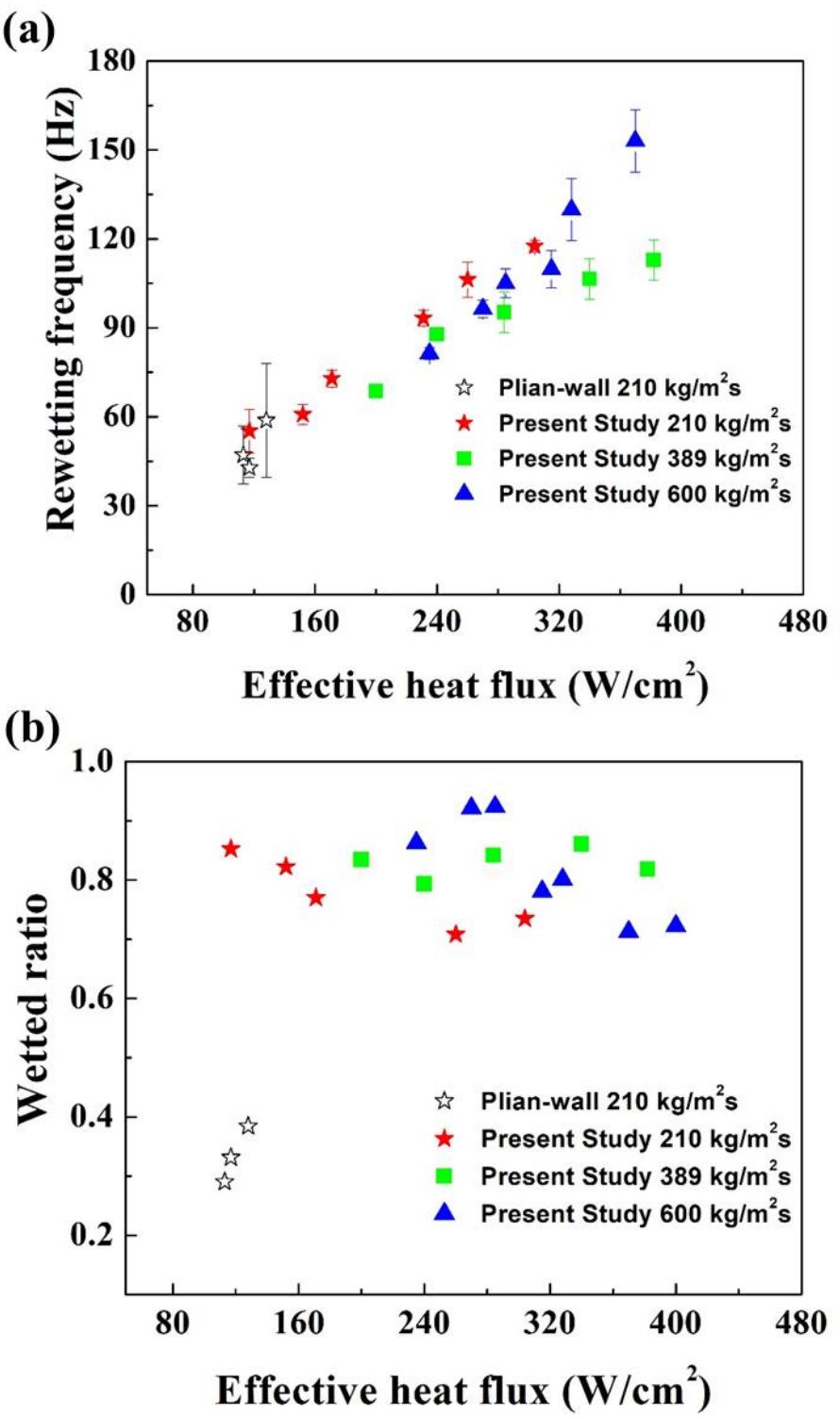

Figure 3.19 (a) Rewetting frequency at different mass fluxes; and (b) Enhanced wetted ratio over plain-wall microchannels

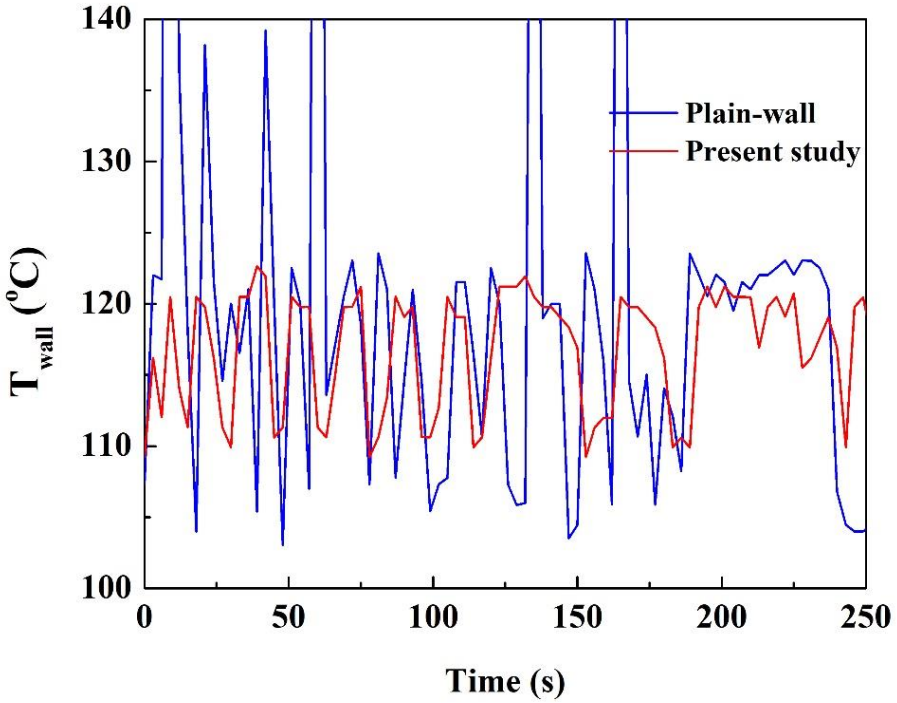

Figure 3.20 Transient wall temperature with G=389 kg/m^{2}s and q''=131 W/cm^2

Figure 3.19 shows the rewetting frequency in the present design at various mass fluxes. The rewetting frequency increases with the increase of heat flux. The highest frequency is about 151 Hz with mass flux of 600 kg/m^{2}s. Even though the rewetting frequency in the plain-wall microchannels is close to that of the present design at a mass flux of 210 kg/m^{2}s, the stability is much lower than the present design, as it is indicated by the error bars. As it is shown in Figure 3.20, the stability of the present design also can be proved by a transient wall temperature. The maximum temperature change in the plain-wall microchannel is 98 °C compared to 18 °C in the present study. Moreover, the wetted ratio shows the superiority of the present design. Figure 3.19 (b) shows the wetted ratio in the present microchannel is about two-fold higher than that in plain-wall microchannels.

The increased wetted ratio indicates a more sustainable liquid film, which would lead to the enhanced CHF.

3.3 Conclusions

This study has experimentally investigated the flow boiling performances in microchannels with parallel microgrooves decorated on the bottom surface. Compared to plain-wall microchannels, both CHF and HTC have been significantly enhanced because of the promoted capillary effect. Thin liquid film is formed at low mass fluxes, promoting the thin film evaporation. Also, rewetting is greatly enhanced on the present design, which increases global liquid supply and delays the dry-out. Briefly, the maximum enhancements of CHF and HTC are about 155% and 72%, respectively, without sacrificing pressure drop.

CHAPTER 4 TRANSIENT STUDY OF FLOW BOILING IN MICRO-GROOVED MICROCHANNELS UNDER HEAT PULSE

The heat and mass transfer associated with flow boiling in microchannels have been extensively studied in the past decades. The thermal performance of the microchannel devices has been significantly promoted with plenty of enhanced technics. Although a significant number of studies have proved that the flow boiling in microchannels is an effective cooling techniques to dissipate high heat flux, most of the studies in the literature were conducted under steady state conditions, in which the boiling process was studied by increasing the heat loads from zero to CHF gradually and allow the system reach steady state condition before each measurement. In practice, it is more challenging for the thermal engineers to dissipate dynamic heat, which is more frequently encountered in electronic devices. The high device temperature and severe temperature fluctuation is one of the major inducements of high device failure rate. However, there is lack of studies investigating the transient nature of the flow boiling in microchannels, especially under dynamic heating conditions. There are three main categories of transient heat loads were used in the transient study, step response, frequency response and impulse response. In this study, the transient flow boiling phenomenon and thermal characteristics were investigated under square heat pulse at frequency of 1 Hz and duty of 50%. Under the sudden application of the heat flux,

we can observe the quick transition of the flow regimes from single phase, bubbly flow, slug flow, annular flow, to dry-out condition.

4.1 Test setup and Experimental procedure

4.1.1 Test setup

The experimental setup and test procedure is similar to what we used in our previous studies on steady-state flow boiling in microchannel [25, 43]. Figure 4.1 depicts the two-phase apparatus used to conduct experiments. Major components of the experimental setup are similar as in the steady-state study, which are customized visualization system, data acquisition/storage system, power supply system and open coolant loop. The tested device was assembled to the test package module and connected to all the measurement and data acquisition systems. Mechanical fasten unit consists of two fasten bolts and two holding clamps and is used to locate and fasten the microchannel devices. The tested devices were supported at two ends and the middle part was suspended on two heating probe fins. The probe fins connected to the power supply were pressed on the heater, two bolts were used to adjust the heights of the probe-pins. The connection of the heating probe fins and the heater was carefully adjusted to minimize contact resistance. Also, this packaging was carefully designed to minimize the stresses on the heater and to reduce heat loss. Six micro o-rings were placed between the silicon tested device and the holding clamps to achieve mechanical seals and balance the stress on the tested device. Two pressure transducers were connected to the pressure ports to measure pressure drops. A high-pressure nitrogen tank was used to supply pumping power and drive the coolant through the tested system and flow to the recycle reservoir. The power supply system consists of a high precision digital programmable power supply to supply electrical power,

a waveform generator to generate periodic voltage and simulate the condition of startup process of high-power devices. Omega flow meter (FLV-4604A) was used to measure the flow rates. Inlet and outlet temperature were measured with two thermocouples. A customized data acquisition system developed from NI LabVIEW was used to record flow rates, pressures, inlet and outlet temperatures. To acquire transient data with high frequency, a constant resistant was added to the electric circuit and the voltage applied to the constant resistant was measured to calculate the current in the circuit. With the overall voltage, the voltage applied to constant resistance and constant in the electric circuit, the power applied to the heater can be computed.

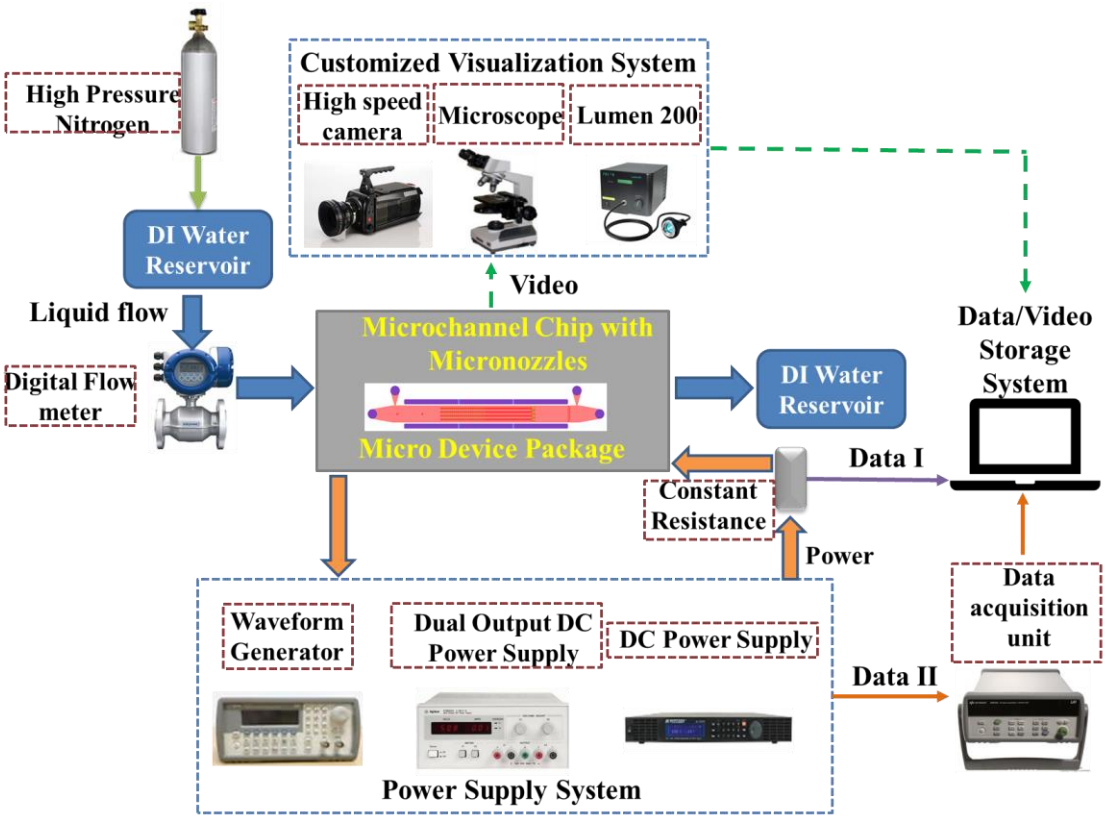

Figure 4.1 Transient test setup

4.1.2 Experimental procedure

Prior to the test, the heater, which also works as a thermistor, is calibrated with a proportional-integral-derivative controller in the isothermal oven to estimate the correlation between the temperature and thermal resistance of the heater. With the correlation, the heater temperature can be estimated with the electrical resistance, which can be obtained from the experimental data. Meanwhile, the heat loss from the system to the surrounding is evaluated as a function of the temperature difference between the heat exchanger temperature and ambient temperature. Both of the heater temperature and heat loss are evaluated with high accuracy. The pressurized DI water tank was degassed with heat supply to maintain the water temperature to 40 ^{o}C prior to the test. With the pumping power of compressed nitrogen and a flow meter of Krohne Optimass 3300c with a ± 0.1% resolution (density with ± 2 kg/m^3), the DI water flowed through the system at a constant mass flow rate. Inlet/outlet pressure and temperature were measured with pressure transducers and K-type thermocouples, respectively. The average temperature of the heater was calculated with the correlation obtained with calibration prior to the test. A high precision digital programmable power supply (BK-PRECISION XLN10014) was used to supply electrical power. The voltage applied to the microheater was measured by an Agilent digital multimeter (34972A). Flow rate, local pressure, inlet and outlet temperature, overall voltage, and current were recorded by a customized data acquisition system developed from NI LabVIEW®. A visualization system comprised of a high-speed camera (Phantom V 7.3) and an Olympus microscope (BX-51) with 400× amplifications were used to study the two-phase flow patterns. All measurements were carried out at 1 atm ambient pressure

and room temperature of ~18 °C and all data were collected by an Agilent 34972A data acquisition system.

Uniform heat flux was applied to the system for 0.5 s then the power was cut and let it cool down for another 0.5s to the condition before boiling. Under the pulsed heating loads, the periodic boiling phenomenon was observed with the entire flow process. The heat amplitude was increased from zero with step of 5 W/cm^2. The data started to be captured when the boiling phenomenon occurred. The heating power and video recorder were triggered simultaneously to obtain synchronous data and video. Voltage data, which is used to calculate heater temperature, was collected at a frequency of 2 kHz and synchronized video was recorded at a frequency of 4 kHz. The inlet/outlet temperature and inlet/outlet pressure were recorded as the average value of 90 data points at 4 min intervals since they cannot response to the change of power input in time with such short heating time.

4.1.3 Data reduction

Before the test procedure calibration is conducted to predict the correlation between temperature and resistance of the thermistor. The average temperature of heater can be calculated as:

$$\overline{T}_{heater} = k(R - R_0) + T_0 \quad (1)$$

Where k is the slope of the heater temperature vs electrical resistance curve which is got from calibration, R_0 is the electrical resistance at room temperature and T_0 is the

room temperature. The resistance of the heater R_{heater} is calculated from the input voltage (V) and current (I).

$$I = \frac{V_R}{R} \tag{2}$$

$$R_{heater} = \frac{V_{total} - V_R}{I} \tag{3}$$

The input power is:

$$P = (V_{total} - V_R) \times I \tag{4}$$

The effective heat input is calculated by deducting heating loss to the surrounding from the original heat input:

$$P_{eff} = P - P_{loss} \tag{5}$$

The heat transferring of the heater and the bottom of microchannel is considered as pure conduction and the average temperature of this surface is computed as:

$$\overline{T} = \overline{T}_{heater} - \frac{q''_{eff} t}{k_s} \tag{6}$$

Where q''_{eff} is the effective heat flux and can be calculated as

$$q''_{eff} = \frac{P_{eff}}{A_b} \tag{7}$$

In additional to that, the overall heat transfer coefficient is calculated as:

$$\bar{h} = \frac{P_{eff}}{A_b(T_{wall} - T_{sat})} \quad (8)$$

4.2 Results and discussion

4.2.1 Thermal performance of the microchannels under heat pulse

Figure 4.2 shows the representative dynamic thermal behaviors under the heat pulse at mass flux of 380 kg/m^{2}s and heat flux of 180 W/cm^2. The flow was in single-phase stage initially, as it is shown in Figure 4.3 (a). The wall temperature increases instantly in the single-phase stage due to direct condensation and single-phase convection. The nucleate boiling was triggered at 0.7s and bubbly flow was observed (Figure 4.3 (b) and (c)) after that. Nucleate boiling dominated the heat transfer mechanism in the bubbly flow stage, which is characterized by a high HTC as it is depicted in

Figure 4.2 (b). With the development of flow boiling, the bubbles started to expand and formed bubble slugs, which suppress the nucleated boiling and cause the reduction in HTC and increase in temperature change rate. With the increase in the vapor volume, annular flow was observed from 0.2 s (Figure 4.3 (d)), where convective boiling dominated. The HTC continually decrease due to the decrease in vapor quality and the occurrence of local and global dry-out.

Figure 4.4 illustrates the thermal responses of the microchannel device under 3 different heating powers which provide initial heat flux of 150 W/cm^2, 168 W/cm^{2,} and 180 W/cm^2. Similarly, under all the heat fluxes, once heat was applied to the device, the wall temperature increased rapidly at the single-phase period. With the increasing of wall temperature, the ONB crisis was triggered and the bubbly flow region was formed after

that. Obviously, the temperature remains in a relative stable level with slightly increase in the bubbly flow period since the system has not reached steady state condition. When slug

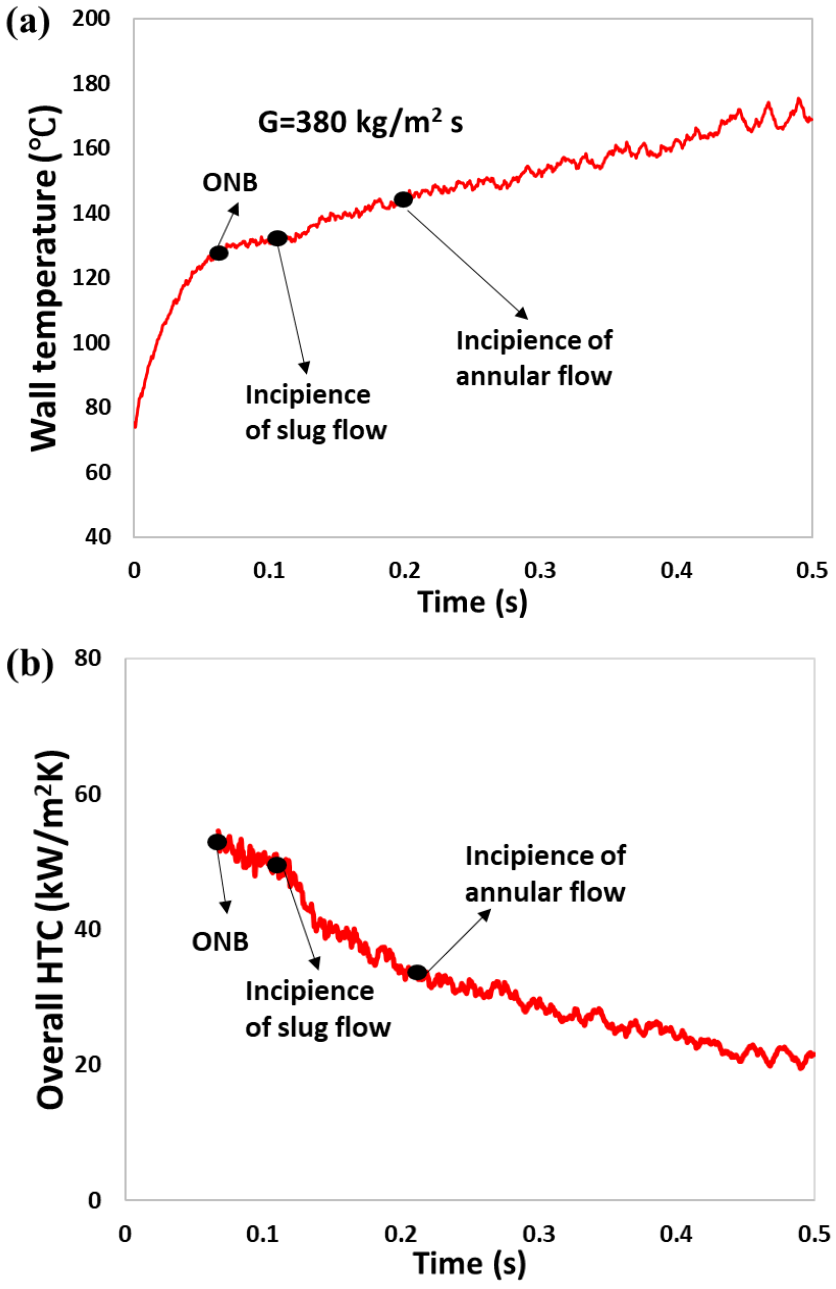

Figure 4.2 Thermal performance response to the heat pulse. (a) Wall temperature (b) Overall HTCs at mass flux of 380 kg/m^{2}s and heat flux of 180 W/cm^2.

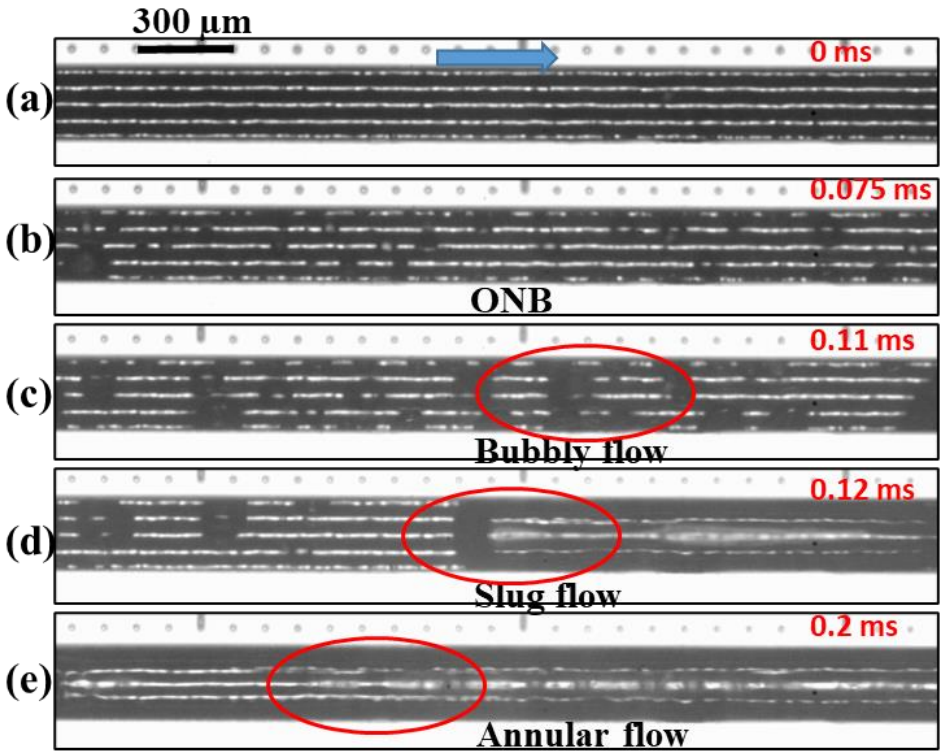

Figure 4.3 Various flow patterns at mass flux of 380 kg/m^{2}s and heat flux of 180 W/cm^2

flow and annular flow were formed in the microchannel, the temperature change rate increase slightly, which suggested reduced heat transfer performance. Moreover, the tested device was heated to a higher temperature before the nucleate boiling was triggered. For example, under the heat flux of 180 W/cm^2, the superheat temperature at ONB is 25 ^{o}C, which is much higher than that in the steady state study. This is caused by the high thermal resistant of the working liquid. The liquid cannot be heated to the saturated temperature in time, which caused a delay in the onsite of nucleate boiling. The characteristic time points represent the transition between each flow regimes were marked in the graph. Clearly, under high heat flux, the boiling phenomenon was triggered earlier than that of low heat flux and the superheat temperature is also higher.

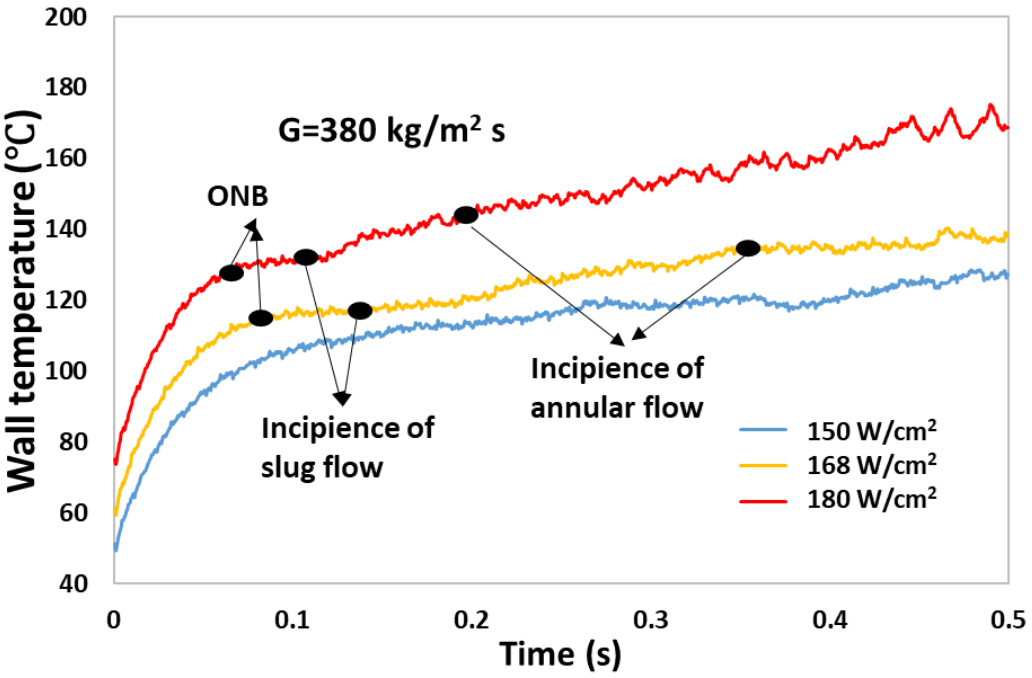

Figure 4.4 Wall temperature response

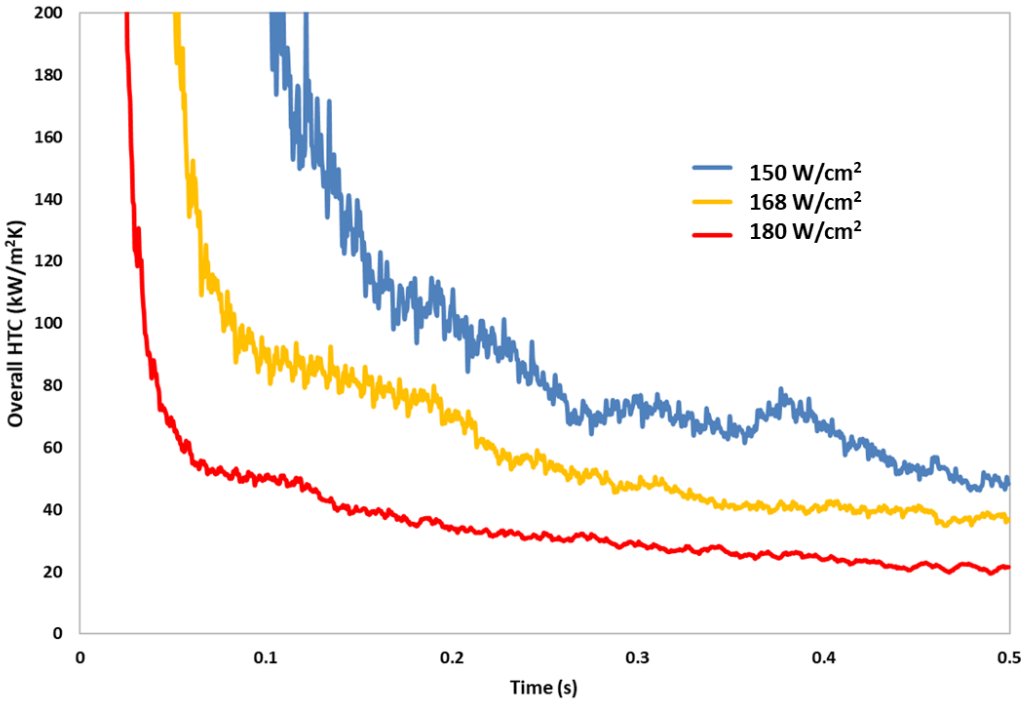

Figure 4.5 Dynamic behavior of Overall HTCs for different heat loads

Figure 4.5 presented the overall HTCs calculated based on the heating area at the three heat loads. Same as it was presented in the steady state study, the HTC reached the highest value at ONB, where nucleate boiling dominated. With the gradually development of flow boiling, the HTC decreases in the slug flow and annular flow stages, where convective boiling dominated. Under low heat flux, the system reached steady state condition before the end of heat pulse. We can observe the typical behaviors of HTCs during different flow regimes. Particularly, an increase in HTC was noticed during film evaporation stage with the gradual thinning of liquid film. However, this cannot be observed at high heat flux due to the quick transition between flow patterns. Moreover, the HTC is lower at high heat loads due to the high superheat temperature caused by lower vapor quality. At heat flux of 168 W/cm^2, the bubbly flow and slug flow dominated more than 55% of the heating period. For the heat flux of 180 W/cm^2, the annular flow was observed from 0.2s and annular film dry-out occurred periodically, which explained the low HTC at high heat flux.

4.2.2 Temperature fluctuation and liquid rewetting

An obvious periodic temperature profile was observed at the end of the heating process when the boiling is fully developed. As it is shown in Figure 4.6, a temperature fluctuation amplitude up to 13 ^{o}C was noticed with frequency of about 33 Hz, which indicates the flow instability. To study on the temperature fluctuation, a visualization study is conducted to match the wall temperature and the corresponding flow patterns.

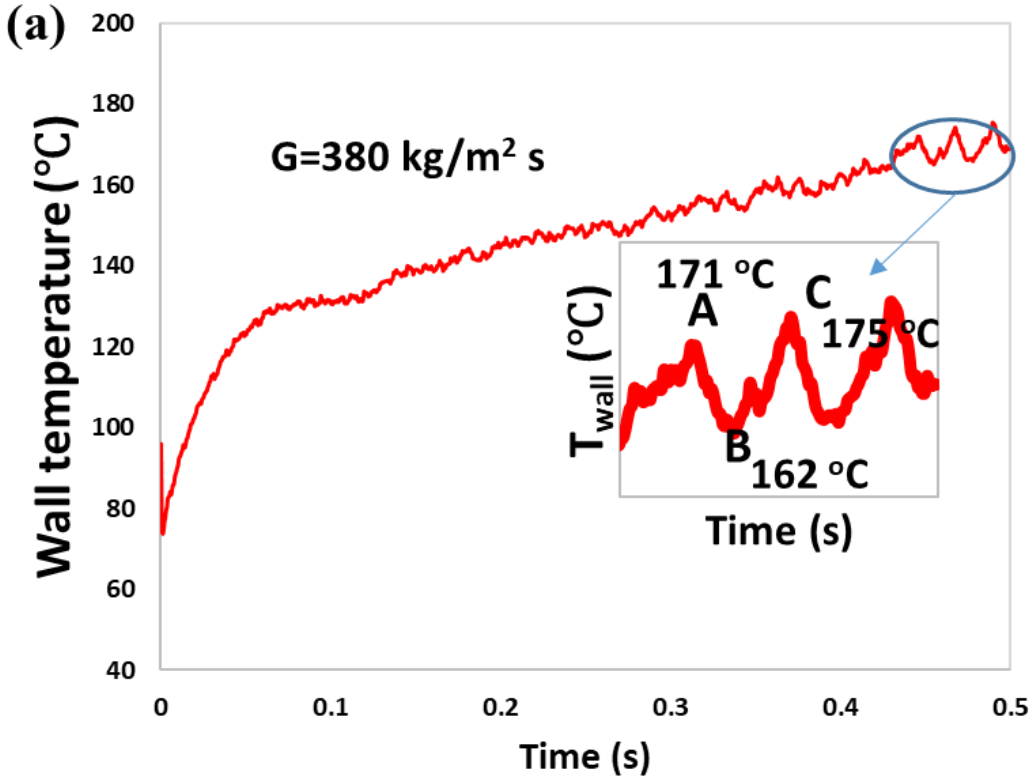

Figure 4.6 Wall temperature time response (G=380 kg/m^{2}s, q"=180 W/cm^2)

Figure 4.7 and Figure 4.8 shows the different flow patterns associated with the wall temperature fluctuation. As it is shown in Figure 4.7, when the temperature reached the highest point on position A, the microchannels were occupied with vapor, which results in the local dry-out and high wall temperature. After that, liquid entered the microchannels gradually and cooled the microchannels to a lower temperature. When the channels are fully rewetted at 0.448s, the lowest temperature was achieved at position B. Figure 4.8 showed the liquid evaporation process. When the liquid started to evaporate, the reducing liquid quality cause the decreasing thermal resistant along the liquid film. In response, the wall temperature grew again till the next dry-out happened at position C.

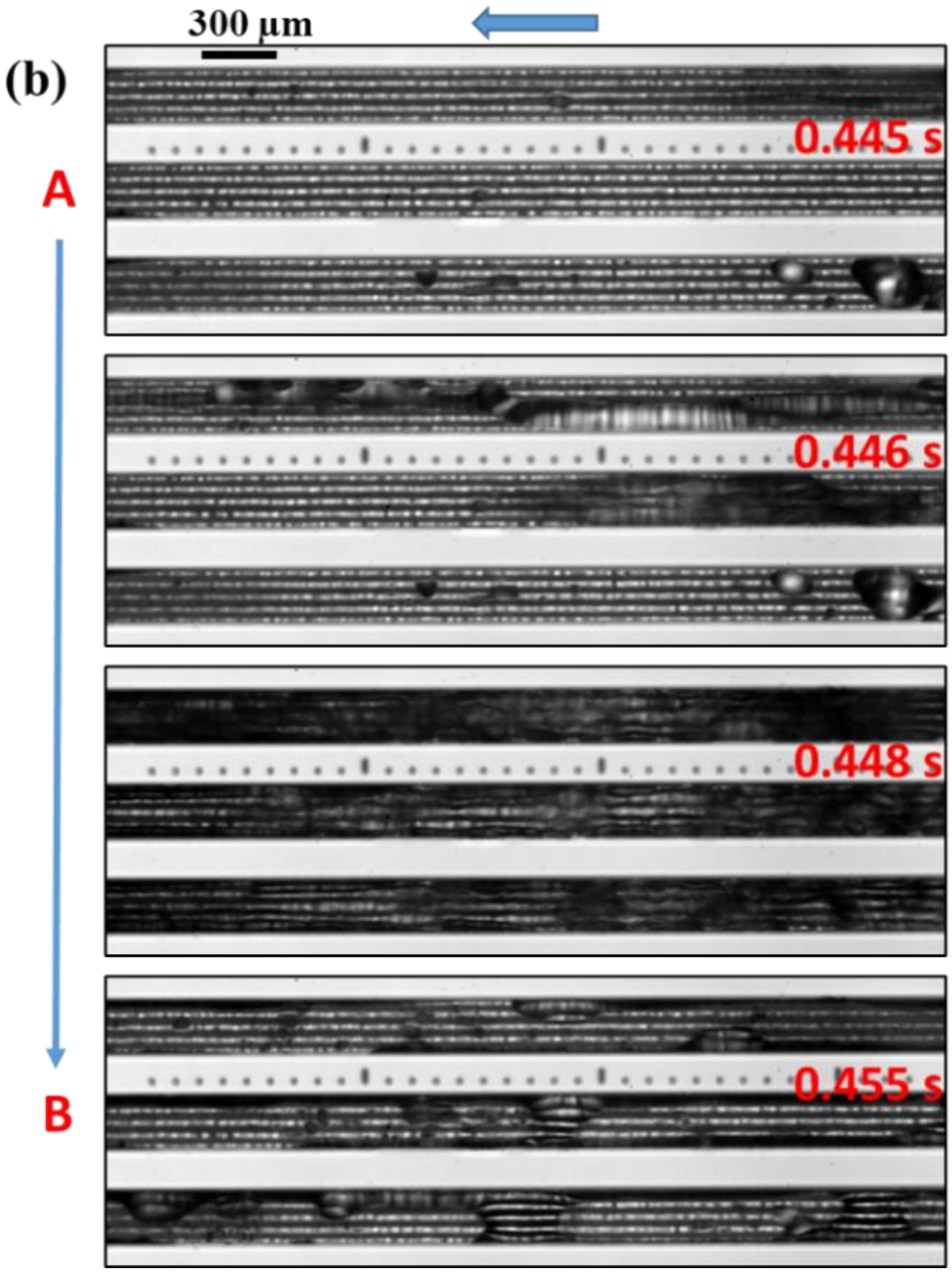

Figure 4.7 Matched flow patterns at corresponding points in Figure 4.6 (A-B: liquid rewetting)

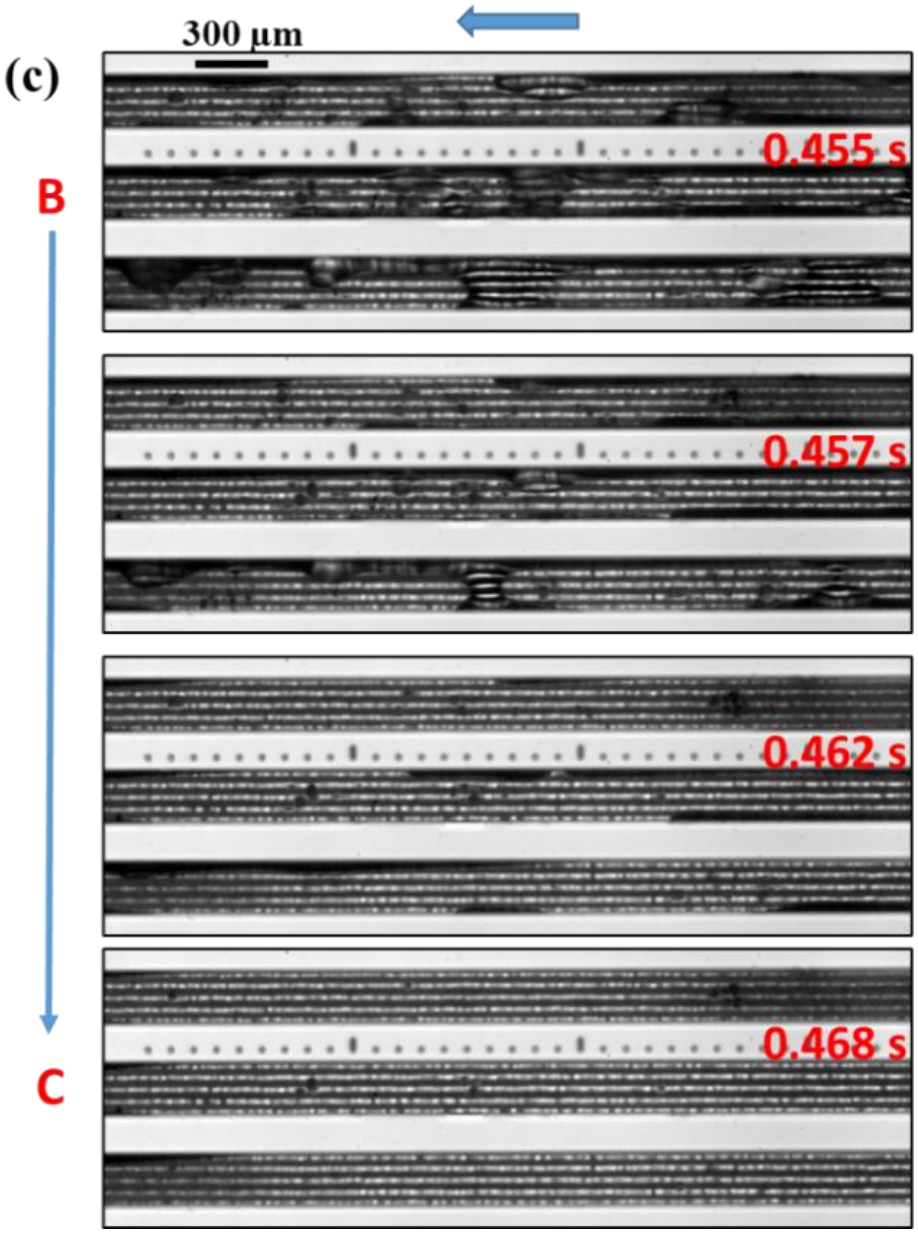

Figure 4.8 Matched flow patterns at corresponding points in Figure 4.6 (B-C: Liquid dry-out)

4.2.3 Enhanced thermal performance

Dynamic behaviors of thermal performance were studied on both plain-wall and micro-grooved microchannels. Obviously, at same heat flux range, the microchannels with microgrooves can maintain the wall temperature at a relative lower level. Moreover, the

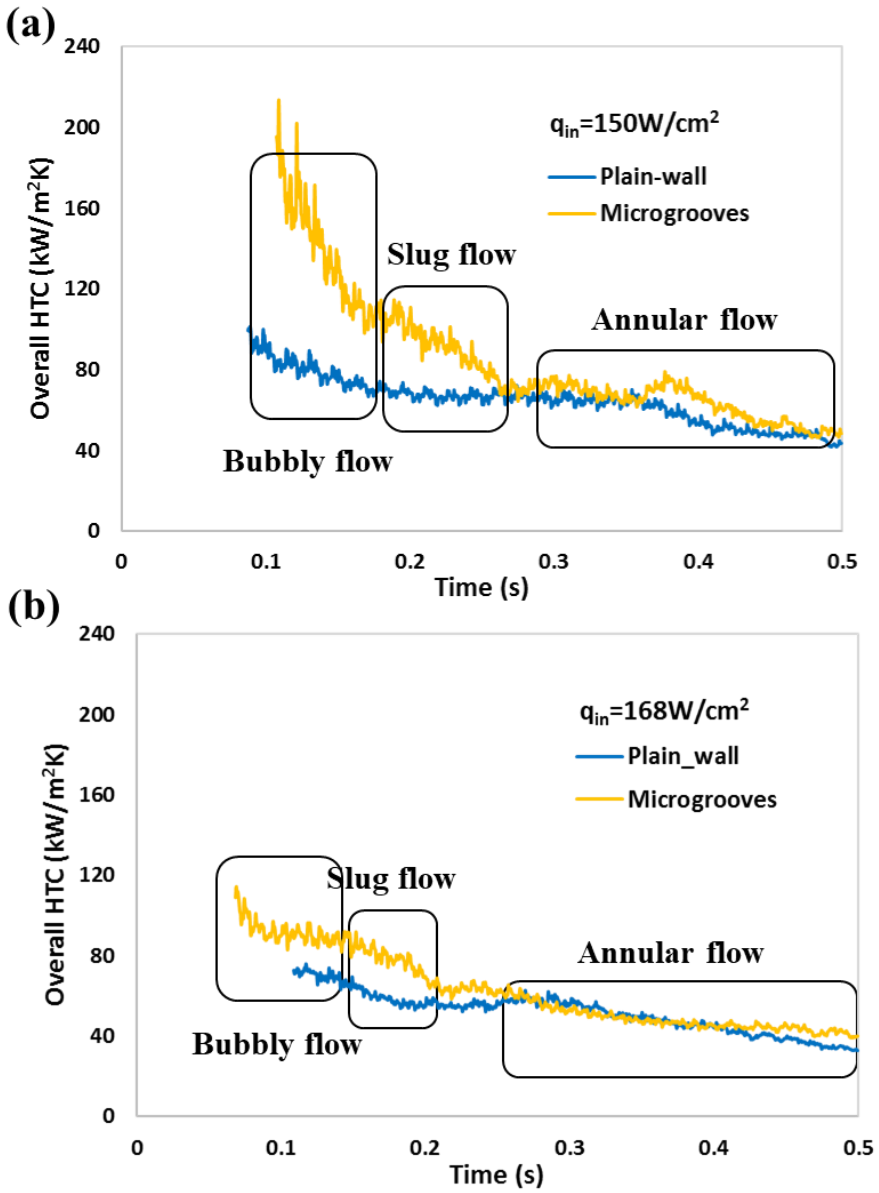

Figure 4.9 Comparison of thermal performance of flow boiling in plain-wall and micro-grooved microchannels (G=380 kg/m^{2}s)

time required to initiate boiling is shorter in the present configuration. However, we cannot observe obvious enhanced stability in the present design. HTCs are calculated based on the heating area. The enhancement of HTCs is maximum at the early boiling stage of all mass fluxes, where nucleate boiling is dominant. A higher nucleate sites density is observed,

which contributes to the enhancement at bubbly flow and slug flow stage. Once the boiling is transited to the annular flow regime, the convective boiling became dominant and the HTCs reduced to a lower level. Thin film evaporation was slightly enhanced due to a more uniform liquid distribution, which results in the increase of HTCs when the boiling is fully developed. However, because of the high capillary pressure in the microgrooves, the liquid was driven to the outlet section more efficiently, which leaded to the relative thick liquid film in the microchannels. As a result, the enhancement in the annular flow regime was limited.

4.3 Conclusions

The transient performance of the flow boiling in the microchannel with microgrooves was investigated. The heat was applied to the system in the form of square heat pulse. The thermal characters of the tested device were captured and the video was recorded synchronously.

- Wall temperature increases rapidly before ONB and the growing rate becomes lower after that
- The flow patterns were matched with wall temperature
- Temperature fluctuation occurred at high heat flux
- HTC is higher in micro-grooved microchannel compared to plain-wall microchannel at same effective heat flux

CHAPTER 5 TRANSIENT STUDY OF FLOW BOILING IN MICROCHANNELS USING AUXILIARY CHANNELS AND MULTIPLE MICRONOZZLES – DI WATER

The transient nature of flow boiling in microchannels with microgrooves under heat pulse was primarily studied. However, the enhancements on HTCs mainly happen during the earlier boiling stages. Fewer advantages were observed at higher mass flux range. Moreover, the flow boiling instability related with temperature fluctuation was noticed in the previous transient study. Moreover, W. Qu and I. Mudawar [89] suggested that CHF could be triggered by flow instabilities, which was caused by vapor backflow into the microchannels' upstream section. Instabilities related to temperature and pressure drop fluctuation were reported in previous studies [90-94]. Generally, the heat transfer performance could be enhanced by suppressing flow instabilities. Various techniques have been developed to suppress flow instability such as inlet restrictors [22, 52]. The compressed gas in upstream is one of the main reasons of flow instability [89, 95]. The inlet restrictor unit can effectively control the flow reversal thus alleviate the flow instability [96, 97]. However, the using of inlet restrictor always come with the cost of extra pressure drop, which means higher pumping power is required. A microchannel device consists of two auxiliary channels and micronozzles in each microchannel was designed

by Yang [49]. A microbubble-excited actuation mechanism, powered by high-frequency bubble growth and collapse, was established to create strong mixing in the microchannels. The HTC and CHF were significantly enhanced without sacrificing pressure drop. Also, the flow stability was significantly enhanced. This device can only induce strong mixing in the downstream section. Developed from the two-micronozzle microchannels, Li [26] built a four-micronozzle configuration to extend the strong mixing to the entire channel. According to the previous steady-state study, the improved microchannel configuration successfully extends the mixing to the entire channel. The HTC and CHF were enhanced by up to 123% and 35% compared to the two-nozzle configuration and the temperature at ONB was found reduced by 14%. Moreover, additional decrease of flow instability was reported in the steady state condition.

The aim of the present work is to investigate the flow boiling performance of the four-nozzle microchannels device under transient working condition. The wall temperature time response and HTC time response will be studied with corresponding flow patterns. The enhancement of the present design compared to plain-wall microchannels device will be evaluated.

5.1 Design and fabrication of the device

A micro cooling device consists of an array of five parallel microchannels (W = 200 μm, H = 250 μm, L = 10 mm), where each main channel is connected to two auxiliary channels (H = 250 μm, W= 60 μm, L = 8 mm), is developed to experimentally characterize flow boiling heat transfer. Each 60-μm-wide auxiliary channel has four 20 μm wide nozzles connected to the main channel. An inlet restrictor (H = 250 μm; W= 20 μm; L = 400 μm)

is integrated in each main channel to trap elongated bubbles. The micronozzles provides additional nucleation sites to promote the nucleate boiling. The strong two-phase mixing induced by the jetting flow generated by the micronozzles through the auxiliary channels will significantly enhance the two-phase heat transfer performance as well as promote rewetting hance increase the CHF.

The fabrication process started with a double-side polished n-type h1 0 0i silicon wafer. First, before fabricating a microheater, a 1 ± 0.01 μm thick thermal oxide layer was grown on both sides of the silicon wafer. The silicon oxide film provides electrical insulation for the micro heater and acts as a mask for deep reactive ion etching (DRIE) in the subsequent microfabrication steps. Next, a thin film heater was fabricated through a liftoff process on the backside of the wafer. In the lift-off process, a pattern mold of a thin film heater was prepared with a negative photoresist by photolithography first. Then, a 1.5 ± 0.05 μm thick layer of aluminum was deposited followed by a 63 Å thick of titanium layer by DC sputtering. Once the thin films were successfully deposited, a thin film heater was formed by a lift-off process. A 1 ± 0.05 μm thick plasma-enhanced chemical vapor deposition (PECVD) oxide layer was then deposited to protect the thin film heater in the subsequent fabrication processes. It which serves as both a micro heater to generate heat flux and a thermistor to measure the wall temperature.

After the heater was formed on the backside, a patterned mask of microchannels on the top side of the wafer were etched in the silicon oxide through photolithography and reactive ion etching (RIE). The area under the oxide mask was protected and the remaining areas were etched out to create 250 ± 3 μm deep trenches by DRIE.

A Pyrex glass wafer was anodically bonded to the silicon substrate to seal the device. The transparent glass cover also serves as a visualization window. RIE was used to remove oxide coatings on the backside to expose the contact pads after anodic bonding. The individual microchannel test chips (length 30 ± 0.005 mm; width 10 ± 0.005 mm; thickness 1 ± 0.005 mm) were cut from the wafer by a dice saw.

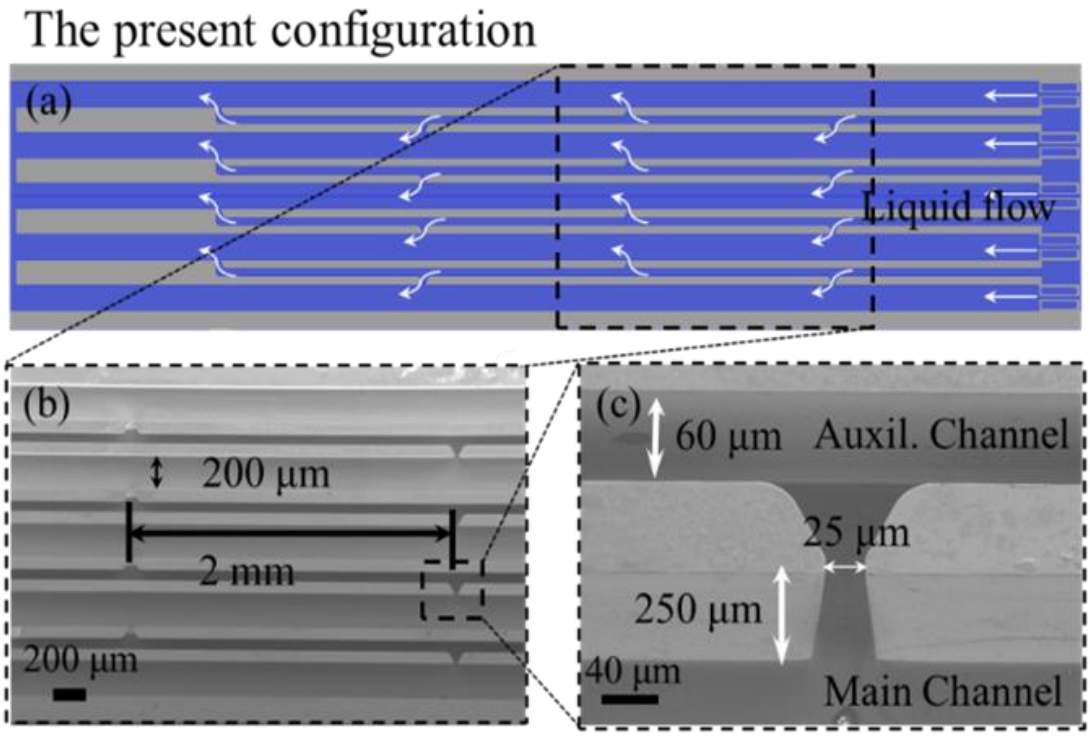

Figure 5.1 The design and major dimensions of the present four-nozzle microchannel configuration. (a) The improved four-nozzle microchannel configuration. (b) SEM image of the micronozzle distribution with a separation of 2 mm. (c) SEM image of the micronozzle.

5.2 Results and discussion

5.2.1 Onsite of nucleate boiling

Figure 5.2 shows the onsite of bubble nucleation at four micronozzles under heat pulse amplitude of 280 W/cm^2 and mass flux of 380 kg/m^{2}s. At 22.57 ms from the trigger

of heating, the bubbled started to nucleate from the first micronozzle (N1) near the outlet. Then the micronozzle N2 was activated at 32.73 ms, which is followed by the activation of N3 at 39 ms and N4 at 50 ms. The sequential activation of these micronozzles suggested the gradually extension of the flow boiling from the downstream to upstream section. The ONB was defined as the first bubble generated from micronozzle N1, which is also the fist bubble appeared in the entire microchannel.

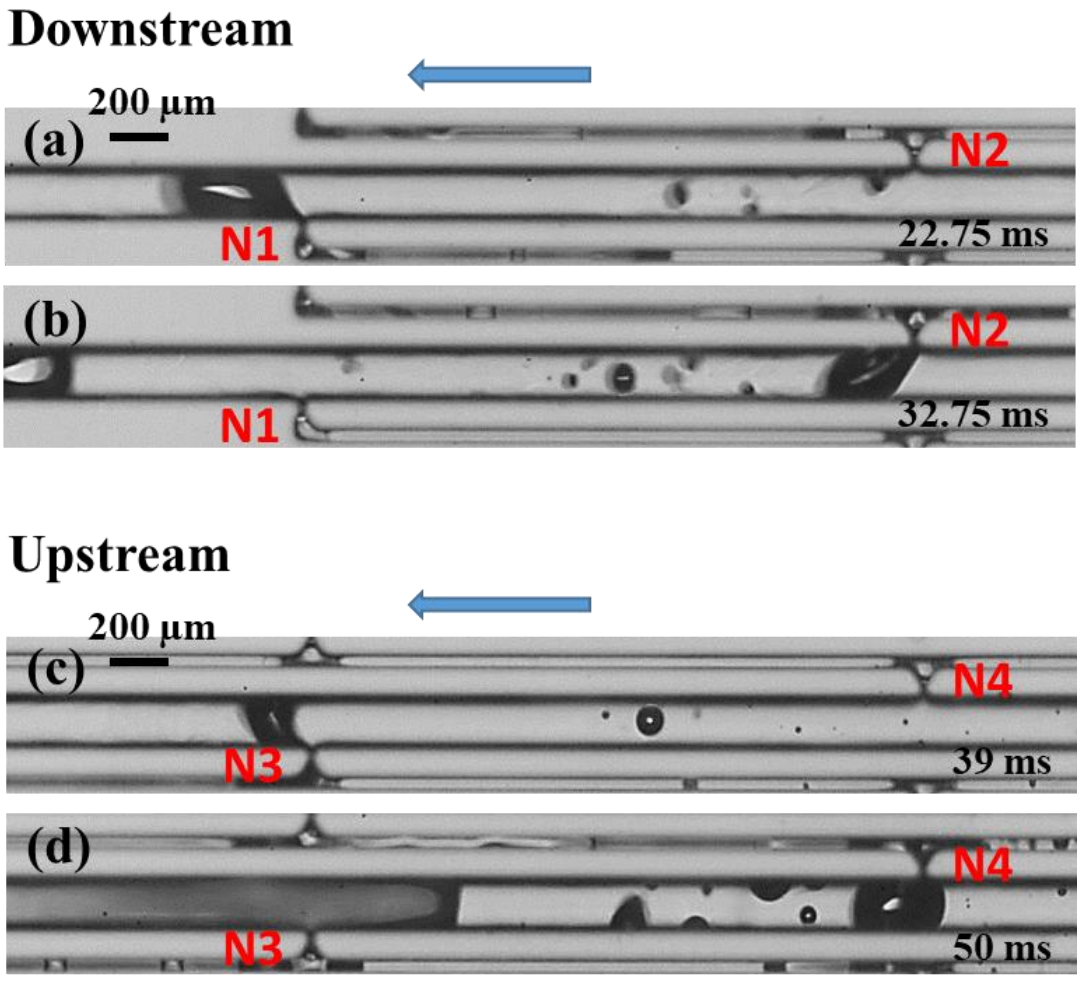

Figure 5.2 Onsite of bubble nucleation from four different micronozzles (G=380 kg/m^{2}s, q”=280 W/cm^2)

Figure 5.3 illustrates the wall temperature that initiated nucleate boiling as a function of effective heat flux. The results were compared with that in the steady state study [26]. In the steady state study, the heat was applied at a constant heat flux to the system and the heat flux was increased gradually, which enabled the fully warming up of the device and working fluid. However, in the transient study, the heat was applied instantly and caused a rapid temperature increase before boiling. As a result, it required a higher heat flux to heat the working fluid to the temperature that initiates boiling. Similarly, the wall temperature at ONB was also larger due to the high heat transfer rate low thermal conductivity of the working fluid. What is more, as it is shown in Figure 5.3, when the ONB temperature increased with the increase in heat flux. Because of the high temperature increase rate, it reached high superheat wall temperature before heating the liquid to the temperature that required to initiate boiling. Similarly, the ONB temperature was also higher with lower mass flux under same heat flux since the temperature increase rate was high compared to higher mass flux.

The ONB was recorded when the nucleation site at the micronozzle N1 was active. Figure 5.4 shows the active time of all the four micronozzles in a microchannel. Under low heat flux, the micronozzles near the outlet was activated, but the boiling was not expanded to the upstream of the microchannels. With the increasing of heat flux, more micronozzles became active and the two-phase mixing was significantly enhanced. Li's study [26] showed that the two-phase mixing was more obvious and frequent in the upstream, which enhanced heat transfer performance of the present configuration under high heat flux. In addition to that, due to the high temperature change rate and high base temperature, the micronozzles were activated earlier under higher heat flux.

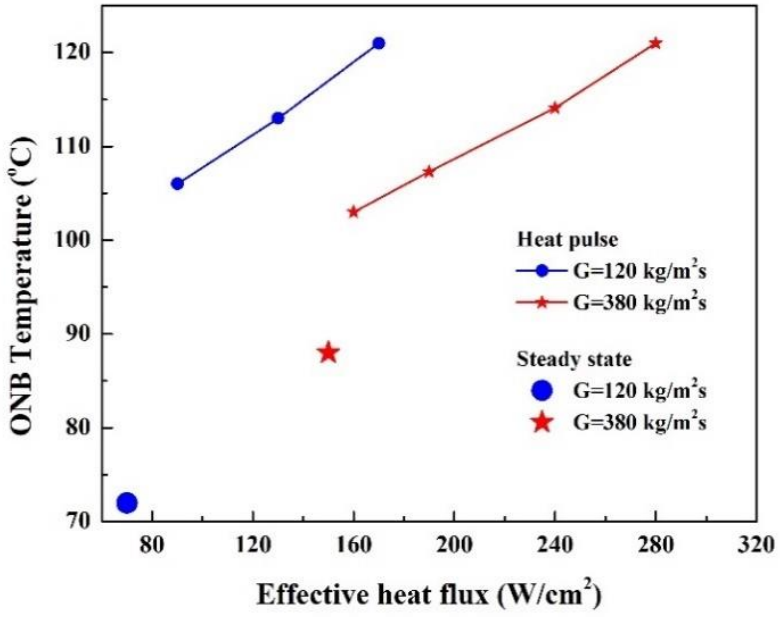

Figure 5.3 Effect of heat flux and mass flux on ONB temperature (G=380 kg/m2s)

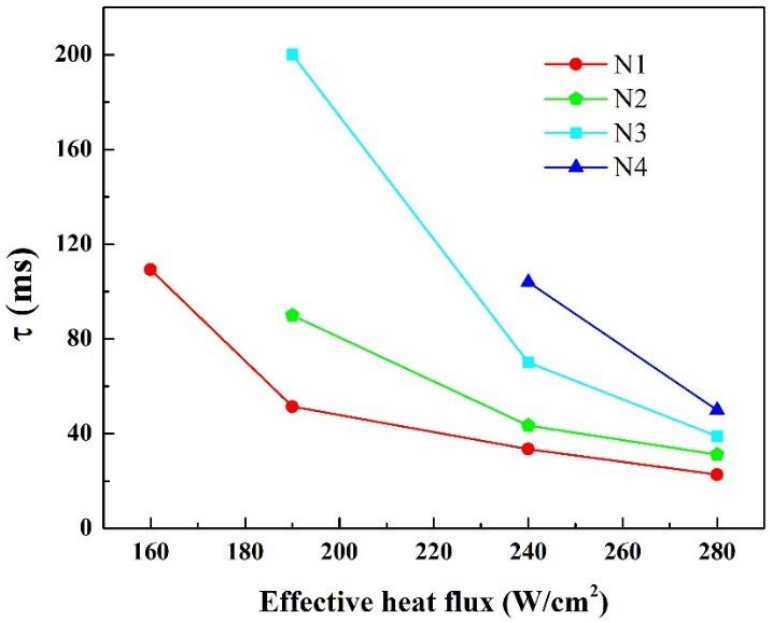

Figure 5.4 Effect of heat flux on time of the activation of four micronozzles (G=380 kg/m^{2}s)

5.2.2 Transient thermal performance under pulsed heating

5.2.2.1 Wall temperature time response of the device

The temperature was captured based on the electrical resistance so there is no current immediately preceding or following the application of the heating pulse. Therefore, the temperature response was only recorded during the heating period but cannot be measured before and after the pulse. The data was recorded after the system reached relative steady-state condition, which means the initial wall temperature or other parameters were repeatable during the recording duration.

Figure 5.5 illustrates a representative wall temperature time response to the square heat pulse with mass flux of 120 kg/m^{2}s and heat pulse amplitude of 170 W/cm^2. Under the sudden application of heat, the wall temperature increased immediately with a very high temperature changing rate. Then the temperature kept increasing with a relative moderate rate. With the increase of wall temperature, various flow regimes were observed with the development of flow boiling. Similar to Basu's [58] study, under sudden application of heat flux, the flow was initially in single-phase and the wall temperature response was characterized by a rapid temperature rise caused by conduction and single-phase convection. The flow was transferred to bubbly flow and rapidly switched to slug flow after the onsite of nucleate boiling (ONB) at 0.05 s. The slug flow was followed by the annular flow during 0.1-0.25 s. With the development of boiling regimes, the temperature increased with a gradually slower rate till the annular film dry-out happened. The obvious dry-out surface and lack of liquid supply were observed from 0.25 s, which characterized with a more rapid temperature rise.

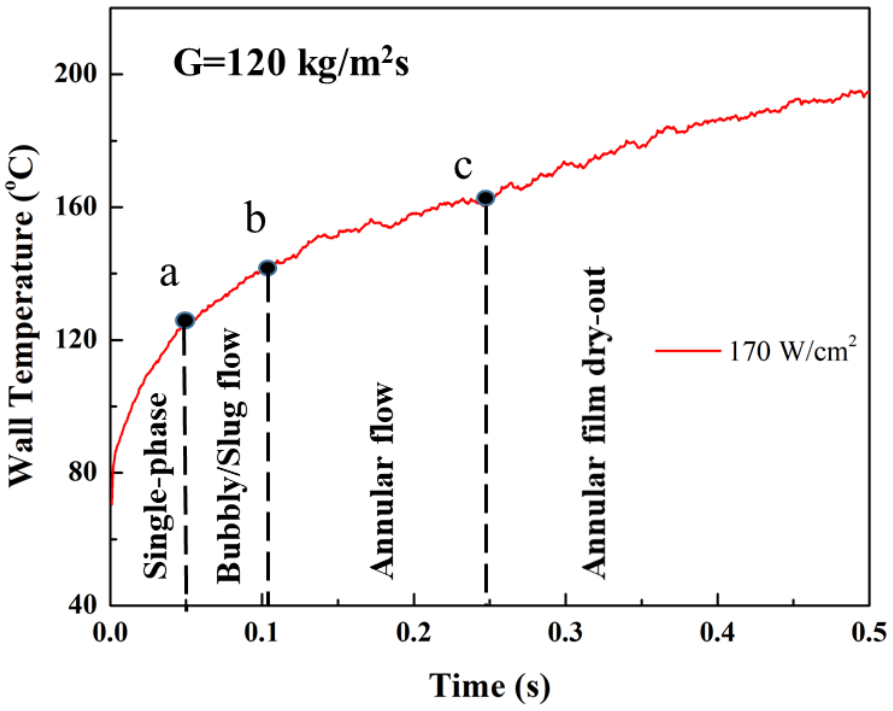

Figure 5.5 Wall temperature time response and flow regimes with heat flux of 170 W/cm^2 (G= 120 kg/m^{2}s)

5.2.2.2 Heat transfer coefficient

Figure 5.6 shows the wall temperature and corresponding overall HTC versus time with heat flux of 240 W/cm^2. Figure 5.7, Figure 5.8, and Figure 5.9 show the different flow regimes at the time marked in Figure 5.6. Under a constant heat flux, the overall HTCs achieved highest value in the earlier boiling stages, when nucleate boiling dominant (Figure 5.7). With the development of flow boiling, convective boiling and thin film evaporation became dominant and HTCs reduces significantly due to the formation of vapor slug induced by rapid increase of wall temperature. Figure 5.8 shows that the microchannel was occupied by annular flow at 0.1s. The jetting flow that came through the microchannel induced strong two-phase mixing and high frequency two phase oscillation. However, with

continually increase of wall temperature, partial dry-out and liquid detaching from the walls were observed in the downstream of the microchannel. Evaporation momentum force dominates over shear force in high heat flux ranges, which leaded to the liquid detaching and reduced heat transfer area. As a result, with the absence of two-phase mixing, liquid rewetting and force convection, the HTC after point (c) reduced compare to the stage between (b) and (c).

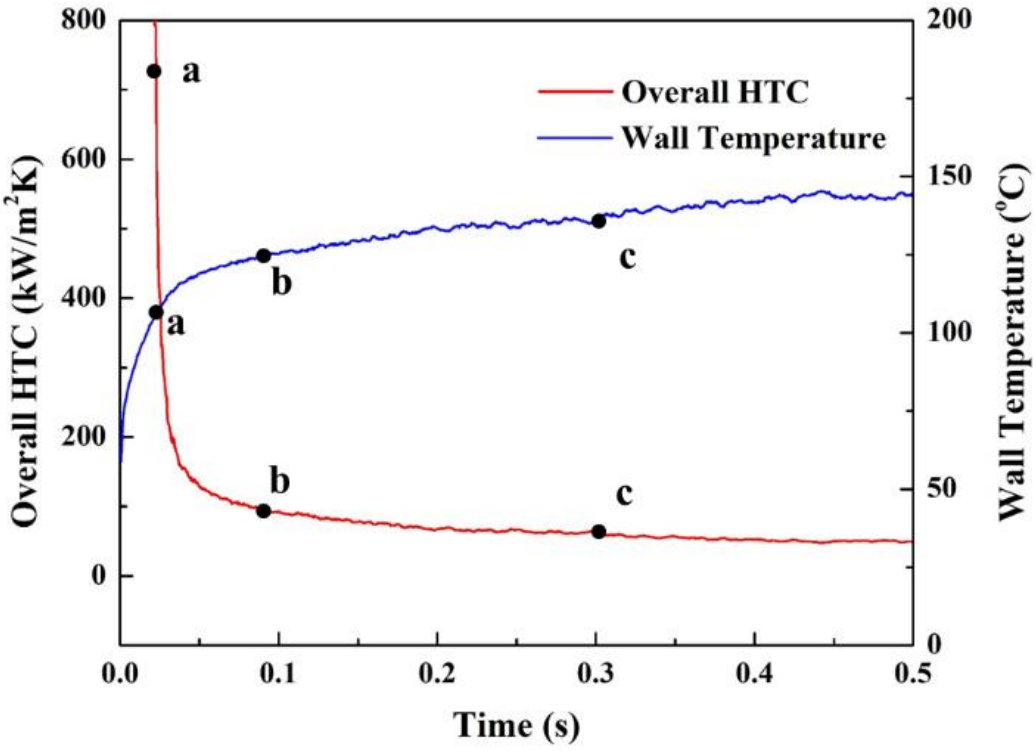

Figure 5.6 Wall temperature response and corresponding HTC at heat flux of 240 W/cm^2 (G=380 kg/m^{2}s)

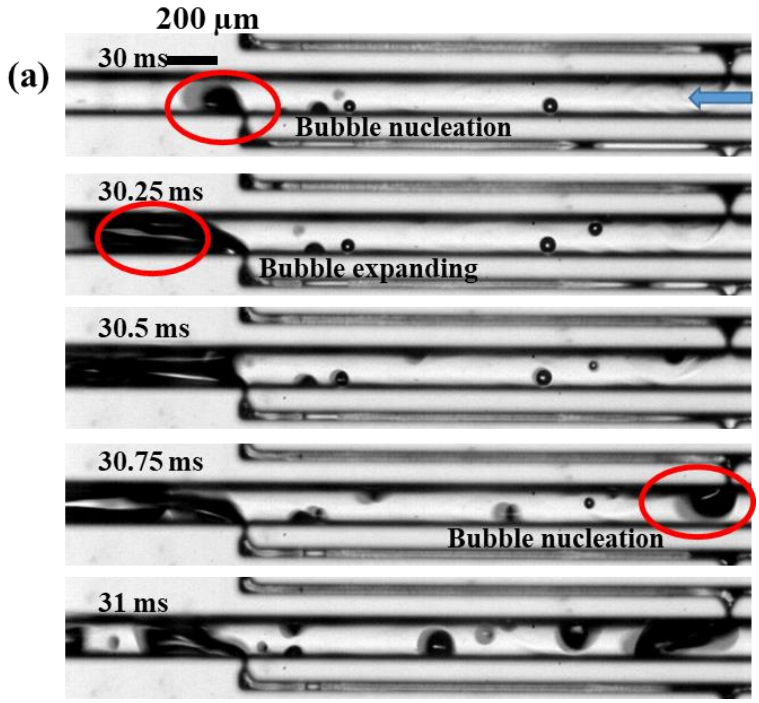

Figure 5.7 Corresponding boiling phenomenon to the points marked in Figure 5.6 – Point a

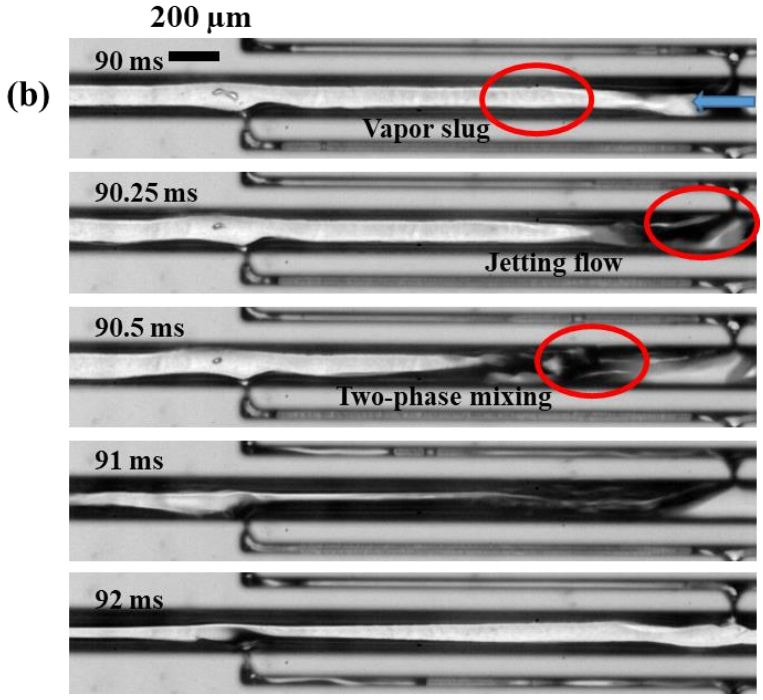

Figure 5.8 Corresponding boiling phenomenon to the points marked in Figure 5.6 – Point B

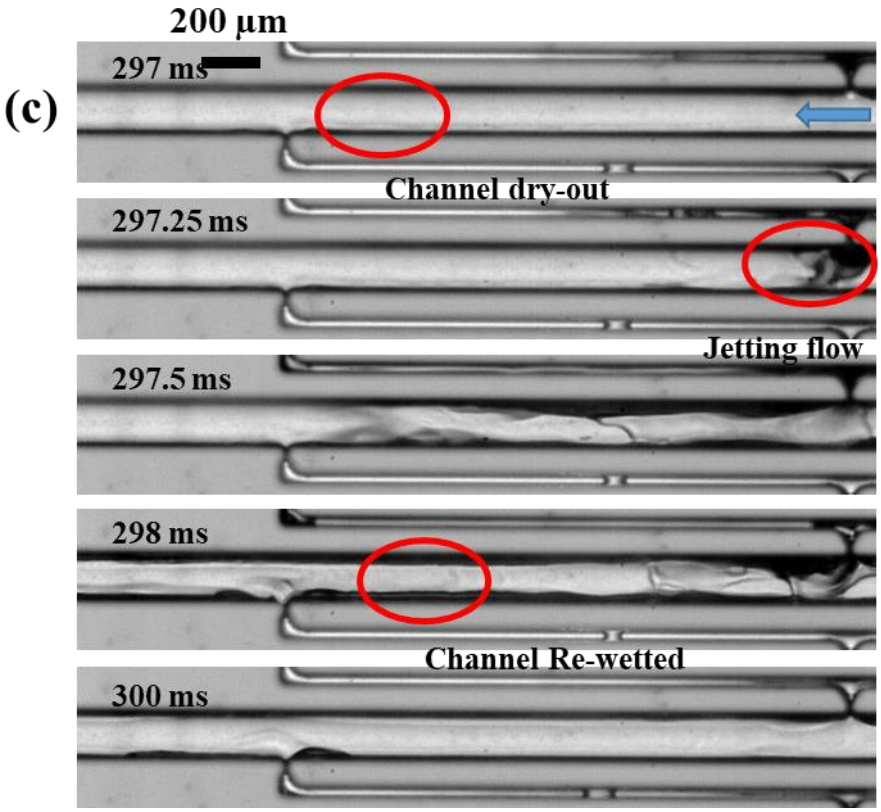

Figure 5.9 Corresponding boiling phenomenon to the points marked in Figure 5.6 – Point c

5.2.3 Effect of heat flux

Figure 5.10 shows the wall temperature time response to the heat pulse with various amplitude. The data were recorded from the lowest heat flux amplitude that can initiate nucleate boiling to the highest amplitude the microchannel device can work at. Clearly, higher heat flux leads to a high wall temperature. Under high heat flux, irregular fluctuation was noticed while the wall temperature is more stable under low heat flux.

A low heat flux (90 W/cm^2) and a high heat flux (170 W/cm^2) were selected to investigate difference on the flow boiling phenomenon. Figure 5.11 illustrates the wall temperature and temperature change rate response marked with turning points of different

flow regimes. Figure 5.13 shows the corresponding flow regimes captured synchronized with the power system. Figure 5.11 suggests that higher heat flux leads to a higher wall temperature and a higher temperature changing rate. The base temperature before the application of heat pulse is also higher. With the increasing of heat flux, it takes a shorter time to active the nucleate boiling. However, a longer time is required to reach steady state. For example, the tested device reached steady state at 0.2 s with heat flux of 90 W/cm^2 while it cannot reach steady state with 170 W/cm^2 before the end of the heat pulse. Moreover, the wall temperature at ONB is higher with higher heat flux, which leads to different behaviors of the two-phase flow. With lower heat input (90 W/cm^2), the nucleate boiling was triggered at 0.12 s. The bubble grew from the micronozzles and expanded in the downstream direction. Regular slug flow was formed after that, but no bubbly flow was observed (Figure 5.13 d). In comparison, for high heat flux (170 W/cm^2), ONB was triggered at a higher temperature. Bubbles grew from both the micronozzle and the microchannel (Figure 5.12 a) then departure and formed bubbly flow. Bubbly flow and slug flow dominated between 0.05 s and 0.1 s. High wall temperature can active the nucleation sites both on the micronozzle and the wall of the microchannel while low wall temperature can only active the nucleation sites on the micronozzle, which leads to the different behaviors of the flow regime under different heat loads. With the development of flow boiling, the temperature experienced a slight rise till the regular boiling was fully established (Figure 5.13 e) for low heat flux. After that the temperature change rate reduced to 0 and wall temperature tends to become flat, which was characterized with a regular annular flow. In comparison, under high heat flux, annular flow prevailed between 0.1-0.25 s and was followed by annular film dry-out happened after 0.25 s with gradually decreased

liquid supply. Critical heat flux (CHF) was triggered once there was not enough liquid supply and cause a more rapid temperature rise.

The HTCs under different heat pulse amplitudes were compared in Figure 5.14. Obviously, higher heat transfer rate was achieved by low heat pulse amplitude due to the earlier development of flow boiling. For example, as it was depicted in Figure 5.13, the microchannels were occupied by bubbly flow and slug flow at 0.12 s under heat pulse of 90 W/cm^2 while annular flow dominated at 0.12s under 170 W/cm^2, which leads to the discrepancy in heat transfer rate. Moreover, large dry-out surface appeared in the relative steady stage also leaded to the reduced HTC.

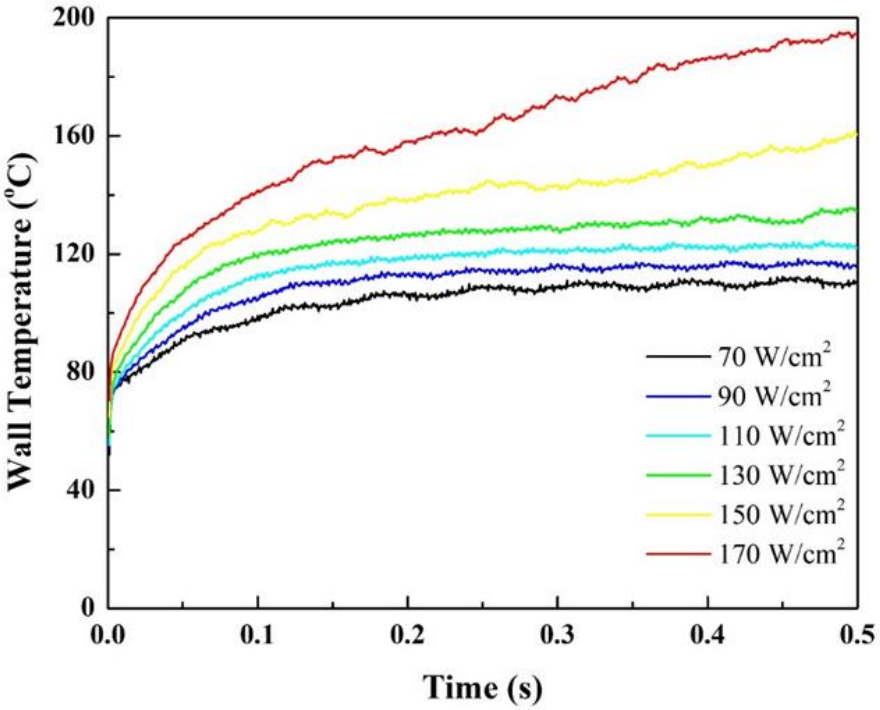

Figure 5.10 Wall temperature response under heat flux of 70 – 170 W/cm^2 with mass flux of 120 kg/m^{2}s

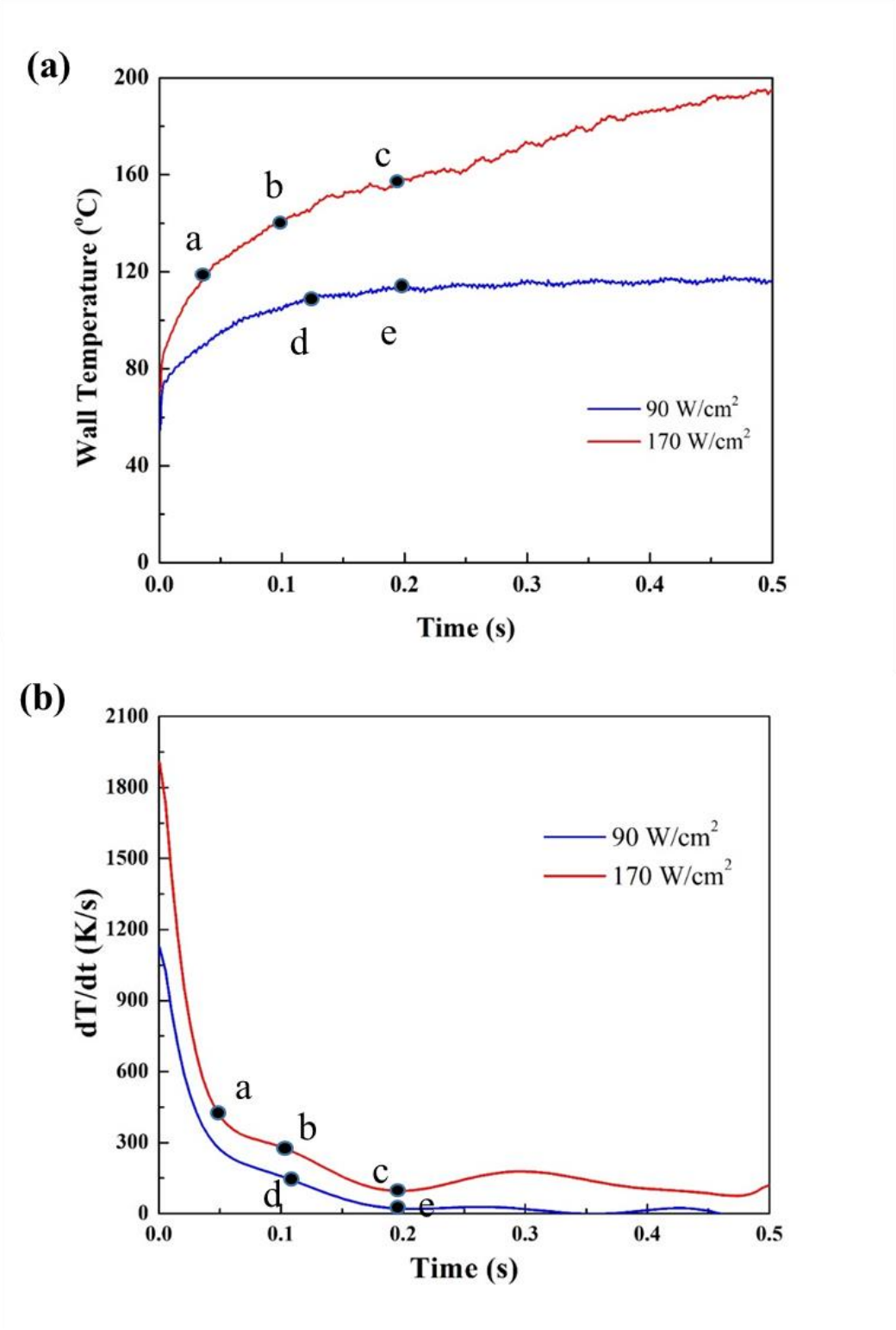

Figure 5.11 Wall temperature (a) and temperature changing rate (b) response to heat flux of 90 W/cm^2 and 170 W/cm^2 (G= 120 kg/m^{2}s)

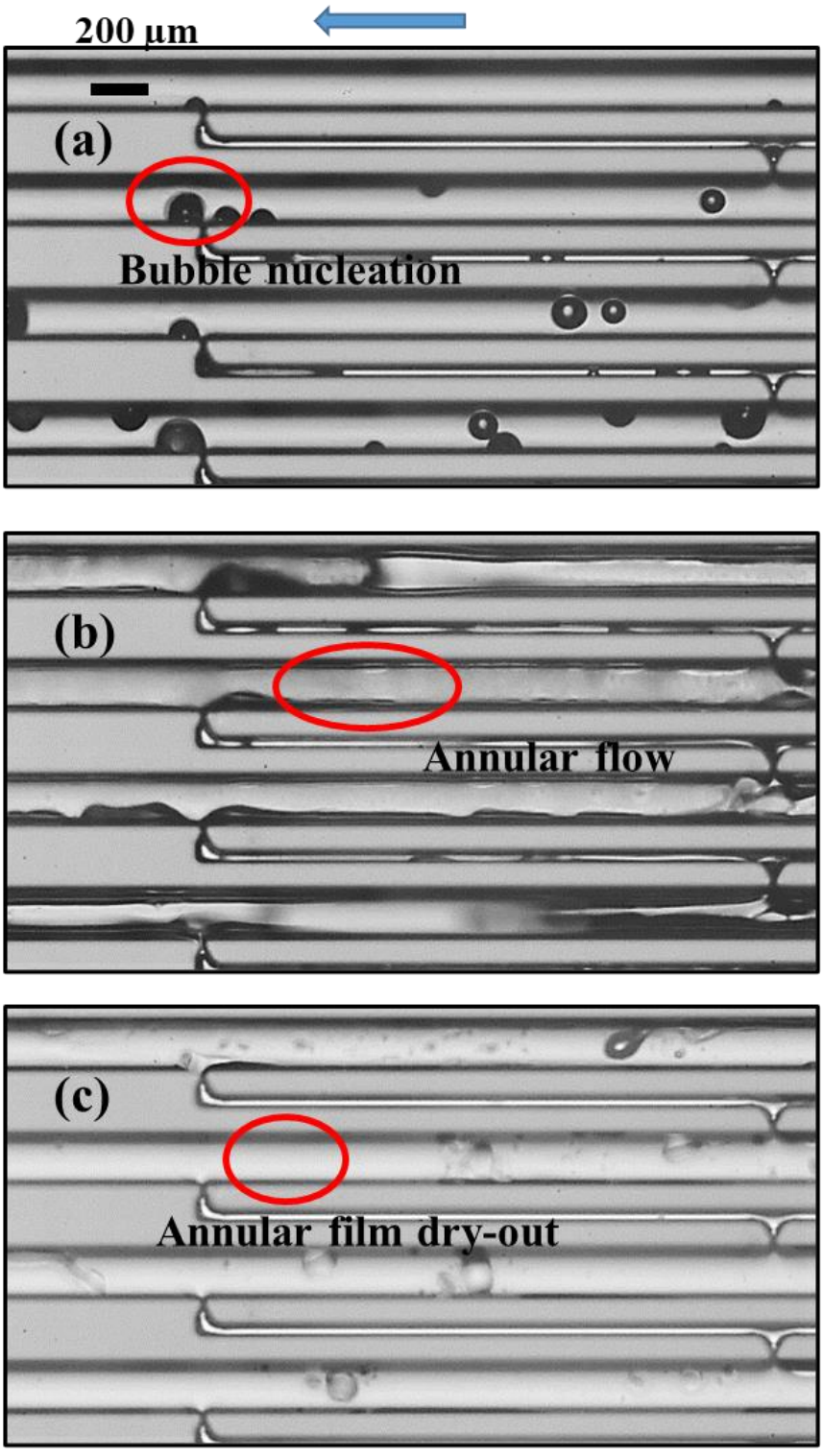

Figure 5.12 Flow regimes at turning point with heat flux of 170 W/cm^2 (a, b and c) (G= 120 kg/m^{2}s) (Scale bars are 200 µm)

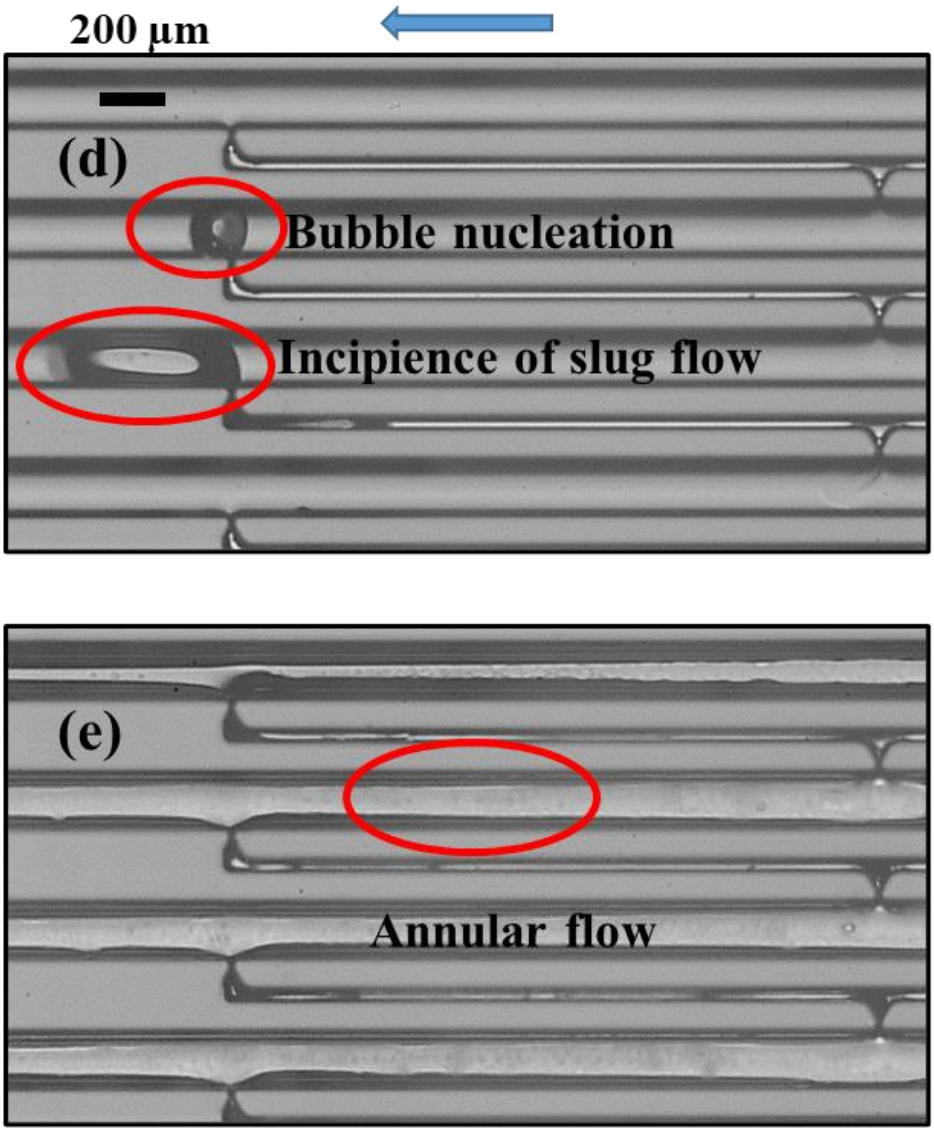

Figure 5.13 Flow regimes at turning point with heat flux of 90 W/cm2 (d and e) (G= 120 kg/m2s) (Scale bars are 200 µm)

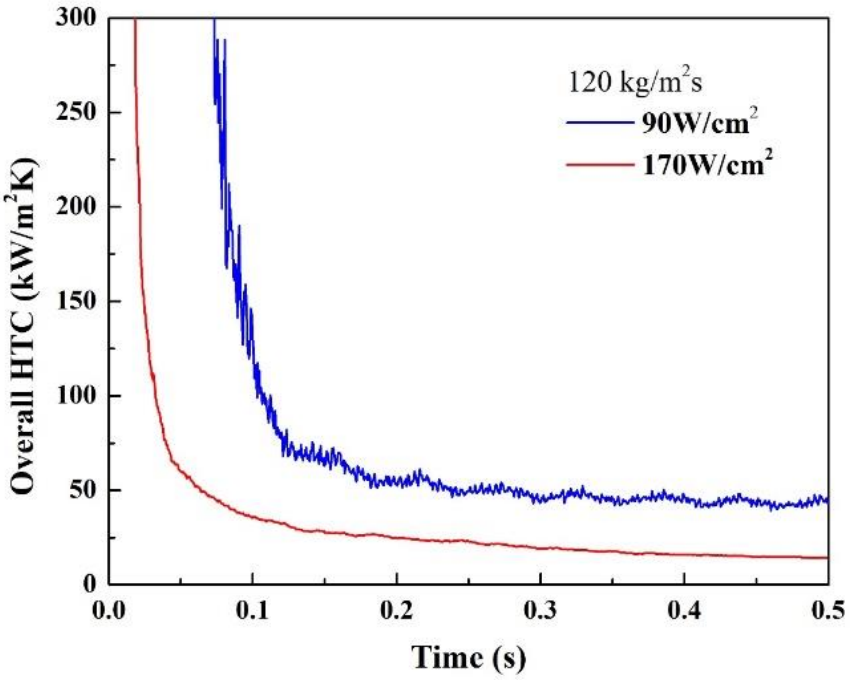

Figure 5.14 Overall HTC under different heat pulse amplitudes

5.2.4 Effects of mass flux

Figure 5.15 presents the wall temperature time response with two different mass fluxes. The heat flux was applied from the smallest value that triggers the flow boiling to the highest value before CHF. Apparently, with the higher mass flux, the tested device can work within a wider heat flux range. With the increase in mass flux, the convective heat transfer is enhanced, which leads to a lower wall temperature. Higher heat flux is required to trigger boiling with increased mass flux. Moreover, the device can work effectively under a higher heat flux, wall temperature, and temperature changing rate.

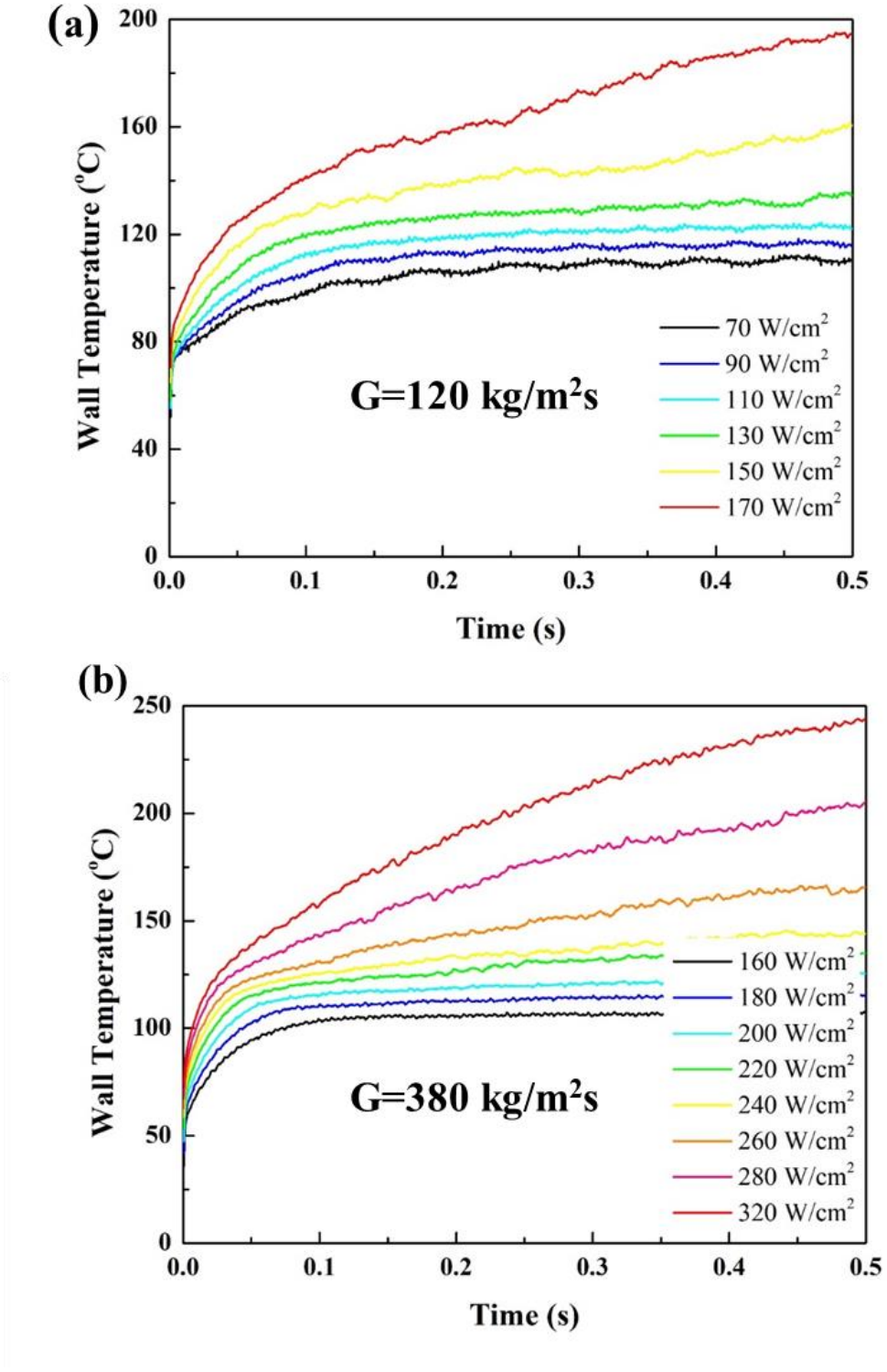

Figure 5.15 Wall temperature response under different heating loads with mass flux of (a) 120 kg/m^{2}s and (b) 380 kg/m^{2}s

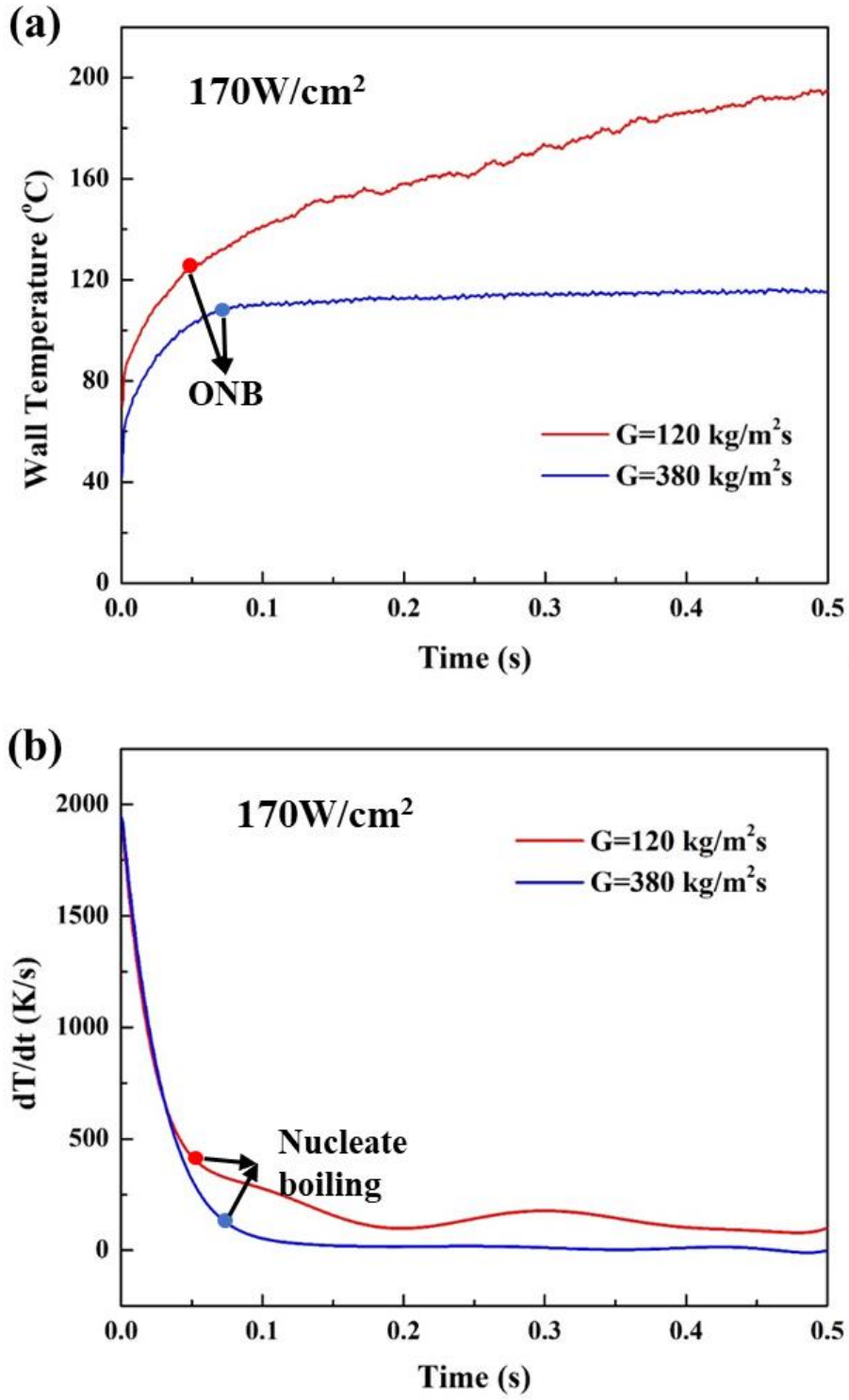

Figure 5.16 Wall temperature (a) and wall temperature increase rate (b) under two mass fluxes (q''=170W/cm^2)

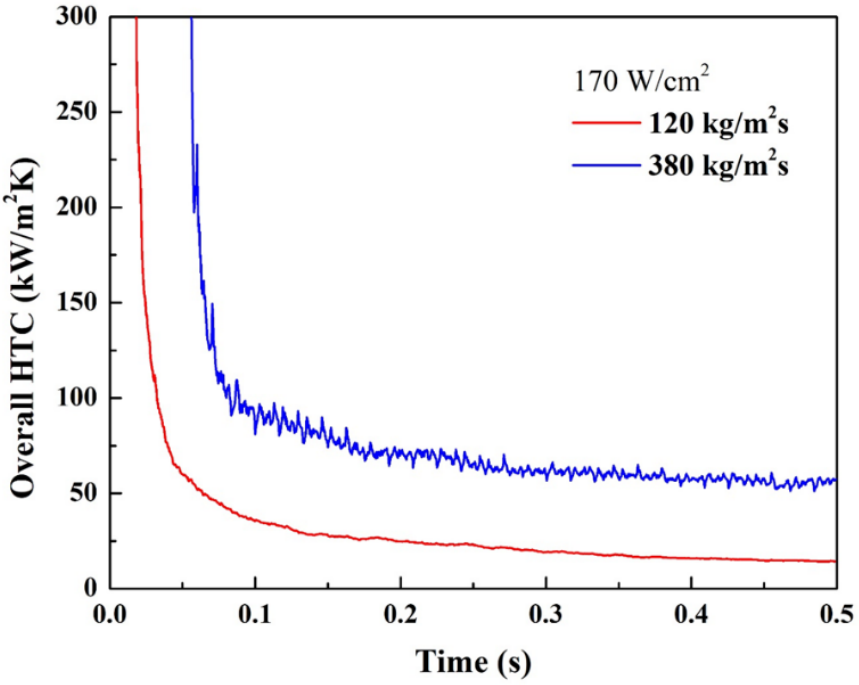

Figure 5.17 Comparison of HTCs with different mass flux

Figure 5.16 shows the wall temperature and wall temperature changing rate under a same heat flux (170 W/cm^2) with four mass flux. Obviously, the wall temperature was higher with reduced mass flux. As the wall superheat temperature increased, the active nucleation site density increased [58]. Therefore, the temperature that initiate nucleate boiling was higher with high mass flux. As shown in Figure 5.16 (b), there was not obvious discrepancy on the temperature changing rate between two mass flux in the single-phase stage. In comparison, the high mass flux showed a better heat transfer performance after ONB. It was explained in the steady state study of the present configuration that two-phase mixing was not so strong at low mass flux as high mass flux, which resulted in a reduced heat transfer performance, as it was depicted in Figure 5.17.

5.2.5 Enhanced transient flow boiling

With most of the mass flux, the flow in a convectional microchannel is dominated with laminar flow because of the shrink of size. The enhancement on mixing is an effective way to improve thermal performance of a microchannel. However, it is hard to achieve passive two-phase mixing during flow boiling in the microchannel. Various methods such as impingement jets [98-100] and embedded staggered herringbone mixers [101] were reported to effectively enhance mixing and increase heat transfer rate. The auxiliary channel and micronozzles that produce high efficiency two phase oscillation was first developed by Yang [25] and achieved a maximum improvement of 149% on HTC compared to the microchannel with inlet restrictors. However, it limited the mixing in the downstream of the microchannel only. The design in this study has successfully extended the two phase oscillation to the entire microchannels and achieved significant enhancement in both HTC and CHF based on our steady state study [26]. To study the transient enhancement under heat pulse, the results were compared with that of plain-wall microchannels.

As is shown in Figure 5.19, the wall temperature of the present design is much lower than that of plain-wall microchannel under the same heat flux, especially during fully developed flow boiling stage. Figure 5.19 suggested that it did not show obvious difference in both wall temperature and temperature change rate in the single-phase stage. With the development of flow boiling, the present configuration showed the better cooling performance with low wall temperature and low temperature change rate, especially in the convective boiling stage. Moreover, the plain-wall microchannels experienced a severe temperature oscillation caused by periodic liquid dry-out. By contract, the two-phase

mixing induced by the micronozzles in the present design can effectively reduce the instability and resulted in a more uniform and stable temperature response.

Figure 5.20 and Figure 5.21 shows the comparison of the HTCs of the present design and plain-wall microchannels at mass flux of 120 kg/m^{2}s and 380 kg/m^{2}s. Two heat fluxes were selected to show the enhancement of the present design at each mass flux. According to the data plots in Figure 5.20, at the same heat flux, the boiling in the plain-wall microchannels was triggered earlier because of high wall temperature. Significant enhancements were observed at all the boiling stages under all the heat fluxes. At mass flux of 120 kg/m^{2}s and a low heat flux of 90 W/cm^2, the flow in the microchannels was initially in slug flow dominated with nucleate boiling and followed with annular flow dominated with convective boiling. The increased nucleation site density contributed to the improvement in nucleate boiling and promoted two-phase mixing contributed to the enhanced convective boiling. An average enhancement of 141% was achieved at the fully developed boiling stage. A higher enhancement of 162% was achieved with higher heat flux. With the increase in heat flux, the two-phase mixing extended to upstream and further enhanced the heat transfer performance. With a mass flux of 380 kg/m^{2}s, the boiling in the plain-wall microchannels was triggered by a lowest heat flux of 140 W/cm^2 while in the present design it was triggered by a lowest heat flux of 160 W/cm^2. As a result, when the present design was occupied with bubbly flow and slug flow under heat flux of 160 W/cm^2, the plain-wall microchannels have achieved fully developed boiling stage. Obviously, the HTCs based on nucleate boiling in the present design was much higher than that based on convective boiling in plain-wall microchannels. When the heat flux was increased to 180 W/cm^2, the boiling in the plain-wall microchannel has reached the threshold to trigger CHF.

However, in the present design, the fully developed boiling was just triggered and strong two-phase mixing was generated. As a result, a more significant enhancement was observed.

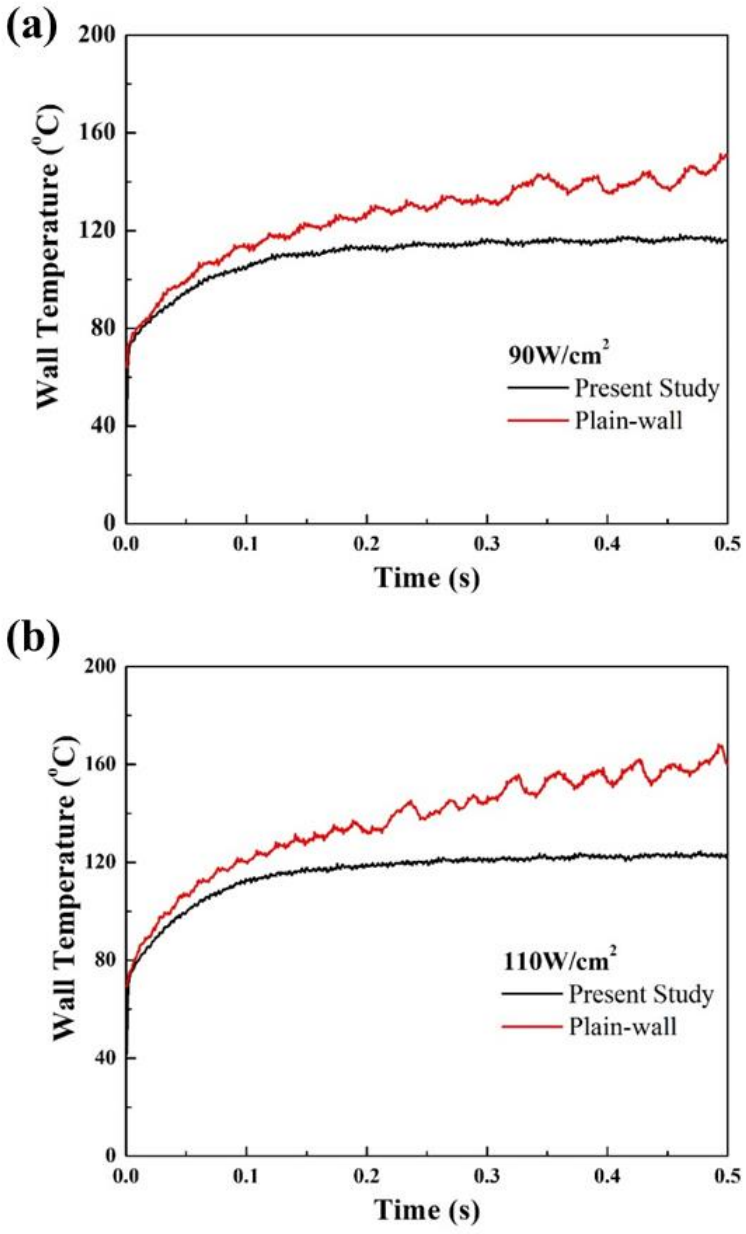

Figure 5.18 Compare of wall temperature time response of plain-wall microchanels and the present ocnfigureation under heat flux of 90W/cm^2 (a) and 110 W/cm^2 (b) (G=120 kg/m^{2}s)

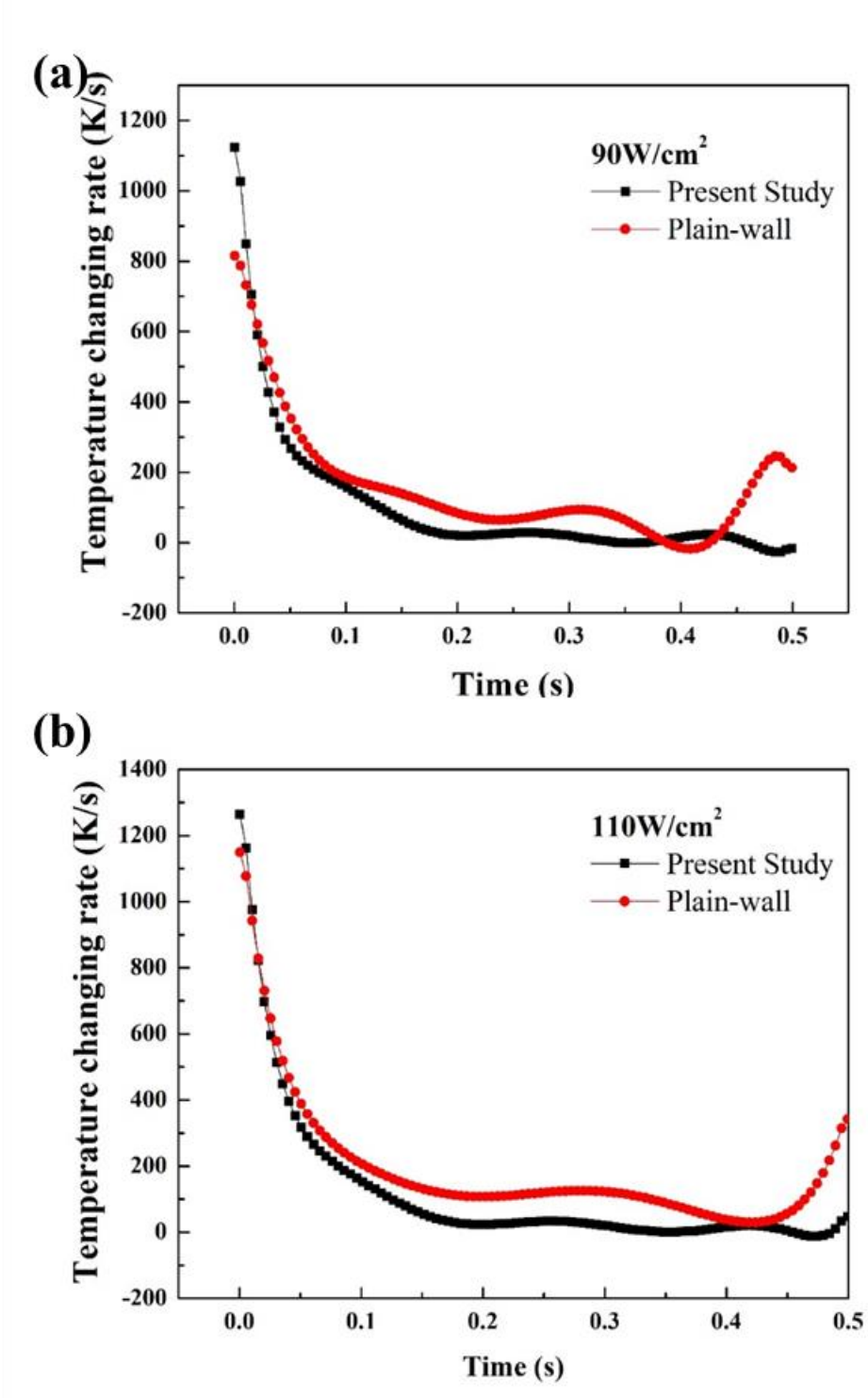

Figure 5.19 Compare of wall temperature change rate time response of plain-wall microchanels and the present ocnfigureation under heat flux of 90W/cm2 (a) and 110 W/cm2 (b) (G=120 kg/m2s)

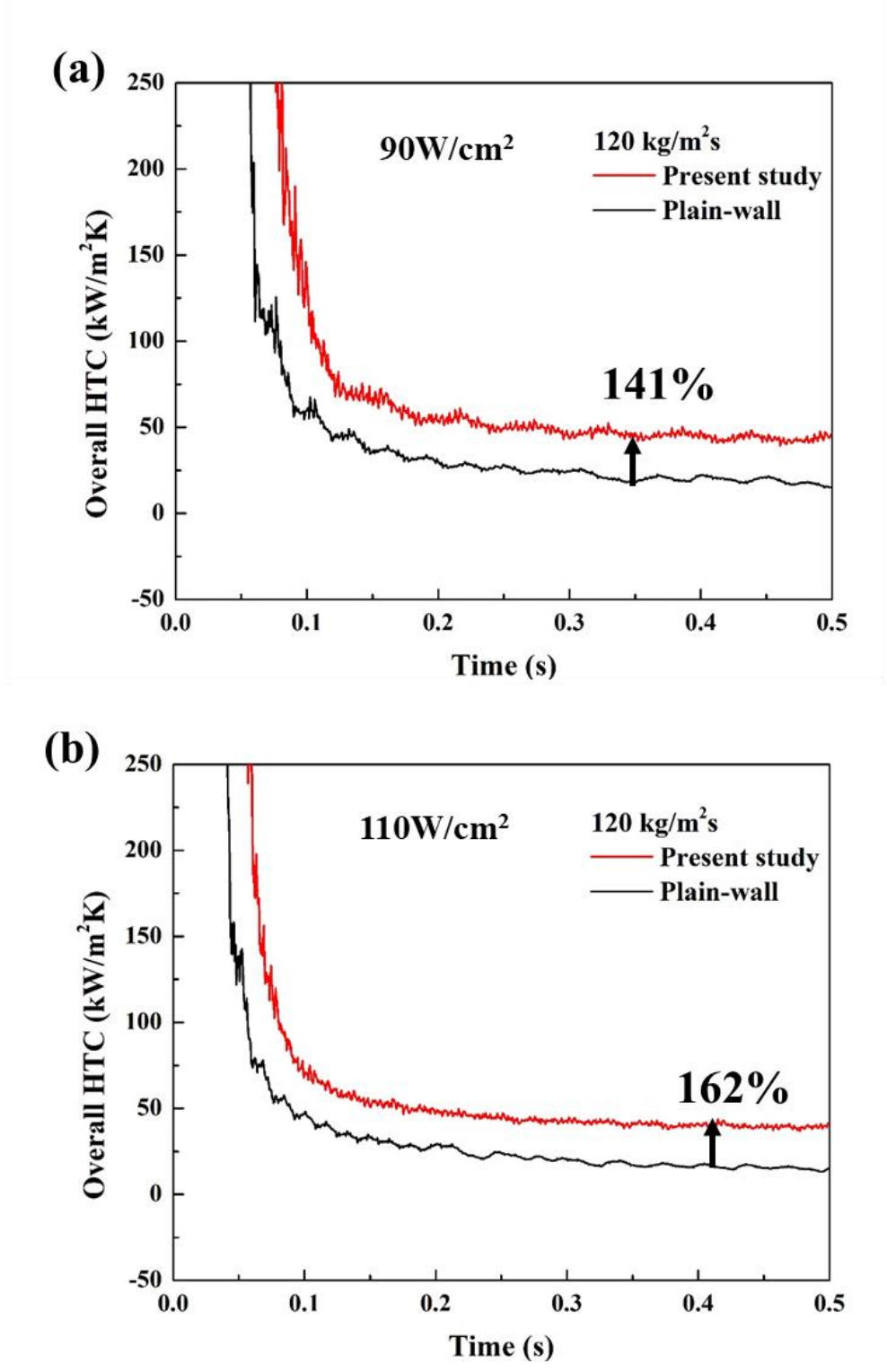

Figure 5.20 The enhancement in HTC of the present configuration at mass flux of 120 kg/m2s

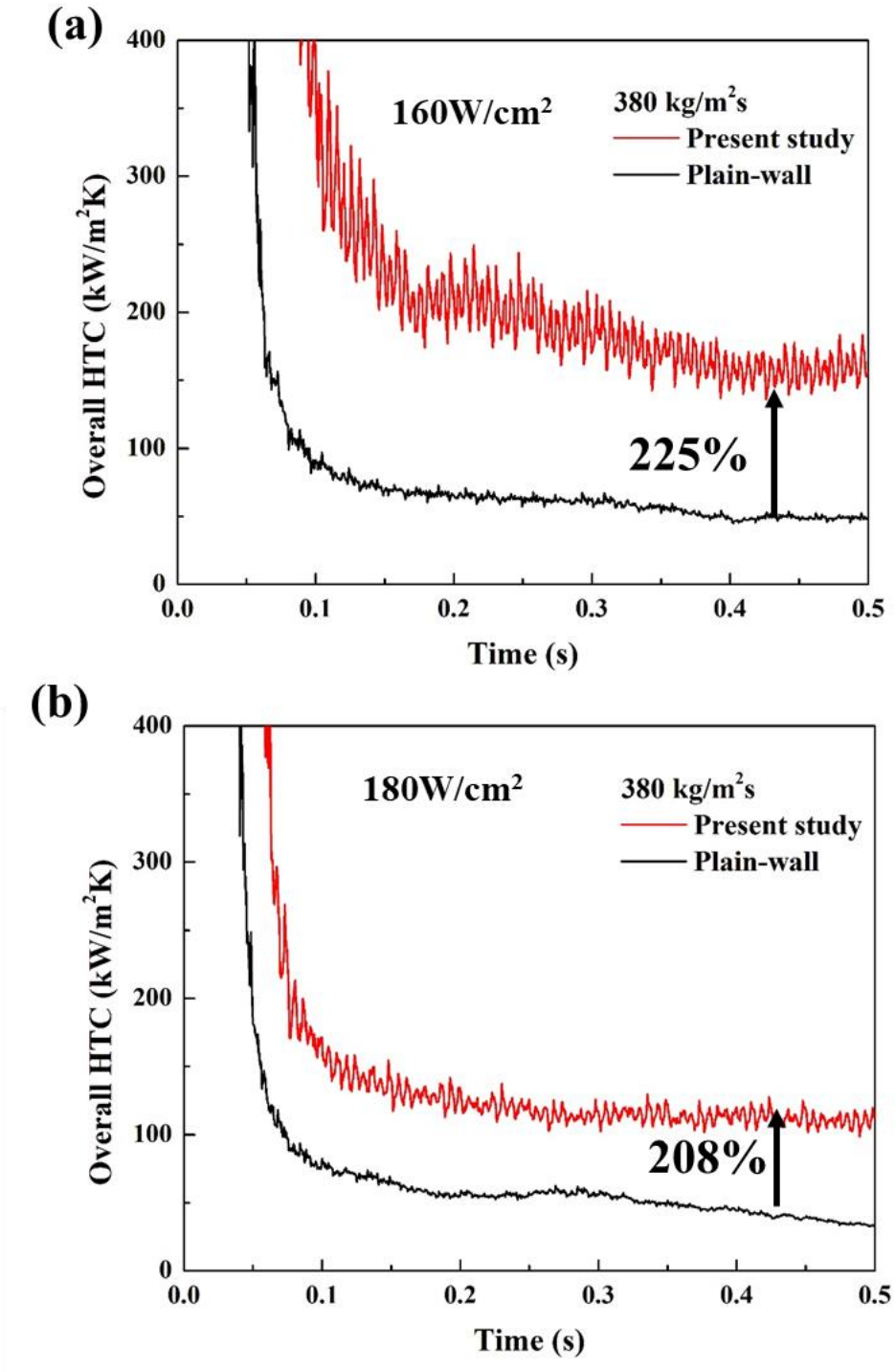

Figure 5.21 The enhancement in HTC of the present configuration at mass flux of 380 kg/m2s

5.3 Conclusion

The transient performance of the flow boiling in the microchannel with auxiliary channels and multiple micronozzles was investigated. The heat was applied to the system in the form of square heat pulse. The thermal characters of the tested device were captured and the video was recorded synchronously.

- The wall temperature and wall temperature increase rate were captured. Various flow regimes, single-phase flow, bubbly flow, slug flow and annular flow were observed with the development of flow boiling. Annular film dry-out characterized by a rapid temperature increase was observed at high heat flux.
- The HTCs were calculated and matched with different boiling regimes. It was noticed that the greatest variation of HTCs during a heating period was found during nucleate boiling stage and it decreased with the development of the flow boiling.
- The effects of heat flux and mass flux were investigated. The wall temperature is more stable under lower heat flux and the HTC is also higher. Under a same heat flux, the HTC is higher with high mass flux.
- Compared to the plain-wall microchannel, the present design showed significant enhancement on HTCs. Moreover, the enhancement is higher with high mass flux and the maximum enhancement achieved 225%.

CHAPTER 6 TRANSIENT STUDY OF FLOW BOILING IN MICROCHANNELS USING AUXILIARY CHANNELS AND MULTIPLE MICRONOZZLES UNDER DYNAMIC HEAT LOADS – HFE-7100

6.1 Introduction

For the safety and reliability of the electronic cooling system, the highly wetting dielectric coolant is one of the most desirable working fluids for high-power density electronics cooling [31, 58, 102, 103]. The thermal conductivity and latent heat of HFE-7100 are 0.069 W/m·K and 111.6 kJ/kg, which make it challenging to significantly increase the thermal performance compared to water. Moreover, due to the low surface tension of the dielectric fluids, is difficult to maintain the thin liquid film on the solid wall in the flow boiling conditions. The liquid film tends to be blown away from the heating surface by the vapor flow in smooth wall microchannels without surface enhancements. Therefore, it is difficult to sustain the efficient heat transfer mechanisms such as thin-film evaporation, convective boiling, and nucleate boiling. As a result, it is challenging to enhance the flow boiling performance in microchannels.

Numerous techniques have been developed to improve the thermal performances of heat transfer rate of flow boiling in microchannels on dielectric fluids. For example, modification of surface topology [31, 32], suppression of vapor flow reversal [32, 104],

delay of nucleate boiling and reduction of bubble size with pre-cooled coolant [104].

Transient microscale flow boiling heat transfer characteristics of HFE-7000 in a single microchannel were experimentally investigated by Basu [58]. A temperature drop or spike were reported at the onsite of the boiling phenomenon and the wall superheat temperature at this point was very high due to low contact angle and high heating rate. The wall superheat at the onset conditions increased with increasing heat flux. The time taken to initiate boiling was studied. It was found that the heat flux affected the time significantly in low heat flux range and less variation was observed in the high heat flux range. Chen [67] also investigated the boiling incipience time with water as working liquid. Similarly, decreased rapidly initially with increasing heat flux but quickly reached a constant value at higher heat fluxes.

6.2 Experimental procedure

This study utilized the same test section as it was described in the transient study with DI water as coolant. The test setup consists of an optical imaging system, a data acquisition unit, and an open coolant loop. The pressurized DI water tank was degassed with heat supply to maintain the water temperature to 40 ^{o}C prior to the test. With the pumping power of compressed nitrogen and a flow meter of Krohne Optimass 3300c with a ± 0.1% resolution (density with ± 2 kg/m^3), the DI water flowed through the system at a constant mass flow rate. Inlet/outlet pressure and temperature were measured with pressure transducers and K-type thermocouples respectively. The average temperature of the heater was calculated with the correlation obtained with calibration prior to the test. A high precision digital programmable power supply (BK-PRECISION XLN10014) was used to

supply electrical power. The voltage applied to the microheater was measured by an Agilent digital multimeter (34972A). A wave form generator was used to trigger the heating signal periodically. A constant resistant was added to the electric circuit and the voltage applied to the constant resistant was captured with high frequence. Flow rate, local pressure, inlet, and outlet temperature, and voltage and current were recorded by a customized data acquisition system developed from NI LabVIEW®. A visualization system comprised of a high-speed camera (Phantom V 7.3) and an Olympus microscope (BX-51) with 400× amplifications were used to study the two-phase flow patterns. The high-speed camera and data acquisition system was triggered at the same time to obtain synchronous data and video. The experimental data were collected with frequency of 2000 Hz and the high-speed images were captured at 4000 Hz. All measurements were carried out at 1 atm ambient pressure and room temperature of ~18 °C and all data were collected by an Agilent 34972A data acquisition system.

Under the control of waveform generator, periodic heat flux was applied to the tested device at a frequency of 0.25 Hz and duty of 25%, which means the heat was on for 1 s and off for 3 s in a heating period. The heat flux amplitude was increased gradually till the condition just before the incipience of flow boiling. The experimental data started to be collected once the heat pulse amplitude was increased to the lowest value that can trigger the flow boiling.

6.3 Results and discussions

An experimental study was conducted to determine the parametric trends governing flow boiling of HFE-7100 at microscale for transient heat loads applied in the form of a

step change in heat flux. A step change causes an instant increase of heat flux applied to the tested system from zero to the maximum value and then remained constant for a settled heating period. The tests were run at different heat flux (112-186 W/cm^2), constant mass flux of 463 kg/m^{2}s, and settled heating period of 1 s. The temperature response was the primary studied parameters and the synchronously captured high-speed video image was matched. Time taken to initiate boiling and wall temperature at that instant were determined at various transient operating conditions. Onset of boiling was followed by a transitional boiling regime that then led to a vigorous boiling regime. The effects of the heat pulse amplitude on the development of different boiling regimes were determined.

6.3.1 Wall temperature response

6.3.1.1 Representative wall temperature response – high heat flux

Figure 6.1 illustrates a representative wall temperature time response to a step change with high heat flux of 142 W/cm^2. Before the onsite of boiling, the wall temperature increased rapidly due to single-phase conduction. A slower increase of wall temperature was noticed caused by convection cooling. An obvious temperature increase was observed at the incipience of flow boiling, which helps to determine the time that taken to initiate boiling. The temperature spike was followed by a gradually slowed rise caused by increased two-phase heat transfer.

A visualization study was carried out to explain the dynamic behaviors of the wall temperature. As it is shown in Figure 6.2, before the onsite of boiling at 231 ms, the flow was in single phase, where single-phase conduction and convection were the primary heat transfer mechanisms. Different form the gradually development of flow boiling of DI water, the boiling of HFE-7100 started with a jetting flow generated by the micronozzles and

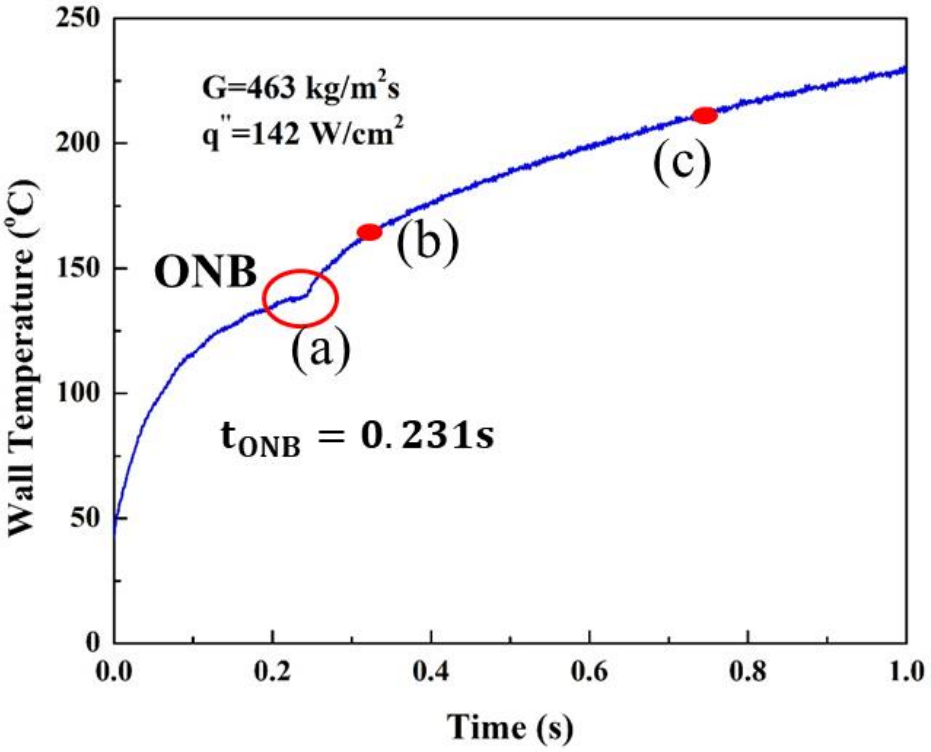

Figure 6.1 Wall temperature responses marked with virous boiling stages (a) ONB (b) Developed boiling (c) Rewetting crisis (high heat flux)

expanded rapidly to the entire microchannels. Strong mixing was observed at 231.75 ms. With the quick increase of vapor volume, obvious vapor layer between the liquid and the wall was observed at 235 ms, which leaded the temperature spike. With the further developed of the flow boiling, strong two-phase mixing (Figure 6.3) induced by the jetting flow came through micronozzles significantly enhance the heat transfer performance and decreased the temperature increase rate. Figure 6.4 shows the boiling phenomena in the late boiling stage. The local dry-out occurred periodically owing to the limit liquid supply from the main channel. The local rewetting was significantly enhanced by the jetting flow from the auxiliary channel. However, local dry-out occurred in the auxiliary channel occasionally and resulted in continually increase of wall temperature.

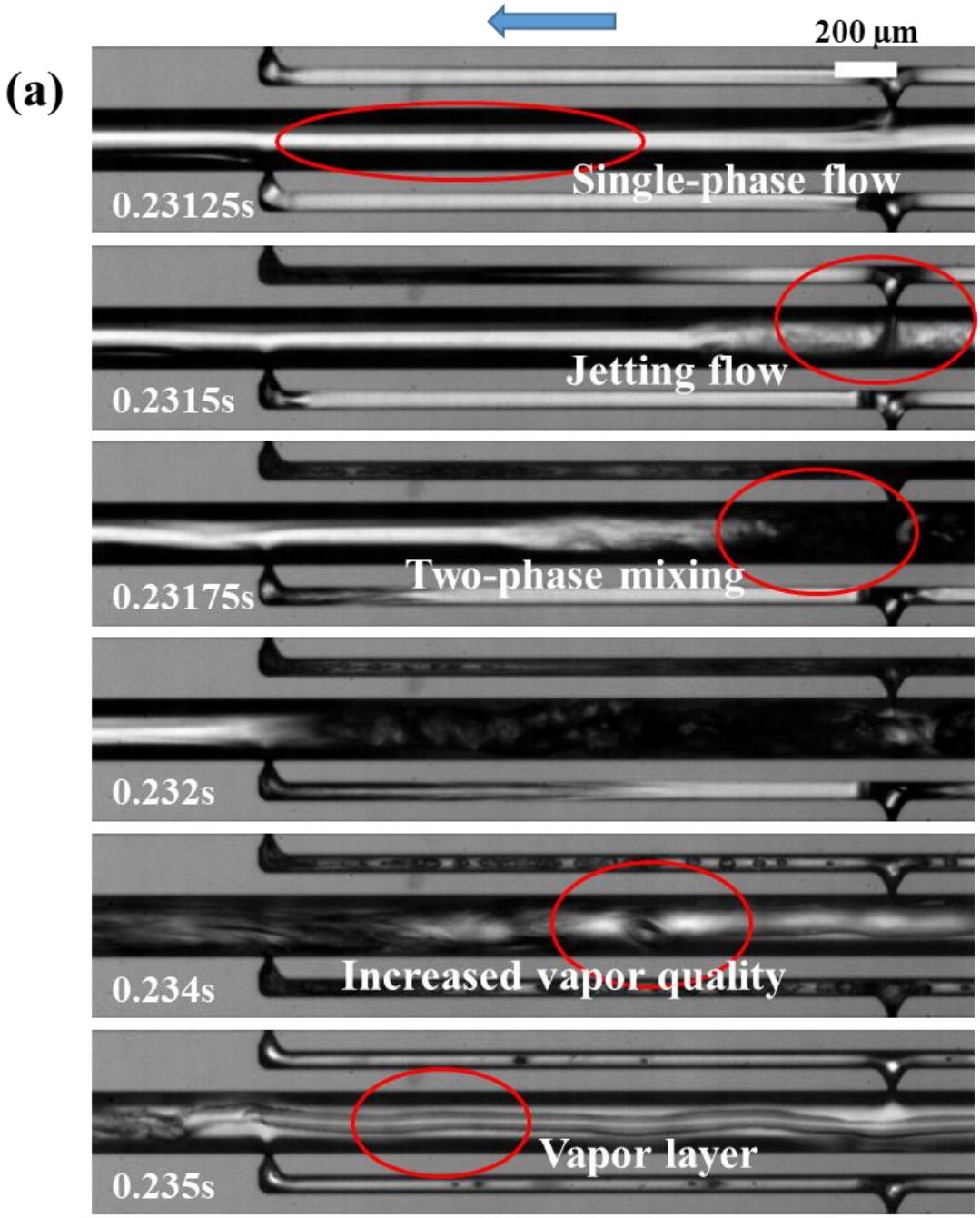

Figure 6.2 Visualization study at the corresponding points (a) marked in Figure 6.1 (downstream)

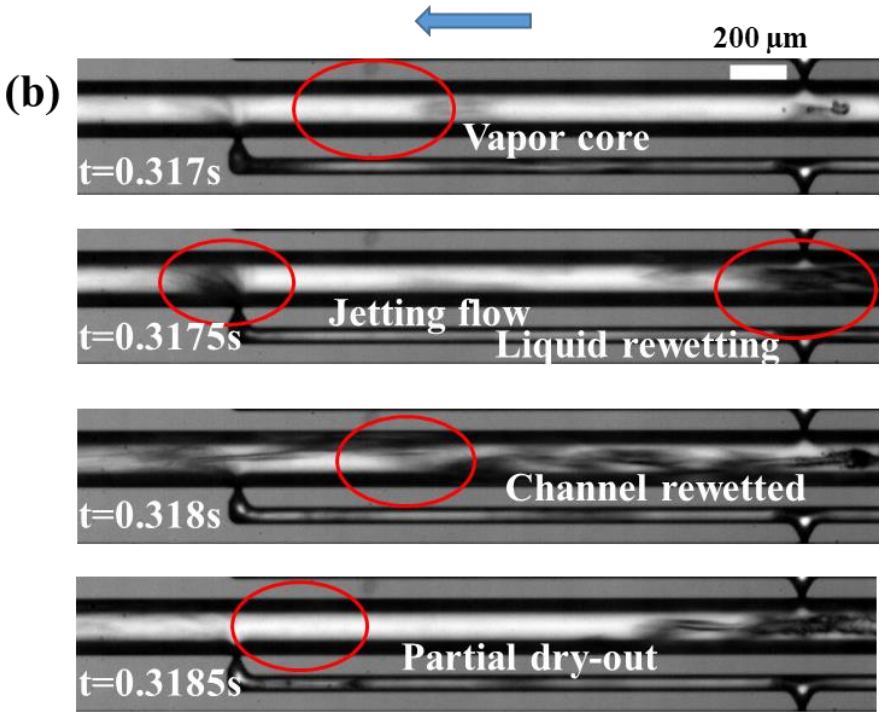

Figure 6.3 Visualization study at the corresponding points (b) marked in Figure 6.1 (downstream)

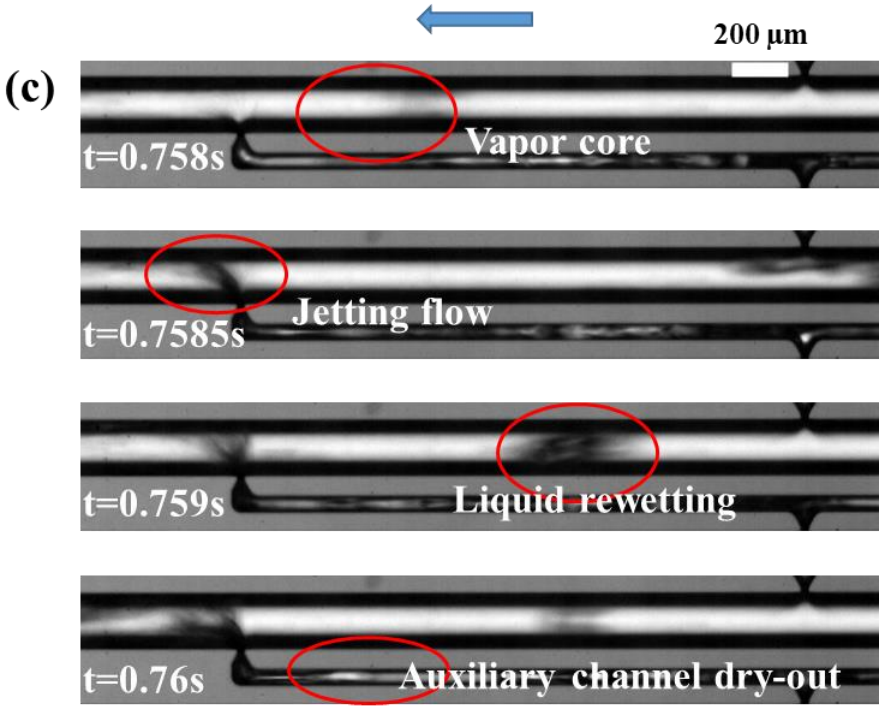

Figure 6.4 Visualization study at the corresponding points (c) marked in Figure 6.1 (downstream)

6.3.1.2 Representative wall temperature response – Low heat flux

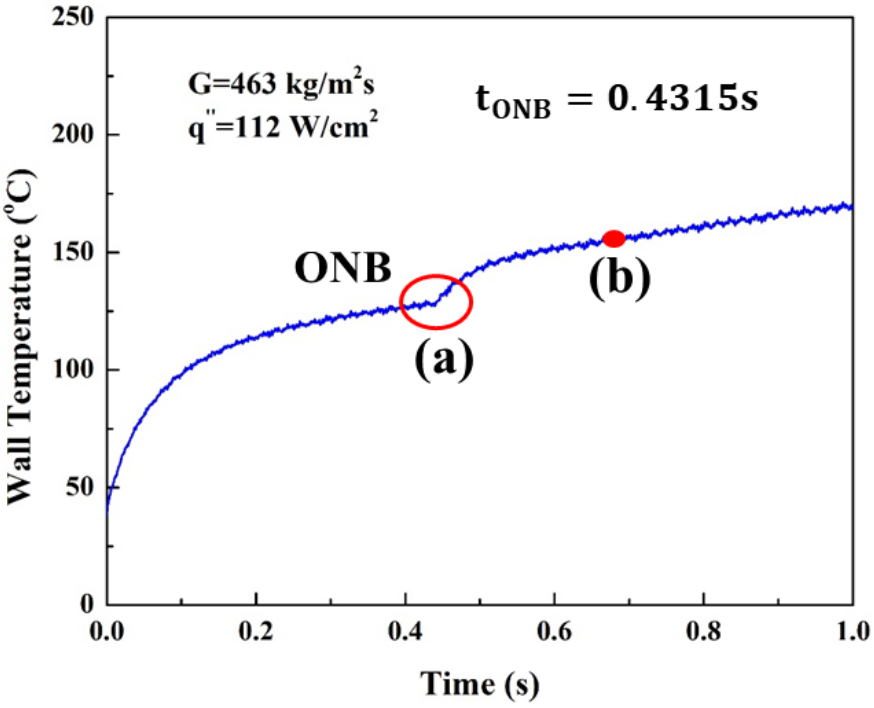

Figure 6.5 Wall temperature response marked with various boiling stage: (a) Onsite of boiling (b) developed boiling (low heat flux)

Like the wall temperature response under high heat flux, a temperature spike was also noticed at the instant of onsite of flow boiling. As it is shown in Figure 6.5, the boiling was initiated at 431.5ms. Figure 6.6 (a) shows that the bubble slug expanded to the upstream in 0.5 ms, which shows disparity in the two working fluids. Similarly, the jetting flow induced by the first micronozzle neat the inlet cracked the bubble slug and generated strong two-phase mixing, which significantly enhanced the thermal performance of the cooling device. After the boiling was fully developed along the entire microchannel, regular nucleate boiling phenomena was observed near the inlet. Figure 6.6 (b) shows the bubble nucleation, bubble growth, bubble expanding process. Once the bubble expanded

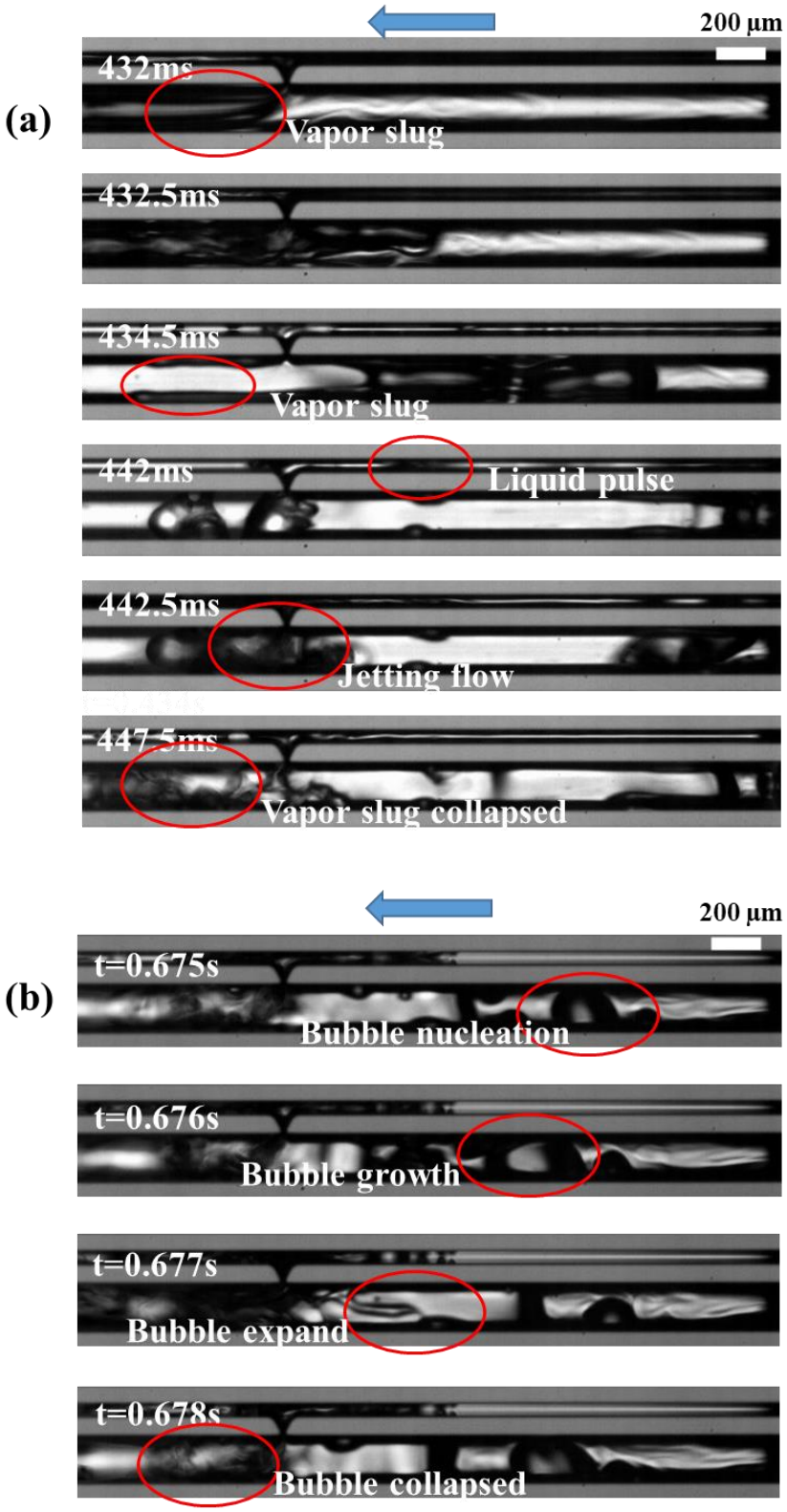

Figure 6.6 Visualization study at the corresponding points marked in Figure 6.5 (upstream)

to the first micronozzle, the jetting flow from the auxiliary channel cracked the bubble slug. The high-frequency jetting flow enable the continuous global liquid supply.

6.3.1.3 Effects of heat flux

Figure 6.7 shows the wall temperature response under heat flux of 112-186 W/cm^2. Different from Basu's study [58], which presented temperature drop at onsite of boiling under low heat flux and temperature spike under high heat flux, the present study shows consistent trend on wall temperature response under different heat flux. The temperature spike happened under all heat fluxes. The highest wall temperature achieved in this study was 300 ºC, which means that the present configuration can maintain efficient rewetting under high wall temperature.

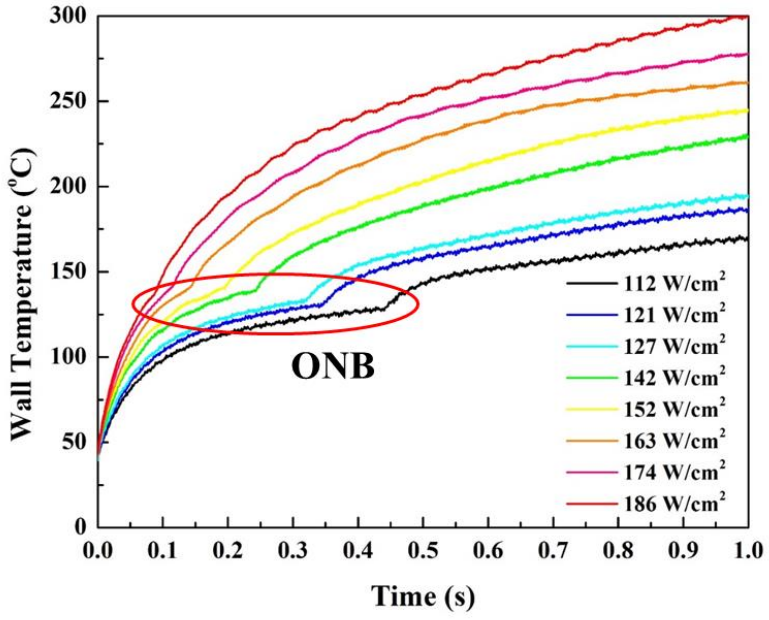

Figure 6.7 Wall temperature response under wide range of heat flux (112 W/cm^2 - 186 W/cm^2)

6.3.2 Onsite of the flow boiling

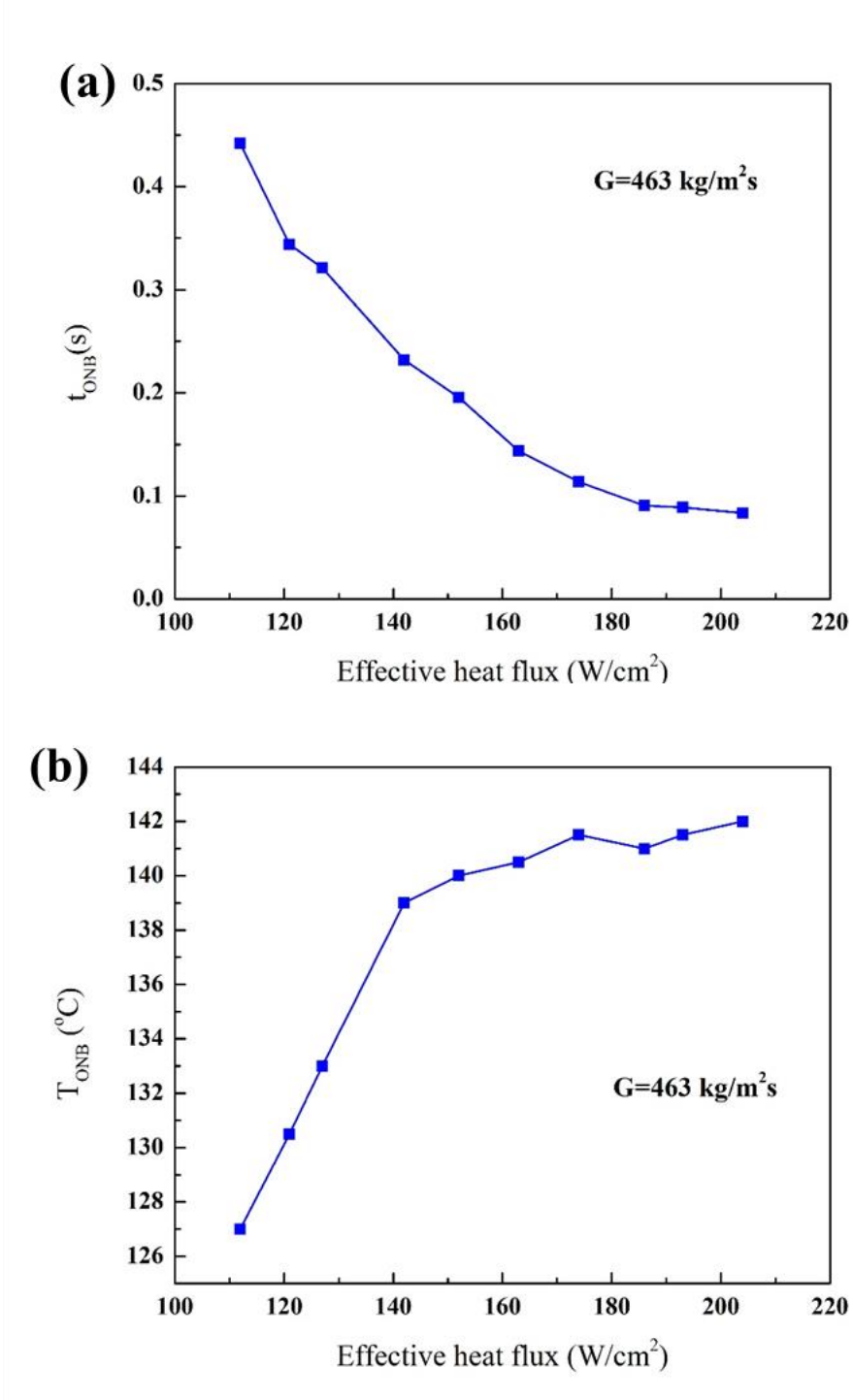

Figure 6.8 The effect of heat flux on (a) time that taken to initiate the boiling (b) wall temperature at the onsite of boiling

As it was discussed previously, the dynamic behaviors of wall temperature were determined by the boiling regime. From a transient perspective, it is important to determine the initial conditions of boiling, such as the time taken to initiate the flow boiling and the wall temperature at that instant. The heat flux has significant effects on the boiling initiate time and temperature. As it was described in Figure 6.8, with the increase in the heat pulse amplitude, less time was required to trigger the flow boiling. When the heat flux was increased to very high value (186 W/cm^2), the boiling initiate time started to converge to a relative stable value. Opposite trend was observed on the onsite boiling temperature, which increase with the increase in heat flux. Similarly, the temperature also reached a stable value when the heat flux was increased higher than 174 W/cm^2. The similar behaviors of the time taken to initiate flow boiling and wall temperature at onsite of flow boiling were reported by Basu [58] and Chen [67].

6.4 Summary

An experimental study was conducted to investigate heat transfer characteristics of a microchannel heat sink with micronozzles under heat pulse at 0.25 Hz for flow boiling of HFE-7100. The main findings are summarized below:

- A temperature spike was noticed at onsite of flow boiling caused by the rapid generation of vapor film on the boiling surface.
- Jetting flow induced by the micronozzles was observed, which enable strong two-phase mixing thus enhanced the heat transfer rate.
- Due to the low thermal conductivity, low surface tension of HFE-7100 and high heating rate, the boiling initiated with a very high wall superheat.

- The time taken to started boiling decreased with the heat flux while the wall temperature at that instant increased.

CHAPTER 7 CONCLUSIONS

Comprehensive studies were conducted on the enhanced flow boiling in the microchannels with both steady-state and transient conditions. The microchannels with microgrooves fabricated on the bottom wall was developed to increase the nucleation site density and the capillary pressure thus promote nucleate boiling and thin film evaporation and enhance liquid rewetting. Steady-state study showed that both the HTC and the CHF were significantly enhanced. Thin liquid film is formed at low mass fluxes, promoting the thin film evaporation. Also, rewetting was greatly enhanced on the present design, which increased global liquid supply and delayed the dry-out. The maximum enhancements of CHF and HTC were about 155% and 72%, respectively, without sacrificing pressure drop. A deteriorated heat transfer performance was observed at high mass flux due to liquid flooding.

To find the transient heat transfer nature of flow boiling in microchannels under dynamic heat loads, transient studies were conducted on microchannels devices with different structures. The time response of wall temperature, wall temperature change rate and overall HTC were plotted and matched with synchronous image. The transient study on the micro-grooved microchannels showed limited enhancement compared to the plain-wall microchannels. Flow instability associated with temperature fluctuation was noticed under high heat flux. Moreover, the enhancement was mainly observed in the early boiling stage. To suppress the boiling instability and enable enhancement along all the boiling

stages, the transient study was also conducted on the microchannel with auxiliary channel and micronozzles. A more uniform wall temperature was observed due to the strong two-phase mixing induced by the micronozzles, especially in the fully developed boiling stages. A maximum enhancement of 225% on HTC was achieved by the microchannel with micronozzles compared to the plain-wall microchannel. The ONB time and temperature was identified. It was found that the heat flux has a significant effect on the time taken to initiate flow boiling and the wall temperature at that instant. To better understand the nature at onsite of boiling, the study was also conducted with HFE-7100 as coolant. Different from the boiling phenomenon of DI-water, the flow boiling of HFE-7100 expanded to the entire channel instantly. A temperature spike was observed at onsite of boiling and helped to determine the onsite boiling time and temperature. The time taken to started boiling decreased with the heat flux while the wall temperature at that instant increased.

REFERENCES

[1] Smakulski, P., and Pietrowicz, S., 2016, "A review of the capabilities of high heat flux removal by porous materials, microchannels and spray cooling techniques," Applied Thermal Engineering, 104, pp. 636-646.

[2] Mudawar, I., 2013, "Recent advances in high-flux, two-phase thermal management," Journal of Thermal Science and Engineering Applications, 5(2), p. 021012.

[3] Green, C., Kottke, P., Han, X., Woodrum, C., Sarvey, T., Asrar, P., Zhang, X., Joshi, Y., Fedorov, A., and Sitaraman, S., 2015, "A review of two-phase forced cooling in three-dimensional stacked electronics: technology integration," Journal of Electronic Packaging, 137(4), p. 040802.

[4] Tran, T., Wambsganss, M., and France, D., 1996, "Small circular-and rectangular-channel boiling with two refrigerants," International Journal of Multiphase Flow, 22(3), pp. 485-498.

[5] Mudawar, I., 2001, "Assessment of high-heat-flux thermal management schemes," IEEE Transactions on Components and Packaging Technologies, 24(2), pp. 122-141.

[6] Lee, H. J., and Lee, S. Y., 2001, "Heat transfer correlation for boiling flows in small rectangular horizontal channels with low aspect ratios," International Journal of Multiphase Flow, 27(12), pp. 2043-2062.

[7] Kim, S.-M., and Mudawar, I., 2014, "Review of databases and predictive methods for heat transfer in condensing and boiling mini/micro-channel flows," International Journal of Heat and Mass Transfer, 77, pp. 627-652.

[8] Karayiannis, T., and Mahmoud, M., 2017, "Flow boiling in microchannels: Fundamentals and applications," Applied Thermal Engineering, 115, pp. 1372-1397.

[9] Mudawwar, I., El-Masri, M., Wu, C., and Ausman-Mudawwar, J., 1985, "Boiling heat transfer and critical heat flux in high-speed rotating liquid films," International journal of heat and mass transfer, 28(4), pp. 795-806.

[10] Escher, W., Brunschwiler, T., Michel, B., and Poulikakos, D., 2010, "Experimental investigation of an ultrathin manifold microchannel heat sink for liquid-cooled chips," Journal of Heat Transfer, 132(8), p. 081402.

[11] Qu, J., Wu, H.-Y., and Wang, Q., 2012, "Experimental investigation of silicon-based micro-pulsating heat pipe for cooling electronics," Nanoscale and Microscale Thermophysical Engineering, 16(1), pp. 37-49.

[12] Yang, B., Wang, P., and Bar-Cohen, A., 2007, "Mini-contact enhanced thermoelectric cooling of hot spots in high power devices," IEEE Transactions on Components and Packaging Technologies, 30(3), pp. 432-438.

[13] Marcinichen, J. B., Olivier, J. A., Lamaison, N., and Thome, J. R., 2013, "Advances in electronics cooling," Heat Transfer Engineering, 34(5-6), pp. 434-446.

[14] Pettersen, J., Hafner, A., Skaugen, G., and Rekstad, H., 1998, "Development of compact heat exchangers for CO2 air-conditioning systems," International journal of refrigeration, 21(3), pp. 180-193.

[15] Mongia, R., Masahiro, K., DiStefano, E., Barry, J., Chen, W., Izenson, M., Possamai, F., Zimmermann, A., and Mochizuki, M., "Small scale refrigeration system for electronics cooling within a notebook computer," Proc. Thermal and Thermomechanical Proceedings 10th Intersociety Conference on Phenomena in Electronics Systems, 2006. ITHERM 2006., IEEE, pp. 751-758.

[16] Trutassanawin, S., Groll, E. A., Garimella, S. V., and Cremaschi, L., 2006, "Experimental investigation of a miniature-scale refrigeration system for electronics cooling," IEEE Transactions on Components and Packaging Technologies, 29(3), pp. 678-687.

[17] Yuan, W., Yang, B., Yang, Y., Ren, K., Xu, J., and Liao, Y., 2015, "Development and experimental study of the characteristics of a prototype miniature vapor compression refrigerator," Applied energy, 143, pp. 47-57.

[18] Stevanovic, L. D., and Solovitz, S. A., 2008, "Heat sink with microchannel cooling for power devices," Google Patents.

[19] Gillot, C., Meysenc, L., Schaeffer, C., and Bricard, A., 1999, "Integrated single and two-phase micro heat sinks under IGBT chips," IEEE Transactions on Components and Packaging Technologies, 22(3), pp. 384-389.

[20] Zhang, G., and Kandlikar, S. G., 2012, "A critical review of cooling techniques in proton exchange membrane fuel cell stacks," international journal of hydrogen energy, 37(3), pp. 2412-2429.

[21] Soupremanien, U., Le Person, S., Favre-Marinet, M., and Bultel, Y., 2012, "Tools for designing the cooling system of a proton exchange membrane fuel cell," Applied Thermal Engineering, 40, pp. 161-173.

[22] Koşar, A., Kuo, C.-J., and Peles, Y., 2005, "Boiling heat transfer in rectangular microchannels with reentrant cavities," International Journal of Heat and Mass Transfer, 48(23-24), pp. 4867-4886.

[23] Li, W., Ma, J., Alam, T., Yang, F., Khan, J., and Li, C., 2018, "Flow boiling of HFE-7100 in silicon microchannels integrated with multiple micro-nozzles and reentry micro-cavities," International Journal of Heat and Mass Transfer, 123, pp. 354-366.

[24] Kuo, C.-J., Koar, A., Peles, Y., Virost, S., Mishra, C., and Jensen, M. K., 2006, "Bubble dynamics during boiling in enhanced surface microchannels," Journal of Microelectromechanical Systems, 15(6), pp. 1514-1527.

[25] Yang, F., Dai, X., Kuo, C.-J., Peles, Y., Khan, J., and Li, C., 2013, "Enhanced flow boiling in microchannels by self-sustained high frequency two-phase oscillations," International Journal of Heat and Mass Transfer, 58(1-2), pp. 402-412.

[26] Li, W., Yang, F., Alam, T., Qu, X., Peng, B., Khan, J., and Li, C., 2018, "Enhanced flow boiling in microchannels using auxiliary channels and multiple micronozzles (I): Characterizations of flow boiling heat transfer," International Journal of Heat and Mass Transfer, 116, pp. 208-217.

[27] Ma, J., Li, W., Ren, C., Khan, J. A., and Li, C., 2019, "Realizing highly coordinated, rapid and sustainable nucleate boiling in microchannels on HFE-7100," International Journal of Heat and Mass Transfer, 133, pp. 1219-1229.

[28] Koşar, A., and Peles, Y., 2007, "Boiling heat transfer in a hydrofoil-based micro pin fin heat sink," International Journal of Heat and Mass Transfer, 50(5-6), pp. 1018-1034.

[29] Krishnamurthy, S., and Peles, Y., 2008, "Flow boiling of water in a circular staggered micro-pin fin heat sink," International Journal of Heat and Mass Transfer, 51(5-6), pp. 1349-1364.

[30] Li, C., Wang, Z., Wang, P. I., Peles, Y., Koratkar, N., and Peterson, G., 2008, "Nanostructured copper interfaces for enhanced boiling," small, 4(8), pp. 1084-1088.

[31] Yang, F., Li, W., Dai, X., and Li, C., 2016, "Flow boiling heat transfer of HFE-7000 in nanowire-coated microchannels," Applied Thermal Engineering, 93, pp. 260-268.

[32] Kuo, C. J., and Peles, Y., 2009, "Flow boiling of coolant (HFE-7000) inside structured and Plain Wall Microchannels," Journal of Heat Transfer, 131(12), p. 121011.

[33] Bar-Cohen, A., and Rahim, E., "Modeling and prediction of two-phase refrigerant flow regimes and heat transfer characteristics in microgap channels," Proc. ASME 2007 5th International Conference on Nanochannels, Microchannels, and Minichannels, American Society of Mechanical Engineers Digital Collection, pp. 1141-1160.

[34] Kabov, O. A., Zaitsev, D., Cheverda, V., and Bar-Cohen, A., 2011, "Evaporation and flow dynamics of thin, shear-driven liquid films in microgap channels," Experimental Thermal and Fluid Science, 35(5), pp. 825-831.

[35] Wang, H., Garimella, S. V., and Murthy, J. Y., 2007, "Characteristics of an evaporating thin film in a microchannel," international journal of heat and mass transfer, 50(19-20), pp. 3933-3942.

[36] Bar-Cohen, A., and Rahim, E., 2009, "Modeling and prediction of two-phase microgap channel heat transfer characteristics," Heat Transfer Engineering, 30(8), pp. 601-625.

[37] Park, K., and Lee, K.-S., 2003, "Flow and heat transfer characteristics of the evaporating extended meniscus in a micro-capillary channel," International Journal of Heat and Mass Transfer, 46(24), pp. 4587-4594.

[38] Cazabat, A., Heslot, F., Troian, S., and Carles, P., 1990, "Fingering instability of thin spreading films driven by temperature gradients," Nature, 346(6287), p. 824.

[39] Gatapova, E. Y., and Kabov, O. A., 2008, "Shear-driven flows of locally heated liquid films," International Journal of heat and mass transfer, 51(19-20), pp. 4797-4810.

[40] Lu, C. T., and Pan, C., 2009, "A highly stable microchannel heat sink for convective boiling," Journal of Micromechanics and Microengineering, 19(5), p. 055013.

[41] Schneider, B., Koşar, A., Kuo, C.-J., Mishra, C., Cole, G. S., Scaringe, R. P., and Peles, Y., 2006, "Cavitation Enhanced Heat Transfer in Microchannels," Journal of Heat Transfer, 128(12), p. 1293.

[42] Li, C., Wang, Z., Wang, P. I., Peles, Y., Koratkar, N., and Peterson, G. P., 2008, "Nanostructured copper interfaces for enhanced boiling," Small, 4(8), pp. 1084-1088.

[43] Li, W., Yang, F., Alam, T., Khan, J., and Li, C., 2015, "Experimental and theoretical studies of critical heat flux of flow boiling in microchannels with microbubble-excited high-frequency two-phase oscillations," International Journal of Heat and Mass Transfer, 88, pp. 368-378.

[44] Chen, R., Lu, M. C., Srinivasan, V., Wang, Z., Cho, H. H., and Majumdar, A., 2009, "Nanowires for enhanced boiling heat transfer," Nano letters, 9(2), pp. 548-553.

[45] Kuo, C. J., and Peles, Y., 2007, "Local measurement of flow boiling in structured surface microchannels," International Journal of Heat and Mass Transfer, 50(23-24), pp. 4513-4526.

[46] Li, W., Qu, X., Alam, T., Yang, F., Chang, W., Khan, J., and Li, C., 2017, "Enhanced flow boiling in microchannels through integrating multiple micro-nozzles and reentry microcavities," Applied Physics Letters, 110(1), p. 014104.

[47] Zhu, Y., Antao, D. S., Chu, K.-H., Chen, S., Hendricks, T. J., Zhang, T., and Wang, E. N., 2016, "Surface Structure Enhanced Microchannel Flow Boiling," Journal of Heat Transfer, 138(9), p. 091501.

[48] Yang, F., Dai, X., Peles, Y., Cheng, P., Khan, J., and Li, C., 2014, "Flow boiling phenomena in a single annular flow regime in microchannels (I): Characterization of flow boiling heat transfer," International Journal of Heat and Mass Transfer, 68, pp. 703-715.

[49] Yang, F., Dai, X., and Li, C., 2012, "High frequency microbubble-switched oscillations modulated by microfluidic transistors," Applied Physics Letters, 101(7), p. 073509.

[50] Galloway, J., and Mudawar, I., 1993, "CHF mechanism in flow boiling from a short heated wall—II. Theoretical CHF model," International journal of heat and mass transfer, 36(10), pp. 2527-2540.

[51] Hetsroni, G., Mosyak, A., Pogrebnyak, E., and Segal, Z., 2005, "Explosive boiling of water in parallel micro-channels," International Journal of Multiphase Flow, 31(4), pp. 371-392.

[52] Koşar, A., Kuo, C.-J., and Peles, Y., 2006, "Suppression of Boiling Flow Oscillations in Parallel Microchannels by Inlet Restrictors," Journal of Heat Transfer, 128(3), pp. 251-260.

[53] Zhu, Y., Antao, D. S., Chu, K., Chen, S., Hendricks, T. J., Zhang, T., and Wang, E. N., 2016, "Surface structure enhanced microchannel flow boiling," Journal of Heat Transfer, 138(091501).

[54] R. Chen, M. C. L., V. Srinivasan, Z. Wang, H.H. Cho, A. Majumdar, , 2009, "Nanowires for Enhanced Boiling Heat Transfer," Nano Letters, 9(2), pp. 548-553.

[55] Morshed, A., Yang, F., Ali, M. Y., Khan, J. A., and Li, C., 2012, "Enhanced flow boiling in a microchannel with integration of nanowires," Applied Thermal Engineering, 32, pp. 68-75.

[56] Kandlikar, S. G., Kuan, W. K., Willistein, D. A., and Borrelli, J., 2006, "Stabilization of flow boiling in microchannels using pressure drop elements and fabricated nucleation sites," Journal of Heat Transfer, 128(4), pp. 389-396.

[57] Li, D., Wu, G., Wang, W., Wang, Y., Liu, D., Zhang, D., Chen, Y., Peterson, G., and Yang, R., 2012, "Enhancing flow boiling heat transfer in microchannels for thermal management with monolithically-integrated silicon nanowires," Nano letters, 12(7), pp. 3385-3390.

[58] Basu, S., Werneke, B., Peles, Y., and Jensen, M. K., 2015, "Transient microscale flow boiling heat transfer characteristics of HFE-7000," International Journal of Heat and Mass Transfer, 90, pp. 396-405.

[59] David, T., Mendler, D., Mosyak, A., Bar-Cohen, A., and Hetsroni, G., 2014, "Thermal management of time-varying high heat flux electronic devices," Journal of Electronic Packaging, 136(2), p. 021003.

[60] Aguiar, G. M., and Ribatski, G., 2019, "The Effect of Transient Power Hotspots on the Heat Transfer Coefficient during Flow Boiling Inside Single Microscale Channels," Heat Transfer Engineering, 40(16), pp. 1337-1348.

[61] Chen, G., and Cheng, P., 2009, "Nucleate and film boiling on a microheater under pulse heating in a microchannel," International Communications in Heat and Mass Transfer, 36(5), pp. 391-396.

[62] Jiang, L., Wong, M., and Zohar, Y., 2000, "Transient temperature performance of an integrated micro-thermal system," Journal of Micromechanics and Microengineering, 10(3), p. 466.

[63] Wang, Y., Shin, J.-h., Woodcock, C., Yu, X., and Peles, Y., 2019, "Local, transient heat transfer measurements for flow boiling in a microchannel with a pin fin," International Journal of Heat and Mass Transfer, 134, pp. 377-387.

[64] Huang, H., Borhani, N., and Richard Thome, J., 2016, "Thermal response of multi-microchannel evaporators during flow boiling of refrigerants under transient heat loads with flow visualization," Journal of Electronic Packaging, 138(3).

[65] Basu, S., Werneke, B., Peles, Y., and Jensen, M. K., 2015, "Thermal behavior of a microdevice under transient heat loads," International Journal of Heat and Mass Transfer, 91, pp. 1078-1087.

[66] Jiang, L., Wong, M., and Zohar, Y., 2000, "Unsteady characteristics of a thermal microsystem," Sensors and Actuators A: Physical, 82(1-3), pp. 108-113.

[67] Chen, G., Quan, X., and Cheng, P., 2010, "Effects of pulse width and mass flux on microscale flow boiling under pulse heating," International Communications in Heat and Mass Transfer, 37(7), pp. 792-795.

[68] Chen, C., Lin, T., and Yan, W.-M., 2017, "Time periodic saturated flow boiling heat transfer of R-134a in a narrow annular duct due to heat flux oscillation," International Journal of Heat and Mass Transfer, 106, pp. 35-46.

[69] Kandlikar, S. G., 2002, "Fundamental issues related to flow boiling in minichannels and microchannels," Experimental Thermal and Fluid Science, 26(2-4), pp. 389-407.

[70] Li, J., and Peterson, G., 2005, "Boiling nucleation and two-phase flow patterns in forced liquid flow in microchannels," International journal of heat and mass transfer, 48(23-24), pp. 4797-4810.

[71] Wojtan, L., Revellin, R., and Thome, J. R., 2006, "Investigation of saturated critical heat flux in a single, uniformly heated microchannel," Experimental Thermal and Fluid Science, 30(8), pp. 765-774.

[72] Vafaei, S., and Wen, D., 2010, "Critical heat flux (CHF) of subcooled flow boiling of alumina nanofluids in a horizontal microchannel," Journal of Heat Transfer, 132(10), p. 102404.

[73] Hsieh, S.-S., and Lin, C.-Y., 2012, "Correlation of critical heat flux and two-phase friction factor for subcooled convective boiling in structured surface microchannels," International Journal of Heat and Mass Transfer, 55(1-3), pp. 32-42.

[74] Li, W. M., Yang, F. H., Alam, T., Khan, J., and Li, C., 2015, "Experimental and theoretical studies of critical heat flux of flow boiling in microchannels with microbubble-excited high-frequency two-phase oscillations," International Journal of Heat and Mass Transfer, 88, pp. 368-378.

[75] Bergles, A., and Kandlikar, S., 2005, "On the nature of critical heat flux in microchannels," Journal of Heat Transfer, 127(1), pp. 101-107.

[76] Chang, K., and Pan, C., 2007, "Two-phase flow instability for boiling in a microchannel heat sink," International Journal of Heat and Mass Transfer, 50(11-12), pp. 2078-2088.

[77] Wang, G., Cheng, P., and Bergles, A., 2008, "Effects of inlet/outlet configurations on flow boiling instability in parallel microchannels," International Journal of Heat and Mass Transfer, 51(9-10), pp. 2267-2281.

[78] Koşar, A., Kuo, C.-J., and Peles, Y., 2006, "Suppression of boiling flow oscillations in parallel microchannels by inlet restrictors," Journal of Heat Transfer, 128(3), pp. 251-260.

[79] Deng, P., Lee, Y.-K., and Cheng, P., 2003, "The growth and collapse of a micro-bubble under pulse heating," International Journal of Heat and Mass Transfer, 46(21), pp. 4041-4050.

[80] Kandlikar, S. G., 2012, "History, Advances, and Challenges in Liquid Flow and Flow Boiling Heat Transfer in Microchannels: A Critical Review," Journal of Heat Transfer, 134(3), pp. 034001-034001-034015.

[81] Thome, J. R., 2006, "State-of-the-art overview of boiling and two-phase flows in microchannels," Heat transfer engineering, 27(9), pp. 4-19.

[82] Jacobi, A. M., and Thome, J. R., 2002, "Heat transfer model for evaporation of elongated bubble flows in microchannels," J. Heat Transf.-Trans. ASME, 124(6), pp. 1131-1136.

[83] Davis, E. J., and Anderson, G., 1966, "The incipience of nucleate boiling in forced convection flow," AIChE Journal, 12(4), pp. 774-780.

[84] Steinke, M. E., and Kandlikar, S. G., 2004, "An experimental investigation of flow boiling characteristics of water in parallel microchannels," Journal of Heat Transfer, 126(4), pp. 518-526.

[85] Yang, F., Dai, X., Peles, Y., Cheng, P., Khan, J., and Li, C., 2014, "Flow boiling phenomena in a single annular flow regime in microchannels (II): Reduced pressure drop and enhanced critical heat flux," International Journal of Heat and Mass Transfer, 68, pp. 716-724.

[86] Kline, S. J., and McClintock, F. A., 1953, "Describing uncertainties in single-sample experiments," Mechanical Engineering, 75(1), pp. 3- 8.

[87] Qu, W., and Mudawar, I., 2003, "Flow boiling heat transfer in two-phase micro-channel heat sinks—I. Experimental investigation and assessment of correlation methods," International journal of heat and mass transfer, 46(15), pp. 2755-2771.

[88] Chen, R., Lu, M.-C., Srinivasan, V., Wang, Z., Cho, H. H., and Majumdar, A., 2009, "Nanowires for enhanced boiling heat transfer," Nano letters, 9(2), pp. 548-553.

[89] Qu, W. L., and Mudawar, I., 2004, "Measurement and correlation of critical heat flux in two-phase micro-channel heat sinks," Int. J. Heat Mass Transf., 47(10-11), pp. 2045-2059.

[90] Wu, H. Y., and Cheng, P., 2003, "Visualization and measurements of periodic boiling in silicon microchannels," Int. J. Heat Mass Transf., 46(14), pp. 2603-2614.

[91] Wu, H. Y., and Cheng, P., 2004, "Boiling instability in parallel silicon microchannels at different heat flux," Int. J. Heat Mass Transf., 47(17-18), pp. 3631-3641.

[92] Wu, H. Y., Cheng, P., and Wang, H., 2006, "Pressure drop and flow boiling instabilities in silicon microchannel heat sinks," J. Micromech. Microeng., 16(10), pp. 2138-2146.

[93] Wang, G., Cheng, P., and Wu, H., 2007, "Unstable and stable flow boiling in parallel microchannels and in a single microchannel," Int. J. Heat Mass Transf., 50(21-22), pp. 4297-4310.

[94] Chang, K. H., and Pan, C., 2007, "Two-phase flow instability for boiling in a microchannel heat sink," Int. J. Heat Mass Transf., 50(11-12), pp. 2078-2088.

[95] Qu, W., and Siu-Ho, A., 2009, "Measurement and prediction of pressure drop in a two-phase micro-pin-fin heat sink," Int. J. Heat Mass Transf., 52(21-22), pp. 5173-5184.

[96] Kosar, A., Kuo, C. J., and Peles, Y., 2006, "Suppression of boiling flow oscillations in parallel microchannels by inlet restrictors," J. Heat Transf.-Trans. ASME, 128(3), pp. 251-260.

[97] Kandlikar, S. G., Kuan, W. K., Willistein, D. A., and Borrelli, J., 2006, "Stabilization of flow boiling in microchannels using pressure drop elements and fabricated nucleation sites," J. Heat Transf.-Trans. ASME, 128(4), pp. 389-396.

[98] Evelyn N. Wang, L. Z., Linan Jiang, Jae-Mo Koo, James G. Maveety, Eduardo A. Sanchez, 2004, "Micromachined Jets for Liquid Impingement Cooling of VLSI Chips," JOURNAL OF MICROELECTROMECHANICAL SYSTEMS, 13, pp. 833-841.

[99] Fabbri, M., and Dhir, V. K., 2005, "Optimized Heat Transfer for High Power Electronic Cooling Using Arrays of Microjets," Journal of Heat Transfer, 127(7), p. 760.

[100] Chen, Y. C., Ma, C. F., Qin, M., and Li, Y. X., 2005, "Theoretical study on impingement heat transfer with single-phase free-surface slot jets," International Journal of Heat and Mass Transfer, 48(16), pp. 3381-3386.

[101] Yang, F. H., Alwazzan, M., Li, W. M., and Li, C., 2014, "Single- and Two-Phase Thermal Transport in Microchannels With Embedded Staggered Herringbone Mixers," Journal of Microelectromechanical Systems, 23(6), pp. 1346-1358.

[102] Chen, T., and Garimella, S. V., 2006, "Measurements and high-speed visualizations of flow boiling of a dielectric fluid in a silicon microchannel heat sink," International Journal of Multiphase Flow, 32(8), pp. 957-971.

[103] Chang, J., and You, S., 1997, "Boiling heat transfer phenomena from microporous and porous surfaces in saturated FC-72," International Journal of Heat and Mass Transfer, 40(18), pp. 4437-4447.

[104] Lee, J., and Mudawar, I., 2008, "Fluid flow and heat transfer characteristics of low temperature two-phase micro-channel heat sinks – Part 1: Experimental methods and flow visualization results," International Journal of Heat and Mass Transfer, 51(17-18), pp. 4315-4326.